

STUDIES OF FLUID FLOW, HEAT TRANSFER,
AND INDUCED STRESSES IN AND AROUND
UNDERGROUND FRACTURES

by

ALAN RICHARD CROCKETT

B.S., BOSTON UNIVERSITY, BOSTON, MASSACHUSETTS
(1978)

SUBMITTED TO THE DEPARTMENT OF
MECHANICAL ENGINEERING IN PARTIAL
FULFILLMENT OF THE
REQUIREMENTS FOR THE
DEGREE OF

MASTER OF SCIENCE IN
MECHANICAL ENGINEERING

at the
MASSACHUSETTS INSTITUTE OF TECHNOLOGY
June 1984

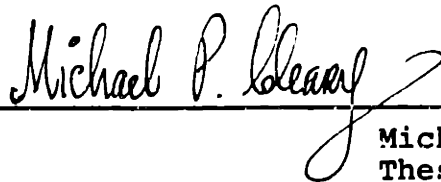
© Massachusetts Institute of Technology

Signature of Author



Department of Mechanical Engineering

Certified by



Michael P. Cleary
Thesis Supervisor

Accepted by



MASSACHUSETTS INSTITUTE
OF TECHNOLOGY

Chairman, Departmental Graduate Committee

Warren M. Rohsenow

JUL 17 1984

LIBRARIES

Archives

STUDIES OF FLUID FLOW, HEAT TRANSFER,
AND INDUCED STRESSES IN AND AROUND
UNDERGROUND FRACTURES

by

ALAN RICHARD CROCKETT

Submitted to the Department of Mechanical Engineering
on March , 1984 in partial fulfillment of the
requirements for the Degree of Master of Science in
Mechanical Engineering

ABSTRACT

The temperature and fluid flow distributions in and around wellbores and fractures must often be considered if stimulation and completion operations in low permeability gas and oil formations are to be modeled accurately. Fracture efficiency and induced reservoir stress (backstress) depend on the fluid exchange between fracture and reservoir, and reservoir fluid properties, such as viscosity, are temperature sensitive. Thus, fluid exchange and variation in temperature can significantly affect concerns of such practical importance as well production rates and hydraulic fracture profiles and growth rates.

Several models of varying accuracy and complexity are developed to describe fluid exchange, heat transfer, and subsequent thermal and pore-pressure-induced backstresses for stationary (e.g. production) and propagating (e.g. hydraulic) fractures. They range from a simple yet effective model which lumps fracture and reservoir related phenomena at the wellbore, to a model providing a precise two dimensional description. Fluid and heat exchanges between fracture and reservoir are determined from (singular) surface integral equations, based on an influence function superposition method, and the temperature variation in the fracture is obtained using an integral control volume technique. Given fluid loss and temperature distributions, the backstresses are determined directly by influence function or misfit wedge (i.e. dislocation) methods.

The fluid loss, temperature distributions, and backstresses are obtained for stationary and propagating fractures, and comparisons are made between the models developed. Additionally, the results indicate that in tight reservoirs convection is not an important mechanism of heat transfer, the heat up of cold fracture fluid occurs in the vicinity of the wellbore, and thermally induced backstresses are small over the time scale of hydraulic fracturing in comparison to those induced by fluid loss.

Thesis Supervisor: Dr. Michael P. Cleary
Title: Associate Professor of Mechanical Engineering

Acknowledgements

Firstly, I would like to thank my advisor, Professor Michael P. Cleary for the inspiration, support, and friendship that he has generously given me. Many thanks also to my undergraduate student, Hai Vo, who went far beyond the call of duty innumerable times to help accomplish this research; to Lauren Zeise of Harvard University who spent many patient hours reviewing the manuscript and supporting me in my work; to Bengi Ambrogi for his excellent drafting of the graphs and figures; to Barbara Rosen for typing the equations; and to Susan Bimbo for her help with the report preparation. Lastly, I would like to thank my parents, Norman and Erica Crockett, for all they have done for me, over so many years.

Financial support for this work came from the M.I.T. UFRAC Project, which is supported by several production and service companies in the energy industry.

Table of Contents

Abstract	ii
Acknowledgements	iii
List of Tables	v
List of Figures	vi
Nomenclature	viii
1. Introduction	1
2. General Modeling Procedures	4
2.1 Coupled Fracture and Reservoir Models	4
2.1.1 Wellbore Lumped Model	9
2.1.2 Pseudo 2D Model	10
2.1.3 2D Model	10
2.2 Reservoir Fluid Flow	11
2.2.1 The Governing Equation	11
2.2.2 1D Fluid Flow	12
2.2.3 2D Fluid Exchange	17
2.3 Backstress	20
2.3.1 General Considerations	20
2.3.2 Reservoir Backstress	22
2.3.3 Discretisation	24
2.4 Heat Transfer in the Reservoir	26
2.4.1 The Governing Equation	26
2.4.2 1D Heat Transfer	27
2.5 Energy Balance in the Fracture	35
2.6 Production	39
2.6.1 2D Drainage Model	39
2.6.2 Discretisation	41
3. Results	43
3.1 Introduction	43
3.2 Reservoir Fluid Flow	44
3.3 Backstress	49
3.4 Heat Transfer	54
3.5 Production	55
4. Summary and Conclusions	57
References	59
Tables	62
Figures	67

List of Tables

Table 1a. Non-dimensionalisation of parameters

Table 1b. Non-dimensional parameters

Table 2a. Typical reservoir parameters for a low to fair permeability oil reservoir

Table 2b. Typical reservoir parameters for a low permeability gas reservoir

Table 3. Fluid, heat penetration and heat exchange characteristics of the typical oil and gas reservoirs

Table 4. Fracture propagation cases generated by a lumped fracture propagation model (ellipsoidal shapes)

List of Figures

- Figure 2.1** Fracture in surroundings with relevant events noted
- Figure 2.2** Heat and fluid penetration into the reservoir normal to the fracture
- Figure 2.3a** Discretisation of fluid exchange with time
- Figure 2.3b** Fracture geometry; discretisation of fracture volume and surface area
- Figure 2.3c** Stationary grid that fracture grows over; variables associated with stationary grid
- Figure 2.3d** Chebyshev grid that stretches over fracture as it grows; variables associated with Chebyshev grid
- Figure 2.3e** Pressure distribution for propagating fractures
- Figure 3.1** 1D exact versus influence function solutions of the fluid loss rate for constant fracture pressure
- Figure 3.2** Lumped and pseudo-2D model predictions of the total fluid lost for propagating fractures: **a)** constant fracture pressure; **b)** constant wellbore pressure; **c)** constant fracture volume growth rate
- Figure 3.3** Predictions of total fluid lost for propagating fractures in gas and oil reservoirs
- Figure 3.4** Two definitions of fracture efficiency shown for various fracture propagation conditions: **a** and **c)** total fracture efficiency; **b** and **d)** fracture volume opposite reservoir efficiency
- Figure 3.5** One and two fluid model predictions of total leakoff for a propagating fracture: **a)** oil reservoir; **b)** gas reservoir
- Figure 3.6** One and two fluid model predictions of fluid loss rate
- Figure 3.7** Comparison of 2D and pseudo-2D fluid loss rates: **a)** stationary fracture; **b)** propagating fracture
- Figure 3.8** 2D fluid loss rates for constant and self-similar pressure distributions along the fracture
- Figure 3.9a** "Approximate", reservoir height, and fracture length model predictions of wellbore backstress for a propagating fracture in an oil reservoir
- Figure 3.9b** Comparison of approximate wellbore backstress predictions

Figure 3.10 Decomposition of wellbore backstress for a propagating fracture in a gas reservoir into a leakoff layer and reservoir components

Figure 3.11a Comparison of 2D and pseudo-2D predictions of backstress for a stationary fracture

Figure 3.11b 2D predictions for a propagating fracture

Figure 3.11c Comparison of 2D and pseudo-2D predictions of backstress for a propagating fracture

Figure 3.12 Comparison of 2D backstress for constant and self-similar pressure distributions along the fracture

Figure 3.13 Comparison of 1D solutions for reservoir heat transfer

Figure 3.14 Sensitivity of the variational heat transfer solution to cubic curve fitting parameter(c)

Figure 3.15 Lumped verses pseudo-2D predictions of average fracture temperature for propagating fracture: **a)** constant wellbore pressure; **b)** constant fracture volume growth rate

Figure 3.16 Lumped predictions of average fracture temperature for propagating fractures

Figures 3.17 Pseudo-2D model predictions of fracture temperature for propagating fractures

Figure 3.18 2D well production model predictions of flow rates into the fracture

Figure 3.19 2D well production model predictions of stabilised flowrates into the fracture

Nomenclature

A	area
A_C	area of fracture cross section
A_{rk}	Chebyshev interpolation matrix
A_{res}	area opposite reservoir
b	backstress constant
c	cubic curve fitting parameter
C_{pl}	specific heat of leakoff fluid
c_R	diffusivity of the reservoir fluid
C_s	specific heat of reservoir rock
E_A	modulus of adjacent stratum
$Ei(x)$	exponential integral function
E_R	reservoir modulus
H_F	half height of reservoir
H, h	reservoir height
h_L	conduction heat exchange rate
K_f	bulk modulus (reservoir fluid)
K_h	conductivity of reservoir rock fluid matrix
K_{hs}	conductivity of the reservoir rock
K_L	effective permeability of the leakoff fluid
K_R	permeability of the reservoir fluid
l, ℓ	characteristic length scale(initial fracture length)

$l(\tau)$	current fracture length
M_F	viscosity of fluid in fracture	
NE	number of reservoir elements	
NNY	number of reservoir nodes	
p	pressure	
Δp	pressure difference between fracture and reservoir	
p_h	pressure at heat penetration depth	
p_L	pressure at the leakoff penetration depth	
p_R	reservoir pressure	
p_w^o	initial wellbore pressure	
p_w	wellbore pressure	
q_L	fluid exchange rate	
\dot{Q}_{rel}	volume flow rate in the fracture	
\dot{Q}_w	wellbore pumping rate	
S_c	fracture surface	
S_r	zeros of the Chebyshev polynomial of the first kind	
S_k	zeros of the Chebyshev polynomial of the second kind	
Δt	time increment	
t, τ	time	
T_1	Chebyshev polynomials of the first kind	
\underline{v}	velocity	
Q_F	total fracture volume	
Q_L	lost fluid volume	

V_R	reservoir volume
Vol	volume of fracture element
$W(1)$	quadratic interpolation weighting
x_o, x	coordinates along the fracture
y_o, y	coordinate normal to fracture
γ_f, Γ_f	pore pressure influence function
γ_h, Γ_h	heat conduction influence function
γ_p, Γ_p	well production influence function
γ_s, Γ_s	backstress influence function
$\Delta\Gamma_h$	convection heat transfer influence function
δ	fracture half-width
δ_f	pore pressure penetration
δ_h	heat penetration
δ_{hc}	conduction heat penetration
δ_L	leakoff penetration
η_T	fracture efficiency based on total fracture volume
η_R	efficiency based on volume opposite reservoir
η	backstress coefficient
ϕ	porosity
θ	temperature
θ_R	reservoir
θ_w	wellbore temperature

κ	thermal diffusivity of the rock and fluid in the reservoir
κ_F	thermal diffusivity of the fracture fluid
κ_L	thermal diffusivity of the leakoff fluid
μ_L	viscosity of the leakoff fluid
$\bar{\mu}_L$	average μ_L
μ_R	viscosity of the reservoir fluid
$\bar{\mu}_R$	average μ_R
ρ	density
ρ_L	density of the leakoff fluid
ρ_S	density of the reservoir fluid
σ_B	pore-pressure induced backstress
σ_B^h	thermal backstress
σ_{BL}	backstress caused by leakoff layer
σ_{BR}	reservoir backstress
σ_{Bv}	backstress based on vertical height
σ_C	confining stress

1 Introduction

The study of diffusive processes and associated stress has a broad range of applications. Classical analyses of heat conduction and thermal stresses, including the work of Carslaw and Jaeger (1959), and Boley and Weiner (1960), are continually extended and implemented to understand and design structures and equipment; newer applications are always appearing, such as in the extraction of heat from geothermal reservoirs (Barr, 1983a and 1983b). Analogous models are used to describe the effects of more general phenomena such as shrinkage (e.g. drying) and solid state diffusion. An area of intense recent interest has been that of stresses induced by fluid flow in porous media (Rice and Cleary, 1976), especially in relation to fracturing processes (Cleary, 1978); such problems, particularly in the context of hydraulic fractures in underground reservoirs, are the main concern of the work presented here.

A variety of techniques have been developed for the analysis of diffusion, many for reservoir engineering applications, and including some that have been oriented toward fracture geometries (Settari and Cleary, 1982a). There has been a predominant preference for volume discretisation techniques (Settari and Price, 1980), especially finite difference (Settari and Cleary, 1982b), and more recently finite element techniques (Advani, 1980). These work well for smoothly varying non-singular, allowably discontinuous fields and finite geometries, with non-linearities and heterogeneities, permitting efficient solution of banded matrices. However, in capturing the behavior around typical reservoir structures, they are limited, because of unavoidable complicating factors, such as severe mesh refinements, "infinite" elements, and moving fracture surfaces. The last is especially difficult to incorporate accurately, and it even requires remeshing for arbitrarily curved trajectories. To deal effectively with these and other difficult characteristics, we have developed so-called surface intergral equation (SIE) techniques (Cleary et al., 1983).

Integral equation approaches are certainly not new in heat conduction (Chang et al., 1973), nor even in this area of application. Although somewhat distinct from conventional boundary integral equation (BIE) methods (Shippy 1975), some limited versions of our formulation have implemented for special case studies of flow around stationary fractures and resulting reservoir production (Cinco et al., 1978). Our methods seem to have advantages in effectiveness and generality; those presented are part of a broader methodology which allows us to correctly determine the growth of one or more fractures. The models presented here simultaneously describe the coupled fluid flow, heat transfer, and induced stresses in and around growing fractures. When coupled with propagation models they provide for a complete description of fracture growth.

The effect of fluid flow and heat transfer in and around hydraulic fractures has considerable importance: accurate predictions of fracture growth length require a knowledge of fluid leakoff; well production rates are determined, in part, by pore pressure distributions; and viscous fracturing fluids often have highly temperature-sensitive viscosities. In addition, accurate fracture growth modeling must often take into account the stresses incurred from fluid and heat interactions between fracture and reservoir.

Our approach provides a succession of models of increasing mathematical complexity and computational difficulty. The SIE method mentioned above is interfaced with other modeling procedures (e.g. volume integrated discretisation of heat transfer in the fracture) to develop the wellbore lumped, the pseudo-2D and the 2D models, each successively providing a more precise description of fluid loss, fracture temperature, and induced stresses for stationary and propagating fractures. In attempting to reduce the computational requirements while providing for physical insight, we incorporate as much analytical structure as possible into even our most complicated models. Using very simple

analytical solutions, the wellbore lumped model, which is compatible with the wellbore lumped propagation models of Cleary, Keck, and Mear (1983), treats the fracture as a lumped system. Both the 2D and pseudo-2D models take into account the variation of properties along the fracture. While the 2D model provides an exact numerical solution for the evolution of fluid loss and backstress, the pseudo-2D model approximates the 2D by assuming fluid loss occurs only normal to the fracture. The pseudo-2D model was designed to be compatible with a fracture propagation model such as P3DH (Settari and Cleary, 1982a), whereas the 2D model can be used with a fully 2D propagation model (Narendran and Cleary, 1983).

2 General Modeling Procedures

2.1 Coupled Fracture and Reservoir Models

Three models of varying accuracy and complexity provide estimates of fluid exchange, fracture temperature, and fluid induced backstress for a fracture in its surroundings (Figure 2.1). Although the models have been developed for 2D planar fractures, the scale of events in typical reservoirs permits their application to curving fractures. Some rudimentary 3D qualities have been built in, to the extent that the models can accommodate P3DH fracture geometry, and out of zone growth; it is also possible to turn any of the models on end, in the P3DH fashion, to model fracture cross-sections. In this section, common attributes of the three models are described and each model is discussed individually. Elements of the modeling (e.g. the fluid loss, backstress, and reservoir/fracture heat transfer components), and a production model which features 2D drainage are described in subsequent sections.

Disturbance propagation

Pressure and temperature difference between fracture and reservoir can be thought of as disturbances in the pressure and temperature fields which gradually diffuse from the fracture out into the reservoir. A criterion is established that, for all practical purposes, determines the distance into the reservoir to which the disturbance propagates. Thus we define the three penetration depths (δ) of interest: δ_p and δ_h are the depths at which the pore pressure and the reservoir temperature are 99% of their reservoir values; δ_L is the position of the leakoff penetration front. In virtually all instances the thermal and leakoff penetrations lag behind (usually far behind) the pore pressure penetration.

Dividing the reservoir up into three regions (thermal and leakoff penetration zones and a reservoir region) is an excellent way of taking into

account some of the reservoir inhomogeneities which unavoidably occur during fracturing. Outside of the thermal and leakoff penetration zones, the reservoir is assumed to be homogeneous. Mathematical analyses pertaining to infinite homogeneous media can be applied to this region; flow fields can be calculated using either 1D or 2D analysis. Within these penetration zones, temperature variation occurs, viscosities vary with temperature, leakoff properties differ from those in the reservoir, and permeabilities depend on the type of fluid present in the zone.

Table 3 shows typical values of these penetrations after one hour for oil and gas reservoirs. We see that the thermal and leakoff penetrations are very small when compared to the fracture length (thermal and leakoff penetrations are less than one foot, fracture lengths on the order of hundreds to thousands of feet). Since the scale of these penetration zones is small, flow within the zones is modeled by simple 1D analysis with flow patterns occurring normal to the fracture surface. All inhomogeneities have therefore been confined to the penetration zones, vastly simplifying the analysis. Coupling occurs at the interfaces between the furthest penetrating zone and the homogeneous reservoir, and between the two penetrating zones (thermal and leakoff).

It is also interesting to note that the scale of pressure penetration (5.5 ft in the gas reservoir, 35 ft in the oil) is also relatively small compared to typical fracture lengths, implying that 1D reservoir region flow analysis (like that used in the lumped and the pseudo-2D models) would probably be adequate in many instances. Comparisons of pseudo-2D and 2D results (Figures 3.7) bear this out.

Coupled equations

All models require that the equations governing fluid loss and fracture/reservoir heat transfer be solved simultaneously. Unfortunately, these equations are coupled nonlinearly. To circumvent this difficulty the governing

equations are solved sequentially; those quantities necessary to decouple the equations are extrapolated from previous time levels. Accurate to second order in time, the extrapolation equation is

$$y_N = \left(1 + \frac{\Delta t_N}{\Delta t_{N-1}}\right) y_{N-1} - \frac{\Delta t_N}{\Delta t_{N-1}} y_{N-2} + O(\Delta t_N^2) \quad (1)$$

To bring the solution from the N to the N+1 time level, we sequentially integrate the governing equations as follows:

- 1) The excess pressure, Δp , and relevant fracture flow and geometry information is passed from a fracture propagation solver.
- 2) The fracture temperature θ , and the leakoff and thermal penetration depths, δ_L and δ_h , respectively, are extrapolated from previous time levels.
- 3) The average viscosities μ_L and μ_R are calculated using the extrapolated values.
- 4) The fluid loss q_L and leakoff depth δ_L are calculated.
- 5) Backstress σ_B is determined
- 6) The fracture temperature and heat penetration δ_h are calculated.
- 7) $N=N+1$

Discretisation

This modeling requires the discretisation of integral equations in which part (multiplicative) of the integrand is an unknown to be determined, and the

other part is integrable in time. We assume that the unknown is constant over short time periods and integrate the remaining part over that period. The cumulative value of the integral can then be attained by summing the constituent elements. As an example, the discretisation of fluid exchange (q_L) with time is shown in Figure 2.3a. Although we show later that for our purposes the accuracy of such a method is very good (Figure 3.1), it can always be improved by taking smaller time steps.

Although the analyses performed are at most 2D planar, some 3D fracture characteristics have been included, as illustrated in Figure 2.3b. The fracture is discretised into volume sections (elements), each having 2 associated surface areas: the total area of the section (A_i) and the section area in contact with the reservoir ($A_{res,i}$). This scheme can accommodate any fracture geometry (we use ellipsoidal geometry with temporally evolving lengths, heights and widths) so long as the volumes and surface areas associated with each element are calculated in accordance with the fracture geometry in question. Fluid in the fracture is assumed to flow only in the direction of the fracture length. With this discretisation heat transfer in the fracture is analysed and total loss and fluid efficiency are estimated.

Two grids are defined on the fracture. One is a stationary grid (Figure 2.3c) with equally spaced nodes extending out beyond the maximum position of the fracture tip; when the fracture grows over a new node, that node becomes "activated". The activation rate of new nodes depends on how fast the fracture grows. All pseudo-2D quantities are determined on this stationary grid, and in the 2D model, the grid is used for the heat transfer analysis.

The stationary grid is perfectly adequate for schemes such as the pseudo-2D models which do not have the capability to resolve the complex backstress and flow patterns at the fracture tip. However, the most important aspect of the fully 2D analysis is the study of these patterns; this requires a

grid with high resolution at the fracture tip. To determine fluid loss and backstress, we use a Chebychev grid (Figure 2.3d) which stretches with the fracture as it grows. Node locations are determined from the location of the zeros of Chebychev polynomials of the first and second kind. The generating functions are graphically depicted in Figure 2.3d. The highest concentration of grid nodes always occurs in the region of the fracture tip, where fluid loss and backstress change rapidly; the lowest concentration occurs at the wellbore where change is slow. The 2D heat transfer variables are evaluated on the stationary grid, and an interpolation scheme (linear) converts quantities required from the fixed grid to the Chebychev grid or vice versa.

Fracture Pressure Distributions

Fluid loss is driven by the difference in pressure ($p_F - p_T$) between the fracture pressure, p_F , and the tectonic pressure, also called the reservoir pore pressure, p_T . The fracture pressure is the sum of the confining stress, σ_c , present in the formation rock, and the excess pressure (over confining stress), σ , which drives hydraulic fracture propagation. The excess pressure usually varies along the fracture according to a self-similar pressure distribution, like that obtained from the P3DH fracture propagation model and shown in Figure 2.3e. Since the excess pressure at the wellbore for the fracture propagation histories considered is of order 100 psi, and since the confining stresses for the oil and gas reservoirs considered are of order 600 and 2500 psi, respectively, the variation along the fracture in total pressure is at most 10% for the oil reservoir and 2% for the gas reservoir. Thus it is doubtful that variation in excess pressure will often have a significant effect on loss, except perhaps at the fracture tip, where marginal effects may be observed. In order to verify this assumption, analyses are performed with both constant fracture pressure and with a distribution whose excess pressure component varies self-similarly along the fracture. Values of the excess pressure at the wellbore are assumed to be the same in both cases.

2.1.1 Wellbore Lumped Model

The wellbore lumped model determines averaged quantities: All quantities including fluid loss, fracture temperature, and backstress, are functions of time only; and the fracture volume is discretised using only one element. The model takes into account time varying pressure and temperature differences between fracture and reservoir, the temperature dependence of viscosity in the reservoir, and the coupling between the governing thermal and fluid equations. Backstress is determined at the wellbore based on both the reservoir height and the fracture length.

The effect of fracture propagation on fluid and heat exchange is determined by an area weighting technique. Current values (at time t_N) are found with respect to current fracture geometry. However, all previous values are known with respect to the previous fracture geometry. In order to determine the previous values with respect to current geometry, the values are weighted by the ratio of previous to current fracture area. For example, fluid loss for any previous time level n is calculated with respect to the current fracture geometry such that the total loss rate at that level is conserved; hence,

$$\hat{q}_L(t_n) = \frac{\hat{A}_n}{\hat{A}_N} \hat{q}_L(\hat{t}_n), \quad \hat{h}_L(t_n) = \frac{\hat{A}_n}{\hat{A}_N} \hat{h}_L(\hat{t}_n) \quad (2)$$

where A_n and A_N are the areas of the fracture at the n and N time levels. Previous values of the penetration depths are also extrapolated according to Eqn. 2; whereas the fracture temperature is extrapolated with respect to a ratio of fracture volumes.

2.1.2 Pseudo-2D Model

The pseudo-2D model represents an improvement over the wellbore lumped model in that it takes into account the variation of quantities along the fracture length. The fracture is divided into I segments or elements and essentially the same equations as in the wellbore lumped model are applied to each segment: 1D equations governing heat transfer and fluid flow in the reservoir provide estimates of heat and fluid exchange; and the fracture temperature is determined by energy interactions of each segment with the adjacent reservoir and fracture segments. Backstress along the length of the fracture is found by substituting the pseudo-2D loss distribution into a 2D formulation for backstress; the wellbore backstress is also found based on the reservoir height assuming there is no vertical variation in loss over the reservoir zone. The pressure differences for each segment, the fracture geometry, and the flow rates in the fracture must be provided by a fracture propagation model.

As described in the fracture discretisation section, all variables are found on a fixed grid over which the fracture grows: New segments must be continually activated during the fracture period. If the pseudo-2D model is used in conjunction with a fracture propagation model that has a grid which stretches with the fracture, the quantities it provides to the pseudo-2D model such as pressure difference and fracture segment geometry must be interpolated to the fixed grid.

2.1.3 2D Model

The 2D model is the most accurate of those developed. Fully 2D analyses are performed on a non-uniform stretching grid in order to calculate distributions of fluid loss and backstress along the length of the fracture; fracture temperature is determined on the fixed grid as in the pseudo-2D model. Interpolation must be performed to pass relevant quantities between the

grids. If the 2D model is used in conjunction with a fracture propagation model, pressure differences and relevant geometry may also have to be interpolated. The 2D model provides precise calculations of fluid loss and backstress at the fracture tip; however, a large amount of computation is required to do the job. A full matrix must be solved for each time step to calculate loss, and the effects of previous fluid loss and heat exchange must be summed at every time step from the initial time in order to calculate current solution values. Such cost, however, is unavoidable even with other methods (e.g. finite difference and element methods) if accurate solutions near the fracture tip are to be found.

2.2 Reservoir Fluid Flow

2.2.1 The governing equation

The equation governing pore pressure for a homogeneous reservoir is obtained by writing the mass conservation equation in terms of pore pressure and reservoir stress. Since for an infinite reservoir domain (or a reasonable approximation to it) the effect of reservoir stress can be neglected, the result is a diffusion equation in terms of pore pressure only:

$$c_R \nabla^2 p = \frac{\partial p}{\partial t} \qquad \nabla^2 \hat{p} = \frac{\partial \hat{p}}{\partial \hat{t}} \qquad (3)$$

The velocity field can be found using D'Arcy's Law:

$$\underline{v} = \frac{-k_R}{\mu_R} \underline{\Delta} p \qquad \underline{\hat{v}} = -\underline{\Delta} \hat{p} \qquad (4)$$

The equations on the right in Eqns. (3, 4) have been non-dimensionalised according to Table 1.

Although it is generally true that the presence of boundaries surfaces, strata, etc. affect pore pressure distributions, the effect is small for a great many cases. For this reason, outside of the leakoff penetration zone and the thermal boundary layer surrounding the fracture the reservoir is treated as an infinite, homogeneous domain.

2.2.2 1D Fluid Flow

Special analytical solution

When a constant pressure difference between the fracture and the reservoir at infinity is specified, one important analytical solution to Eqn. 3 provides the transient pressure distribution in the reservoir:

$$\hat{p} = \Delta\hat{p} \operatorname{erfc}\left(\frac{\hat{y}_0}{2\sqrt{\hat{t}}}\right) \quad (5a)$$

$$\hat{q}_L = 2\Delta\hat{p}/\sqrt{\pi\hat{t}} \quad (5b)$$

$$\delta_f = 3.6\sqrt{c_R t} \quad \delta_f = 3.6\sqrt{\hat{t}} \quad (5c)$$

q_L is the fluid loss rate out of the fracture obtained from Eqns. 4 and δ_f the depth into the reservoir to which pore pressure diffusion has occurred.

The leakoff penetration depth is defined as

$$\hat{\delta}_L = \frac{\hat{\kappa}_L \hat{\beta}_v}{2\phi} \int_0^{\hat{t}} \hat{q}_L d\hat{\tau} \quad (6)$$

For q_L defined in Eqn. 5b the resulting leakoff penetration is

$$\delta_L = \frac{2}{\sqrt{\pi}} \frac{\Delta p k_R}{\phi \mu_R} \sqrt{c_R t} \quad \hat{\delta}_L = \frac{2}{\sqrt{\pi}} \frac{\Delta \hat{p} \hat{\kappa}_L \hat{\beta}_v}{\phi} \sqrt{\hat{t}} \quad (7)$$

Influence function solution

Beyond the penetration depths of the leakoff fluid (δ_L) and of the heat transfer (δ_h) the reservoir properties are considered to be constant. The pressure drop ($p_h - p_R$) between the pressure at the larger penetration depth (either δ_L or δ_h) and the reservoir pressure at infinity can be related to the reservoir fluid flow at that depth by an influence function solution:

$$\hat{p}_h - \hat{p}_R = \int_0^{\hat{t}} d\hat{\tau} \int_{\hat{s}_c(\hat{\tau})} \hat{q}_L \hat{\gamma}_f d\hat{s} \quad (8a)$$

$$\gamma_f = \frac{\mu_R}{4\pi k_R (t-\tau)} \exp \left[\frac{-[(x_0-x)^2 + y_0^2]}{4c(t-\tau)} \right] \quad (8b)$$

where γ_f is the fundamental solution to Eqns. 4 for a single instantaneous

source of strength unity, and q_L is the fluid flow at the relevant penetration depth.

Since Eqns. 8 contain two unknowns, $(p_h - p_R)$ and q_L , more information is required to determine reservoir flow. Closure is achieved by including the equations that govern flow within the heat and leakoff penetration zones and which relate fracture quantities to the unknowns of Eqns. 8. Suppose that the leakoff penetration (δ_L) is less than the heat penetration (δ_h) and that both are much smaller than the scale of the fracture ($\delta_h, \delta_L \ll \ell$); then the flow between the fracture and the heat penetration depth is essentially 1D, a function of time only and is specified by D'Arcy's law. Within the leakoff penetration zone the relation is

$$.5\hat{q}_L = -(\hat{C}_L \hat{\mu}_L(\hat{\theta}))^{-1} \frac{\partial \hat{p}}{\partial \hat{y}} \quad (9a)$$

where q_L is the fluid exchange between fracture and reservoir, C_L is a non-dimensional grouping of permeabilities and viscosities, and $\mu_L(\theta)$ is the non-dimensional viscosity of the leakoff fluid. Since the viscosity of typical leakoff fluid (principally water) can change by a factor of 3 or 4 between fracture and reservoir temperatures, the effect of temperature on viscosity can not always be neglected. (In many reservoirs the leakoff layer has little effect on loss and can be neglected.) Integration of Eqn. 9a yields

$$\hat{p}_L = \hat{p}_F - .5\hat{C}_L \bar{\mu}_L \hat{\delta}_L \hat{q}_L \quad (9b)$$

The average viscosity μ_L for the leakoff fluid is

$$\bar{\mu}_L = \frac{1}{\delta_{L0}} \int_0^{\hat{\delta}} \hat{\mu}_L(\hat{\theta}) d\hat{y}, \quad \hat{\mu}_L(\hat{\theta}) = A_L + B_L \hat{\theta}^{C_L} \quad (9c)$$

The constants A_L , B_L , and C_L can be obtained from viscosity data for the leakoff fluid. An identical argument can be made for calculating the flow in the region between the leakoff fluid penetration δ_L and the heat penetration δ_h except that within this zone the relevant viscosities and permeabilities are those related to the reservoir fluid. The governing equations for this region are

$$.5\hat{q}_L = -\hat{\mu}_R(\hat{\theta})^{-1} \frac{\partial \hat{p}}{\partial \hat{y}} \quad (10a)$$

$$\hat{p}_h - \hat{p}_L = -.5g\bar{\mu}_R(\hat{\delta}_h - \hat{\delta}_L)\hat{q}_L, \quad g = \begin{cases} 1 & \hat{\delta}_h - \hat{\delta}_L > 0 \\ 0 & \hat{\delta}_h - \hat{\delta}_L \leq 0 \end{cases} \quad (10b)$$

$$\bar{\mu}_R = \frac{1}{\hat{\delta}_h - \hat{\delta}_L} \int_{\hat{\delta}_L}^{\hat{\delta}_h} \hat{\mu}_R(\hat{\theta}) d\hat{y}, \quad \hat{\mu}_R(\hat{\theta}) = A_R + B_R \hat{\theta}^{C_R} \quad (10c)$$

A_R , B_R , and C_R can be found for reservoir fluid viscosities. The equations derived are valid regardless of the relative values of δ_h and δ_L . However, when $\delta_h < \delta_L$, Eqns. 10 are simply irrelevant. In that case, as shown in Eqn. 10b, $g=0$.

Equations 8, 9b and 10b can be combined to form an expression relating

Δp , the difference between fracture pressure and reservoir pressure, to q_L , the fluid exchange. Thus reservoir flow is defined in terms of fracture quantities only.

$$\Delta \hat{p}(\hat{t}) = .5 [\hat{C}_L \bar{\mu}_L(\hat{t}) \hat{\delta}_L(\hat{t}) + g \bar{\mu}_R(\hat{t}) (\hat{\delta}_h(\hat{t}) - \hat{\delta}_L(\hat{t}))] \int_0^{\hat{t}} \hat{q}_L(\hat{t}) \hat{\gamma}_f(\hat{t}, \hat{\tau}) d\hat{\tau} \quad (11a)$$

$$\hat{\gamma}_f(\hat{t}, \hat{\tau}) = 1/2\sqrt{\pi(\hat{t}-\hat{\tau})} \quad (11b)$$

The time integral can be written as a sum of integrals over intervals Δt , with integrands consisting of an unknown part (τ) and an integrable part $g(\tau)$. If the time increment is small, the integral may be approximated by

$$\int_{t_{n-1}}^{t_n} f(\tau) g(\tau) d\tau \approx f(t_n) \int_{t_{n-1}}^{t_n} g(\tau) d\tau \quad (12)$$

Equations 11a and 6 are discretised using Eqn. 12:

$$\Delta \hat{p}(\hat{t}_N) = .5 [\hat{C}_L \bar{\mu}_L(\hat{t}_N) \hat{\delta}_L(\hat{t}_N) + g \bar{\mu}_R(\hat{t}_N) (\hat{\delta}_h(\hat{t}_N) - \hat{\delta}_L(\hat{t}_N))] \hat{q}_L(\hat{t}_N) = \sum_{n=1}^N \hat{q}_L(\hat{t}_N) \hat{\Gamma}_f(\hat{t}_N, \hat{t}_n) \quad (13a)$$

$$\hat{\Gamma}_f(\hat{t}_N, \hat{t}_n) = \frac{1}{\sqrt{\pi}} [(\hat{t}_N - \hat{t}_{n-1})^{1/2} - (\hat{t}_N - \hat{t}_n)^{1/2}] \quad (13b)$$

$$\hat{\delta}_L(\hat{t}_N) = \frac{\hat{\kappa}_L \hat{\beta}_v}{4\phi} \sum_{n=1}^N (\hat{q}_L(\hat{t}_n) + \hat{q}_L(\hat{t}_{n-1})) \Delta \hat{t}_n \quad (13c)$$

Given the current pressure difference ($\Delta p(t_N)$) and the previous exchange history (q_L for $t < t_N$), the current fluid exchange can be directly calculated from Eqns. 13.

2.2.3 2D Fluid Exchange

The influence function solution for fluid exchange along the 2D fracture is similar to its 1D counterpart, except the effect of fluid exchange must be integrated along the fracture (Cleary et al., 1983). The result, valid for propagating fractures, is

$$\begin{aligned} \Delta \hat{p}(\hat{x}_0, \hat{t}) - .5 [\hat{C}_L \bar{\mu}_L(\hat{x}_0, \hat{t}) \hat{\delta}_L(\hat{x}_0, \hat{t}) \\ + g \bar{\mu}_R(\hat{x}_0, \hat{t}) (\hat{\delta}_h(\hat{x}_0, \hat{t}) - \hat{\delta}_L(\hat{x}_0, \hat{t}))] \hat{q}_L(\hat{x}_0, \hat{t}) \end{aligned} \quad (14a)$$

$$= \int_0^{\hat{t}} d\hat{\tau} \hat{\ell}(\hat{\tau}) \int_{-1}^1 q_L(\eta, \hat{t}) \hat{\gamma}_f(\hat{x}_0, \eta; \hat{t}, \hat{\tau}) d\hat{x}, \quad \eta = \hat{\ell}(\hat{\tau}) \hat{x}$$

where

$$\hat{\gamma}_f(\hat{x}_0, \eta; \hat{t}, \hat{\tau}) = \frac{1}{4\pi(\hat{t}-\hat{\tau})} \exp\left(-\frac{(\hat{x}_0 - \eta)^2}{4(\hat{t}-\hat{\tau})}\right) \quad (14b)$$

The discretisation of the time integral is the same as in the 1D case Eqn. 12. The remaining integral along the fracture is a singular integral that can be solved by a global interpolation scheme which employs Chebyshev polynomials. Valid for all (including singular) kernels K , the standard integration formula is

$$\int_{-1}^1 f(x) K(x_0, x) dx = \frac{\pi}{M} \sum_{k=1}^M \frac{1}{\sqrt{1-s_k^2}} f(s_k) K(x_0, s_k) \quad (15a)$$

$$K(x_0, s_M) = 0.5(K(x_0, s_M) + K(x_0, -s_M)) \quad (15b)$$

$$s_k = -\cos(\pi k/M), \quad k=1, \dots, M \quad (15c)$$

$$s_r = -\cos(\pi(2r-1)/2M), \quad r=1, M \quad (15d)$$

having set $f(s_M) = f(-s_M)$ for closure in Eqn. 15b. Unless K is singular, the integral can be evaluated at any convenient set of x_0 , if its integrand is weighted at the zeroes s_k of the M^{th} order Chebyshev polynomial of the first kind. If K is singular, then it must be evaluated at the zeroes s_r of the $(M-1)^{\text{th}}$ order Chebyshev polynomial. It is also necessary to define a matrix which interpolates from the s_r points to the s_k points since the temperature is needed at the s_k points. A global interpolation matrix using Chebyshev polynomials accomplishes this as follows:

$$A_{rk} = \frac{2}{M} \left(\frac{1}{2} + \sum_{\ell=1}^M T_{\ell}(s_r) T_{\ell}(s_k) \right) \quad (16a)$$

$$T_{\ell}(s) = \cos(\ell \cos^{-1} s) \quad (16b)$$

where the functions $T_{\ell}(s)$ are Chebyshev polynomials of the first kind. Given the accuracy afforded by the stretched grid, local interpolation could probably

be used with equal success. Remembering that the exponential integral function of the first kind is defined as

$$Ei(x) = \int_x^{\infty} \frac{1}{\eta} \exp(-\eta) d\eta \quad (17)$$

the discretised version of Eqns. 14 becomes

$$\begin{aligned} \Delta \hat{p}(s_{rN}, \hat{t}_N) - .5 \sum_{k=1}^M A_{rk} [\hat{C}_L \bar{\mu}_L(s_{kN}, \hat{t}_N) \hat{\delta}_L(s_{kN}, \hat{t}_N) \\ + g \bar{\mu}_R(s_{kN}, \hat{t}_N) (\hat{\delta}_h(s_{kN}, \hat{t}_N) - \hat{\delta}_L(s_{kN}, \hat{t}_N))] \hat{q}_L(s_{kN}, \hat{t}_N) \\ = \frac{\pi}{M} \sum_{n=1}^N \hat{\ell}(\hat{t}_n) \sum_{k=1}^M \sqrt{1-s_k^2} \hat{q}_L(s_k, \hat{t}_n) \hat{f}_f(s_{rN}, s_k; \hat{t}_N, \hat{t}_n) \\ s_{rn} = \hat{\ell}(\hat{t}_n) s_r, \quad s_{kn} = \hat{\ell}(\hat{t}_n) s_k, \quad r=1, M \end{aligned} \quad (18a)$$

$$\hat{f}_f(s_r, s_k; \hat{t}_N, \hat{t}_n) = \frac{1}{4\pi} Ei\left(\frac{(s_r - s_k)^2}{4\sigma}\right) \left| \begin{array}{l} \sigma = \hat{t}_N - \hat{t}_{n-1} \\ \sigma = \hat{t}_N - \hat{t}_n \end{array} \right. \quad (18b)$$

If the pressure difference along the fracture is known, Eqns. 18 represent a system of M equations with M unknowns ($q_L(s_k, t_N)$). When the system is solved at the current time level (t_N), the current value of fluid exchange is found at each s_k point. The procedure is then repeated for the t_{N+1} level.

2.3 Backstress

2.3.1 General Considerations

In addition to being a major determinant of well pumping rates, fluid leakoff causes swelling of the rock adjacent to the fracture which in turn creates a stress normal to the fracture surface called the backstress. This stress, often a significant percentage of the excess pressure, works against hydraulic fracture propagation.

The nature of backstress can best be understood by analogy to the effects of a dislocation in an elastic medium. Fluid loss from the fracture can be thought of as a misfit wedge of material stuck into the reservoir along the fracture up to its tip. A uniform leakoff penetration depth corresponds to a misfit wedge of constant width; such a wedge creates compressive stress increasing toward the tip as $1/r$, the inverse of the distance to the fracture tip. A detailed explanation of the theories of dislocations can be found in Hirth and Lothe (1968); for applications to induced stresses in porous media, see Rice and Cleary (1976).

The stress effect can be modeled by putting a dislocation at each end of the wedge: The solution for the compressive stress at the middle of the wedge is given by

$$\sigma_B = \frac{G\bar{b}}{\pi l(1-\nu)} \quad (19a)$$

where G is the shear modulus, ν the Poisson ratio, and \bar{b} the misfit wedge width. \bar{b} can be deduced from the amount of uniaxial strain the reservoir material undergoes when the pore pressure is increased by Δp . If \bar{b} is replaced by such an expression, the backstress becomes

$$\sigma_B = \frac{2\delta\eta\Delta p}{\pi l(1-\nu)} \quad (19b)$$

where δ is the appropriate penetration depth (see discussion of Eqns. 20 below) and Δp the pressure difference across the layer. η , the dominant poroelastic stress parameter (backstress coefficient) is given by

$$\eta = \frac{2(1-\nu)}{(1-2\nu)} \xi, \quad \xi = 1 - \frac{K}{K_s}, \quad \eta = 0.3 \quad (19c)$$

K and K_s are the bulk moduli of the overall porous matrix and solid constituent, respectively, under drained conditions. Equation 19b is also valid for non-uniform misfit wedges if the right hand side is multiplied by a coefficient which accounts for wedge geometry.

It is useful to separate the backstress into two components, one due to the leakoff layer, and the other to the diffusion of pressure out through the reservoir fluid:

$$\sigma_B = \sigma_{B_L} + \sigma_{B_R} \quad (20a)$$

where,

$$\sigma_{B_L} = \frac{2\delta_L \eta (p_F - p_I)}{\pi k (1-\nu)} \quad (20b)$$

and

$$\sigma_{B_R} = \frac{2b\eta (p_I - p_R)}{l} \sqrt{c_R t} \quad (20c)$$

The pressure differences are the ones across the leakoff ($p_F - p_I$) and reservoir ($p_I - p_R$) regions; δ_L is the leakoff penetration. The diffusion of pressure into the reservoir occurs over a depth proportional to $\sqrt{c_R t}$. b (as distinct from \bar{b} , the misfit wedge width) has been found in this study to be constant (approximately 0.7) for short to medium times. Looking at the two effects separately can be advantageous: For instance, if the leakoff fluid is liquid and the reservoir fluid a gas, the leakoff component dominates because the reservoir diffusivity is small and most of the pressure drop occurs across the leakoff layer; however, in a liquid reservoir the reservoir component dominates because the effective penetration depth of the pressure difference into the reservoir is large relative to leakoff extent.

2.3.2 Reservoir backstress

The reservoir backstress component (as opposed to the leakoff component) can be modelled for more complex fracture conditions (fluid exchange variation, fracture propagation, etc.) by a Green's function method analogous to the one used for fluid exchange. Ignoring the leakoff component, the equations governing axisymmetric deformation in an infinite medium (for which $C=0$) are

$$\sigma_{rr} + \sigma_{\theta\theta} + 2\eta p = C(t) \equiv 0, \quad \hat{\sigma}_{rr} + \hat{\sigma}_{\theta\theta} + 2\eta \hat{p} = 0 \quad (21a)$$

$$\frac{\partial}{\partial r} (r^2 \sigma_{rr}) = -2\eta r p \quad \frac{\partial}{\partial \hat{r}} (\hat{r}^2 \hat{\sigma}_{rr}) = -2\eta \hat{r} \hat{p} \quad (21b)$$

If the equation for an instantaneous line source of fluid (Eqn. 8b) is substituted for the pore pressure, the equations become

$$\hat{\sigma}_{rr} = \frac{\eta \hat{q}_L}{\pi \hat{r}^2} \left(\exp\left(\frac{-\hat{r}^2}{4(\hat{t}-\hat{\tau})}\right) - 1 \right) \quad (22a)$$

$$\hat{\sigma}_{\theta\theta} = \frac{\eta \hat{q}_L}{\pi \hat{r}^2} \left(1 - \left(1 + \frac{\hat{r}^2}{2(\hat{t}-\hat{\tau})} \right) \exp\left(\frac{-\hat{r}^2}{4(\hat{t}-\hat{\tau})}\right) \right) \quad (22b)$$

The equation for stress normal to the fracture can now be found by integrating the effects of all sources:

$$\hat{\sigma}_B = -\hat{\sigma}_{\theta\theta} = \eta \hat{p}_0 - \eta \int_0^{\hat{t}} d\hat{\tau} \int_{-\hat{l}}^{\hat{l}} d\hat{x} \hat{q}_L(\hat{x}, \hat{\tau}) \frac{\partial \hat{\Gamma}_s}{\partial \hat{\tau}}(\hat{x}_0, \hat{x}, \hat{t}, \hat{\tau}) \quad (23a)$$

$$\hat{\Gamma}_s(\hat{x}_0, \hat{x}, \hat{t}, \hat{\tau}) = \frac{1}{4\pi\xi} (\exp(-\xi) - 1) \quad \xi = \frac{(\hat{x}_0 - \hat{x})^2}{4(\hat{t} - \hat{\tau})} \quad (23b)$$

Thus, as time goes to infinity (q_L goes to zero), the backstress achieves its steady state value of ηp_0 .

2.3.3 Discretisation

Although Eqns. 23 show well the structure of the 2D backstress solution, some numerical difficulties arise if the fluid exchange distribution is not exactly compatible with the pressure difference. Such a condition results either from numerical error or from the use of a 1D loss distribution (or any loss distribution other than the 2D solution). The problem is alleviated by replacing the pressure p_0 with Eqn. 8 (with $p_b = p_l$), which consists of fluid loss effects. With the backstress now expressed in terms of fluid loss, the equation is discretised by integrating the resulting influence function while assuming q_L to be constant locally in both time and across each element along the fracture. Such a technique eliminates the need for global interpolation; hence, the numerical difficulties caused by the oscillatory nature of the Chebychev polynomials are circumvented. Also, because the summation is conservative, additive effects incurred in long summation operations are eliminated. The resulting equation is

$$\hat{\sigma}_B(\hat{x}_0, \hat{t}_N) = \eta \sum_{n=1}^N \sum_{k=1}^M \hat{q}_L(\hat{x}(k, n), \hat{t}_n) \hat{\Gamma}_{sf}(\hat{x}_0, \hat{x}(k, n); \hat{t}_N, \hat{t}_n) \quad (24a)$$

$$\hat{\Gamma}_{sf}(\hat{x}_0, \hat{x}; \hat{t}_N, \hat{t}_n) = \frac{2\sqrt{\hat{t}_N - \tau}}{\pi} \left[\frac{1}{\xi} (1 - \exp(-\xi)) + \xi E_i(\xi^2) \right] \begin{vmatrix} \hat{t}_{n-1} \\ \hat{t}_n \end{vmatrix} \begin{vmatrix} \hat{x}(k, n) \\ \hat{x}(k-1, n) \end{vmatrix} \quad (24b)$$

$$\xi = \frac{\hat{x}_0 - \hat{x}(k, n)}{2\sqrt{\hat{t}_n - \tau}}$$

In the 2D model the spatial elements are centered on the sr points and run between adjacent sk points, whereas in the pseudo-2D model the elements are centered on the stationary grid nodes. A useful wellbore backstress approximation can be obtained by substituting the constant pressure solution for 1D loss into Eqn. 23a, integrating the influence function over space and time, substituting the 1D loss expression for p_0 , and combining terms. If a parameter b (determined by comparison with the exact solution) is introduced, this approximation has the same form as Eqn. 20c for short to medium times; however, for long times the backstress remains finite and, depending on the choice of b , converges to a value near to ηp : a b value of .56 produces a backstress of exactly ηp for long times. The equation is

$$\sigma_B = 2b\eta(p_f - p_T) \frac{\sqrt{c_R t}}{l} \left((1 - \exp(-\frac{l^2}{4c_R t})) + \frac{\sqrt{\pi l}}{2\sqrt{c_R t}} \operatorname{erfc}(\frac{l}{2\sqrt{c_R t}}) \right), \quad (25)$$

It should be noted that the poro-induced backstress equations are equally valid for thermal induced backstress, with only minor modification. ηp is replaced by $\alpha \tilde{E} \Delta T$ where α is the thermal expansion coefficient, \tilde{E} is a reservoir modulus, and ΔT the temperature difference between fracture and reservoir. If

the temperature of the fracture is lower than the temperature of the reservoir, the thermal induced backstress will tend to open the fracture rather than close it, as the poro-induced backstress does. Over the time scale of most fracture applications in low to fair permeability reservoirs, the thermal backstresses are second order relative to the poro-induced backstresses. A general discussion for heated fractures appears in Clossmann and Phocas (1978).

2.4. Heat Transfer in the Reservoir

2.4.1 Governing equation

The governing equation for heat transfer in the porous reservoir surrounding a fracture is obtained by applying energy conservation to a differential control volume of reservoir material:

$$\underline{\nabla} \cdot \underline{K}_h \underline{\nabla}(T) - (\rho C)_{L\underline{\nabla}} \cdot (\underline{\nabla}T) = (\rho C)_{SL} \frac{\partial T}{\partial t} \quad (26a)$$

$$\underline{\nabla} \cdot \underline{\nabla}(\hat{\theta}) - \hat{\beta}_v \underline{\nabla} \cdot (\underline{\nabla}\hat{\theta}) = \hat{\kappa}^{-1} \frac{\partial \hat{\theta}}{\partial t} \quad (26b)$$

Eqn. 26a is non-dimensionalised according to the relations presented in Table 1. There are two non-dimensional groupings: κ , a ratio of thermal to fluid diffusivities, and β_v which, in effect, non-dimensionalises velocity. In deriving this equation, the following assumptions were made: equivalent thermal

properties of the leakoff and reservoir fluids; negligible kinetic energy of pore fluid; thermal equilibrium between the rock and pore fluid; and constant "thermal" properties, eg., those properties associated with the heat transfer equation such as thermal conductivity, heat capacity, and density. The convection heat transfer term appears in this and all subsequent equations for completeness; later it will be shown that for most low permeability reservoir applications the effect of convection can be neglected. A fuller discussion of heat transfer in geothermal systems can be found in Cheng (1978).

A word or two should be said about boundary conditions. In typical reservoirs there are discontinuities in thermal properties such as those produced by strata, sand lenses, etc., that could be treated as boundaries to local regions at which governing equations are coupled through boundary conditions. As will be shown below, in typical fracture applications the heat transfer occurs in a region very close to the fracture. Consequently, the solution is not affected by such boundaries and the heat is transferred from (to) the fracture as though the reservoir were a semi-infinite region on each side of the fracture. There are local complications where a fracture crosses a discontinuity (interface) but these will be neglected. The temperature in the fracture must either be specified as a boundary condition or the heat transfer in the reservoir must be found simultaneously with the heat transfer, as described in the section on energy balance in the fracture below. Similar modeling of reservoir-heat transfer has been done by Sinclair (1971).

2.4.2 1D Heat transfer

Special analytical solutions

There are three special analytical solutions to the transient, conduction and convection heat transfer problem that provide substantial physical insight into the problem of heat and mass transfer around fractures. Additionally,

accuracy of more sophisticated modeling schemes may be determined by comparing the model results to these solutions.

When the fracture temperature is constant, the non-dimensional temperature θ varies from 1 at the fracture to 0 at infinity regardless of the variation in actual reservoir temperature. Initially, the non-dimensional temperature throughout the reservoir is zero. Solutions of the heat transfer equation with these boundaries and initial conditions can be found for a constant velocity field and for one proportional to $\frac{1}{\sqrt{t}}$, the latter, being extremely relevant to hydraulic fracturing. The constant velocity solution is

$$\hat{\theta}(\hat{y}_0, \hat{t}) = .5 \left[\operatorname{erfc} \left(\frac{\hat{y}_0 - \hat{\beta}_v \hat{\kappa} \hat{v} \hat{t}}{2\sqrt{\hat{\kappa} \hat{t}}} \right) + \exp(\hat{\beta}_v \hat{y}_0) \operatorname{erfc} \left(\frac{\hat{y}_0 + \hat{\beta}_v \hat{\kappa} \hat{v} \hat{t}}{2\sqrt{\hat{\kappa} \hat{t}}} \right) \right], \quad (27)$$

$v = \text{constant}$

The pure conduction solution is

$$\hat{\theta}_c(\hat{y}_0, \hat{t}) = \operatorname{erfc}(\hat{\eta}), \quad \hat{\eta} = \hat{y}_0 / 2\sqrt{\hat{\kappa} \hat{t}} \quad (28a)$$

where the heat exchange per unit area \hat{h}_L is given by

$$\hat{h}_{Lc} = \frac{-2\partial\hat{\theta}}{\partial\hat{x}} = 2/\sqrt{\pi\hat{\kappa}\hat{t}} \quad (28b)$$

and the thermal penetration by

$$\delta_{hc} = 3.6\sqrt{\kappa t}, \quad \hat{\delta}_{hc} = 3.6\sqrt{\hat{\kappa} \hat{t}} \quad (28c)$$

When the velocity distribution is defined by $\frac{1}{\sqrt{\pi t}}$, the convective heat transfer solution is

$$\hat{\theta}(\hat{y}_0, \hat{t}) = \frac{\text{erfc}(\hat{\eta} - \hat{\beta}_v \sqrt{\hat{\kappa}/\pi})}{1 + \text{erf}(\hat{\beta}_v \sqrt{\hat{\kappa}/\pi})}, \quad \hat{\eta} = \hat{y}_0 / 2\sqrt{\hat{\kappa} \hat{t}} \quad (29a)$$

$$\hat{h}_L = \hat{h}_{L\text{conv.}} + \hat{h}_{L\text{cond.}} = \hat{\beta} \hat{q}_L \hat{\theta} - 2 \frac{\partial \hat{\theta}}{\partial \hat{x}} \quad (29b)$$

$$\hat{h}_L = 2(\hat{\beta}_v \sqrt{\hat{\kappa}} + 1) / \sqrt{\pi \hat{\kappa} \hat{t}} \quad (29c)$$

$$\hat{\delta}_h = 2(B + \hat{\beta}_v \sqrt{\hat{\kappa}/\pi}) \sqrt{\hat{\kappa} \hat{t}}, \quad \text{erfc}(B) = .01(1 + \text{erf}(\hat{\beta}_v \sqrt{\hat{\kappa}/\pi})) \quad (29d)$$

The heat penetration depth, δ_h , is defined as the distance into the reservoir from the fracture to the point where the temperature is .01 of the fracture temperature. Note that the solution for the $\frac{1}{\sqrt{\pi t}}$ velocity field propagates into the reservoir proportional to \sqrt{t} (Eqns. 29d). Remembering that the heat penetration depth for the transient conduction problem (δ_{hc}) also propagates proportional to \sqrt{t} it can be concluded that 1) the penetration depths δ_h and δ_{hc} differ only by a constant at any time, and that 2) such a constant depends on reservoir permeability, fluid viscosity, pressure difference between fracture and reservoir, and the fluid and thermal diffusivities. A

simple relation that determines the extent to which the heat exchange with the reservoir is dominated by convection can be obtained from Eqns. 28b and 29c:

$$\% \text{ convection} = \frac{(\hat{h}_L - \hat{h}_{Lc})}{\hat{h}_L} \times 100 = \frac{\hat{\beta}_v \sqrt{\bar{k}}}{(\hat{\beta}_v \sqrt{\bar{k}} + 1)} \times 100 \quad (30)$$

Variational method

The variational method provides a more general solution than either of the two special analytical solutions in that it provides the temperature distribution in the reservoir as a function of time for arbitrary time histories of fracture temperature and fluid leakoff. It is an approximate solution, however, that assumes a non-spatially varying velocity through the heat penetration zone (later to be seen as a good approximation) and a cubic curve fit between the known temperature at the fracture and the zero temperature at the heat penetration depth δ_h . Beyond δ_h the temperature is assumed to be that of the reservoir. The conduction heat exchange at the fracture is obtained by differentiating θ with respect to y and setting $y=0$.

$$\hat{\theta}(\hat{y}_o, \hat{t}) = \begin{cases} \hat{\theta}(0, \hat{t}) \left(1 + \frac{c\hat{y}_o}{\hat{\delta}_h(\hat{t})}\right) \left(1 - \frac{\hat{y}_o}{\hat{\delta}_h(\hat{t})}\right)^2 & \hat{y}_o \leq \hat{\delta}_h(\hat{t}) \\ 0 & \hat{y}_o > \hat{\delta}_h(\hat{t}) \end{cases} \quad (31a)$$

$$\hat{h}_L(\hat{t}) = \frac{2\hat{\theta}(0, \hat{t})(c-2)}{\hat{\delta}_h(\hat{t})}, \quad 0 < c < 2 \quad (31b)$$

The cubic curve fitting parameter, c , and the heat penetration depth, δ_h , are determined using the variational principle (Ritz analysis)

$$\int_0^{\hat{\delta}_h(\hat{t})} \left[\frac{\partial^2 \hat{\theta}}{\partial \hat{y}^2} - \hat{\beta}_v \hat{v} \frac{\partial \hat{\theta}}{\partial \hat{y}} - \hat{\kappa}^{-1} \frac{\partial \hat{\theta}}{\partial \hat{t}} \right] \partial \hat{\theta} d\hat{y} = 0 \quad (32)$$

Invoking the variational principle results in two coupled non-linear differential equations governing c and δ_h . Numerical investigation has shown that the solution is reasonably insensitive to c , so that any value of c between .25 and .75 provides a good temperature curve fit (See Figure 3.14). Once c has been specified, the equation governing δ_h becomes drastically simplified:

$$\begin{aligned} \hat{\delta}_h(\hat{t})^2 = & \hat{\theta}(0, \hat{t})^{-c_1} [\hat{\kappa} d_1 \int_0^{\hat{t}} \hat{\theta}(0, \hat{\tau})^{c_1} d\hat{\tau} \\ & + \hat{\beta}_v \hat{\kappa} d_2 \int_0^{\hat{t}} \hat{\theta}(0, \hat{\tau})^{c_1} \hat{v}(0, \hat{\tau}) \delta_h(\hat{t}) d\hat{\tau}] \end{aligned} \quad (33a)$$

$$c_1 = \left(\frac{1}{10} + \frac{c}{30} + \frac{c^2}{210} \right) / c_2, \quad c_2 = \left(\frac{1}{15} + \frac{c}{30} + \frac{c^2}{105} \right) \quad (33b)$$

$$d_1 = \left(\frac{2}{3} - \frac{c}{6} + \frac{c^2}{15} \right) / c_2, \quad d_2 = \left(\frac{1}{3} + \frac{c}{15} + \frac{c^2}{30} \right) / c_2 \quad (33c)$$

A quadratic equation for δ_h is easily obtained once the time integrals are approximated through linear or quadratic interpolation.

Influence function method

The most general solution to the transient heat transfer equation (Eqn. 26a) is the influence function solution. It is formally valid for any number of spatial dimensions and takes into account arbitrarily varying fracture temperatures and velocity fields. The convection term of the governing equation $-\nabla \cdot (\beta_v \underline{V} \theta)$ is treated as a heat source and not as part of the differential equation; hence, the differential equation solved is the conduction equation, with convection sources included wherever and whenever convection has occurred. Essentially, the solution is constructed by the superposition of the effects of instantaneous heat sources that are each related to the temperature by the fundamental solution γ_h . For an infinite domain with a single instantaneous heat sources of strength one at position x and time τ the solution of the transient heat conduction equation at x_0 and time t is γ_h (See Eqn. 35b below). Chang et al. (1973) use the analogous Green function superposition method to solve similar heat conduction problems in an anisotropic medium; and Keung and Domolo (1980) apply superposition methods for heat conduction problems with change of phase in arbitrary domains.

The temperature distribution is calculated by "adding up" or integrating the effects of both the conduction sources on the fracture surface and the convection sources throughout the region for all previous time levels up to the current one. The resulting equation is

$$\hat{\theta}(\hat{y}_o, \hat{t}) = \int_0^{\hat{t}} d\hat{\tau} \left[\int_{\hat{S}_c(\hat{\tau})} \hat{h}_L \hat{\gamma}_h d\hat{S} - \int_{\hat{V}_R(\hat{\tau})} \nabla \cdot (\hat{\beta}_v \hat{v} \hat{\theta}) \hat{\gamma}_h d\hat{V} \right] \quad (34)$$

The equation can be changed to a more desirable form by integrating the convection term by parts, exploiting the symmetry of the solution on either side of the fracture, and restricting the reservoir integration to inside the heat

penetration zone, outside the effect of convection is negligible. For one dimensional heat transfer the solution becomes

$$\hat{\theta}(\hat{y}_0, \hat{t}) = \int_0^{\hat{t}} d\hat{\tau} [(\hat{h}_L(\hat{\tau}) + \hat{\beta}_v \hat{q}_L(\hat{\tau})) \hat{\theta}(0, \hat{\tau})] \hat{\gamma}_h(\hat{y}_0, 0; \hat{t}, \hat{\tau}) \quad (35a)$$

$$+ \hat{\beta}_v \int_0^{\hat{\delta}_h(\hat{t})} \hat{v}(\hat{y}, \hat{\tau}) \hat{\theta}(\hat{y}, \hat{\tau}) \frac{\partial}{\partial \hat{y}} [\hat{\gamma}_h(\hat{y}_0, \hat{y}; \hat{t}, \hat{\tau}) + \hat{\gamma}_h(\hat{y}_0, -\hat{y}; \hat{t}, \hat{\tau})] d\hat{y}$$

where

$$\hat{\gamma}_h(\hat{y}_0, \hat{y}; \hat{t}, \hat{\tau}) = \left[\frac{\hat{\kappa}}{4\pi(\hat{t}-\hat{\tau})} \right]^{1/2} \exp\left[\frac{-(\hat{y}_0 - \hat{y})^2}{4\hat{\kappa}(\hat{t}-\hat{\tau})} \right] \quad (35b)$$

The term $(h_L(\tau) + \beta_v q_L(\tau)\theta(0, \tau))$ conveniently represents the non-dimensional energy rate exchange between reservoir and fracture. In order to obtain a solvable relation between energy rate exchange and fracture temperature, the integrals of Eqn. 35a must be discretised.

The spatial integration between the fracture and the heat penetration depth is obtained by approximating the integrand using quadratic interpolation and performing the integration:

$$\int_0^{\hat{\delta}_h(\hat{t}_n)} \hat{f}(\hat{y}) d\hat{y} = \hat{\delta}_h(\hat{t}_n) \sum_{\ell=2}^{NNY-1} w(\ell) \hat{f}(\hat{y}(\ell, n)) \quad (36a)$$

$$w(\ell) = (1, 4, 2, 4, 2, \dots, 4, 1) / 6NE \quad (36b)$$

$$\hat{y}_n = \hat{y}(\ell, n) = (\ell-1) \hat{\delta}_h(\hat{t}_n) / NNY, \quad \hat{y}_{0N} = (\ell-1) \hat{\delta}_h(\hat{t}_N) \quad (36c)$$

w is the weighting function of the integration and y_n are the positions at which the integrand is to be evaluated. When these approximations are substituted into Eqn. 35a, the result is a discretised equation with unknown reservoir temperatures at each weighting location y_N and an unknown heat exchange h_L .

$$\hat{\theta}(\hat{y}_{0N}, \hat{t}_N) = \sum_{n=1}^N [(\hat{h}_L(\hat{t}_n) + \hat{\beta}_v \hat{q}_L(\hat{t}_n) \hat{\theta}(0, \hat{t}_n)) \hat{f}_h(\hat{y}_{0N}, 0; \hat{t}_N, \hat{t}_n)] \quad (37a)$$

$$+ \hat{\beta}_v \hat{\delta}_h(\hat{t}_n) \sum_{\ell=2}^{NNY-1} w(\ell) \hat{v}(\hat{y}_0, \hat{t}_n) \hat{\theta}(\hat{y}_n, \hat{t}_n) \Delta \hat{f}_h(\hat{y}_{0N}, \hat{y}_n; \hat{t}_N, \hat{t}_n)]$$

$$\hat{y} = 1, NNY$$

$$\hat{f}_h(\hat{y}_0, 0; \hat{t}_N, \hat{t}_n) = \left[\left(\frac{\hat{\kappa}\sigma}{\pi} \right)^{1/2} \exp\left(\frac{-\hat{y}_0}{4\hat{\kappa}\sigma}\right) + \frac{\hat{y}_0}{2} \operatorname{erf}\left(\frac{\hat{y}_0}{2\sqrt{\hat{\kappa}\sigma}}\right) \right] \Bigg|_{\sigma = \hat{t}_N - \hat{t}_n}^{\sigma = \hat{t}_N - \hat{t}_{n-1}} \quad (37b)$$

$$\Delta \hat{f}_h(\hat{y}_0, \hat{y}; \hat{t}_N, \hat{t}_n) = 1/2 \left[\operatorname{erf}\left(\frac{\hat{y}_0 - \hat{y}}{2\sqrt{\hat{\kappa}\sigma}}\right) - \operatorname{erf}\left(\frac{\hat{y}_0 + \hat{y}}{2\sqrt{\hat{\kappa}\sigma}}\right) \right] \Bigg|_{\sigma = \hat{t}_N - \hat{t}_n}^{\sigma = \hat{t}_N - \hat{t}_{n-1}} \quad (37c)$$

By applying Eqn. 37a to each weighting location ($y_0 = y_N$) and to the fracture ($y_0 = 0$), a set of equations can thus be obtained and solved at each new time level (t_N), for the unknown reservoir temperatures and the conduction heat exchange. δ_h need only be roughly approximated at each time level (such as by Eqns. 33) since there are no contributions from integrating beyond the heat penetration depth, δ_h , and only very small contributions in approaching δ_h . If convection can be neglected, Eqn. 37a reduces to the very simple form, similar

to that for 1D fluid exchange:

$$\hat{\theta}(\hat{t}_N) = \sum_{n=1}^N \hat{h}_L(\hat{t}_n) \hat{\Gamma}_h(\hat{t}_N, \hat{t}_n), \quad (38a)$$

$$\hat{\Gamma}_h(\hat{t}_N, \hat{t}_n) = \left(\frac{\hat{\kappa}_\sigma}{\pi}\right)^{1/2} \begin{cases} \sigma = \hat{t}_N - \hat{t}_{n-1} \\ \sigma = \hat{t}_N - \hat{t}_n \end{cases} \quad (38b)$$

2.5 Energy balance in the fracture

No matter how modeling of reservoir fluid flow and heat transfer is approached, if the fluid and heat exchange between fracture and reservoir are unknown, then either the pressure and temperature differences along the fracture must be specified, at least incrementally, or additional equations provided that are to be solved simultaneously with the reservoir equations. It is assumed that pressure differences along the fracture can be supplied by fracture propagation models such as P3DH or the lumped model. However, since temperature along the fracture is unknown, an equation governing heat transfer in the fracture must be included.

As shown in Figures 2.3b and c, the fracture can be divided into I elements. Each element has a volume (Vol) and an area (A). $Q_{rel}(i+1, t_N)$ is the flow rate from the i^{th} element into the $(i+1)^{\text{th}}$ element and $Q_{rel}(i, t_N)$, from the $(i-1)^{\text{th}}$ into the i^{th} element. It is assumed that the fracture propagation model can supply volume, area, and flow rates for the set of I elements. Two different kinds of grids can be used: a large stationary grid covering the final

expected fracture length, or a grid the length of the fracture which grows as the fracture does. If the grid is fixed, then Q_{rel} is the velocity of the fluid flowing within the fracture; if the grid grows with the fracture, Q_{rel} is equal to the difference between the fluid velocity and the fracture propagation rate. For the fixed grid (Figure 2.3c), new nodes must be activated as the fracture tip grows over them, and quantities such as pressure differences must be extracted from the fracture propagation model grid; for the propagating grid, values at previous time levels (hence different locations) must be interpolated then assigned to the new element locations.

When heat transfer in the fracture is principally determined by convection, energy exchange with the reservoir, and the difference in temperature between the wellbore and the reservoir at infinity, the energy balance for the i^{th} fracture element can be written

$$\left(\begin{array}{l} \Delta \text{energy/time} \\ \text{in the } k\text{th} \\ \text{fracture element} \end{array} \right) = \left(\begin{array}{l} \Delta \text{energy/time flowing} \\ \text{into the } k\text{th element} \\ \text{from other fracture} \\ \text{elements} \end{array} \right) - \left(\begin{array}{l} \Delta \text{energy/time} \\ \text{lost to the} \\ \text{reservoir} \end{array} \right) \quad (39a)$$

$$\begin{aligned} \text{or } \frac{d}{dt} [\hat{Vol}(i, \hat{t}_N) \hat{\theta}(\hat{x}_i, \hat{t}_N)] \\ = \hat{\kappa}_L \hat{\beta}_V [0.5(\hat{\theta}(\hat{x}_{i-1}, \hat{t}_N) + \hat{\theta}(\hat{x}_i, \hat{t}_N)) \hat{Q}_{rel}(i, \hat{t}_N) \\ - 0.5(\hat{\theta}(\hat{x}_i, \hat{t}_N) + \hat{\theta}(\hat{x}_{i+1}, \hat{t}_N)) \hat{Q}_{rel}(i+1, \hat{t}_N)] \\ - \hat{\kappa}_F \hat{A}(i, \hat{t}_N) [\hat{h}_L(\hat{x}_i, \hat{t}_N) + \hat{\beta}_V \hat{q}_L(\hat{x}_i, \hat{t}_N) \hat{\theta}(\hat{x}_i, \hat{t}_N)] \end{aligned} \quad (39b)$$

If both the fracture-reservoir interactions and the quantities to be determined by a fracture propagation model are specified, Eqns. 39 can be discretised and then solved to obtain the current temperature of each fracture element. The

time derivative appearing in Eqns. 39 can be written in terms the current temperature and the temperature at the last two previous time levels:

$$\left. \frac{df}{dt} \right|_{t_n} = \frac{1}{\Delta t_n (dtr^2 - dtr)} [(dtr^2 - 1)f_n - dtr^2 f_{n-1} + f_{n-2}] + O(\Delta t^2), \quad (40)$$

$$dtr = \frac{(t_n - t_{n-2})}{(t_n - t_{n-1})}$$

This expression, known as a three point backward difference operator, is accurate to the second order in Δt_N . If Eqn. 40 is substituted into Eqns. 39 a matrix expression of the following form is obtained:

$$\underline{a} \underline{\theta} = \underline{r} \quad (41a)$$

$$\text{or} \quad a(i, i-1) \hat{\theta}(\hat{x}_{i-1}, \hat{t}_N) + a(i, i) \hat{\theta}(\hat{x}_i, \hat{t}_N) + a(i, i+1) \hat{\theta}(\hat{x}_{i+1}, \hat{t}_N) = r(i), \quad i = 2, I-1 \quad (41b)$$

$$r(i) = (dtr^2 \hat{Vol}(i, \hat{t}_{N-1}) \hat{\theta}(i, \hat{t}_{N-1}) - \hat{Vol}(i, \hat{t}_{N-2}) \hat{\theta}(i, \hat{t}_{N-2})) / \Delta \hat{t}_N (dtr^2 - dtr) - \hat{\kappa}_F \hat{A}(i, \hat{t}_N) \hat{h}_L(\hat{x}_i, \hat{t}_N) \quad (41c)$$

$$a(i, i-1) = -.5 \hat{\kappa}_L \hat{\beta}_v \hat{Q}_{rel}(i, \hat{t}_N) \quad (41d)$$

$$a(i, i+1) = .5 \hat{\kappa}_L \hat{\beta}_v \hat{Q}_{rel}(i+1, \hat{t}_N) \quad (41e)$$

$$a(i, i) = .5 \hat{\kappa}_L \hat{\beta}_v (\hat{Q}_{rel}(i+1, \hat{t}_N) - \hat{Q}_{rel}(i, \hat{t}_N)) + \hat{\kappa}_F (\hat{A}(i, \hat{t}_N) \hat{q}_L(\hat{x}_i, \hat{t}_N) + \frac{(dtr^2 - 1) \hat{Vol}(i, \hat{t}_N)}{\Delta \hat{t}_N (dtr^2 - dtr)}) \quad (41f)$$

The boundary conditions required to complete Eqn. 41a are

$$\hat{\theta}(0, \hat{t}) = \hat{\theta}_w(\hat{t}) \quad (42a)$$

at the wellbore and

$$\hat{\theta}(\hat{x}_I, \hat{t}_N) = \hat{\theta}_R, \quad \text{or} \quad \hat{\theta}(\hat{x}_I, \hat{t}_N) = \hat{\theta}(\hat{x}_{I-1}, \hat{t}_N) \quad (42b)$$

at the fracture tip. It is suspected that for most propagating fractures both conditions stated in Eqns. 42 are satisfied, therefore we assume either condition will suffice. Note that in order to solve Eqn. 41a it is only necessary to know relevant quantities back two time levels and not their entire previous history. Also, the matrix \underline{a} is tridiagonal; hence, the computational cost is much less than for the a full matrix case.

2.6 Production

2.6.1 2D Drainage Model

A fracture that has been created and propped, and is now being produced, can be modeled by simultaneously considering flow in the reservoir and in the fracture. Within the fracture, the flow is described by mass conservation:

$$\frac{\partial}{\partial x_0}(\rho Q) + \rho H q_L = \frac{\partial}{\partial t}(\rho A_c) = 0 \quad (43)$$

where H is the height of the reservoir, and A_c the cross-sectional area of the fracture; fluid compressibility in the fracture is neglected. Q , the volume flowrate along the fracture, is written in terms of the pressure drop along the fracture through D'Arcy's law:

$$Q = -A_c \frac{K_F}{\mu_F} \frac{\partial p}{\partial x_0} \quad (44)$$

where K_F and μ_F are the fracture permeability and viscosity, respectively. Substituting this expression into Eqn. 43 yields

$$\frac{\partial}{\partial x_0} \left(\frac{A_c K_F}{\mu_F} \frac{\partial p}{\partial x} \right) + H q_L = 0 \quad (45a)$$

This equation can be integrated:

$$\frac{-A C K_F}{\mu_F} \frac{\partial p}{\partial x_0} \Big|_{x_0} + \int_{x_0}^{\ell} H q_L dx = 0 \quad (45b)$$

The pressure is eliminated by substituting the expression for pressure written in terms of 2D fluid exchange (Eqn. (8) with $p_h = p_F$) and differentiating. An expression with only one unknown, q_L , is produced:

$$\frac{A C K_F}{\mu_F} \int_0^t d\tau \int_{-\ell}^{\ell} dx q_L \frac{\partial \Gamma_f}{\partial x} (x_0, x; t, \tau) + \int_{x_0}^{\ell} H q_L dx = 0 \quad (46a)$$

A boundary condition at the wellbore must be supplied: Either the drawdown pressure, given by

$$p_w(t) = \int_0^t d\tau \int_{-\ell}^{\ell} dx q_L \Gamma_f(0, x; t, \tau) \quad (46b)$$

can be specified, or the wellbore flowrate

$$\dot{Q}_w(t) = 2 \int_0^{\ell} H q_L dx \quad (46c)$$

Given one, the other can be determined from the fluid exchange once the problem is solved.

2.6.2 Discretisation

The three above equations are non-dimensionalised and then discretised on a Chebychev grid in the same fashion as in the case of 2D fluid loss (Eqns. 18). The resulting equations are

$$\frac{\hat{C}_F}{4M} \sum_{n=1}^N \sum_{k=1}^M \sqrt{1-s_k^2} \hat{q}_L(s_k, \hat{t}_N) \hat{\Gamma}_P(s_r, s_k; \hat{t}_N, \hat{t}_n) \quad (47a)$$

$$+ \frac{1}{\hat{A}_c(s_r)} \sum_{k=r}^M \hat{q}_L(s_k, \hat{t}_N) \hat{A}_{res}(s_k) = 0, \quad r = 2, M$$

$$\hat{\Gamma}_P(s_r, s_k; \hat{t}_N, \hat{t}_n) = \frac{\exp\left[-\frac{(s_r - s_k)^2}{4\sigma}\right]}{s_r - s_k} \begin{cases} \sigma = \hat{t}_N - \hat{t}_{n-1} \\ \sigma = \hat{t}_N - \hat{t}_n \end{cases} \quad (47b)$$

$$\hat{Q}_w(\hat{t}_N) = 2 \sum_{k=1}^M \hat{q}_L(s_k, \hat{t}_N) \hat{A}_{res}(s_k) \quad (47c)$$

$$\hat{P}_w(\hat{t}_N) = \frac{\hat{l}}{4M} \sum_{n=1}^N \sum_{k=1}^M \sqrt{1-s_k^2} \hat{q}_L(s_k, \hat{t}_N) \hat{\Gamma}_F(0, s_k; \hat{t}_N, \hat{t}_n) \quad (47d)$$

When multiplied by the width and divided by the length of the fracture, the

fracture coefficient C_F is equal to the fracture conductivity. Note that this model is valid for fractures of varying geometry, and for fractures that have grown out of zone. It is also valid for both short and long time drainage periods.

3 Results

3.1 Introduction

The results section is divided into subsections on fluid loss, backstress, heat transfer, and well production. In each subsection, model performance is evaluated and physical insights are discussed. The fracture propagation data and the properties of oil and gas reservoirs, required as input for the models, are described below. Because the figures so concisely present and summarise our findings, they are used as the basis for discussion; this section is written to bring attention to the most important points shown. It is hoped that the reader will take additional time to study the figures and note those things of interest not explicitly discussed here.

Fracture propagation data

At the time of this study it was not possible to run the fluid loss, fracture temperature, and backstress models simultaneously with a fracture propagation model. Instead the required fracture growth and wellbore pressure histories were generated with a lumped fracture propagation model, neglecting the fluid loss, heat transfer and backstress effects. Although the influence of these effects on fracture propagation has not been taken into account, this approach provides the basis for the evaluation and comparison of model performance and it allows qualitative insight into the nature of fluid loss, fracture temperature, and backstress for propagating fractures.

Summarised in Table 4 are the four fracture propagation and wellbore pressure histories generated by the lumped fracture propagation programs. One history was obtained for constant wellbore pressure and three for a constant pumping rate into fractures with different levels of confinement. Since fluid loss was not taken into account, the prescribed wellbore flowrate actually corresponds to the volume rate of growth of the fracture. In the models

developed, the wellbore flowrate is the sum of the total fluid loss rate and the volume rate of fracture growth as predicted by the propagation model. A small subroutine (mascon) which conserves mass in the fracture was implemented, in order to recalculate the wellbore flowrate and to calculate flowrates along the fracture, taking into account the lost fluid.

Oil and gas reservoirs

Two sets of reservoir parameters were chosen for the study: one corresponds to a oil reservoir, the other to a gas (Tables 2a and 2b). Although these reservoirs will be referred to from time to time as 'typical' reservoirs, the author acknowledges that no such thing exists. Some effort has been made, however, to choose common values of reservoir properties, as opposed to extreme ones. Extreme properties might provide interesting numerical results, but would have little relevance to the reservoirs most frequently encountered.

3.2 Reservoir fluid flow

Error due to temporal discretisation of the influence integral

For a constant pressure difference, Figure 3.1 compares the exact 1D loss rate to the 1D single fluid influence function solution (Eqn. 13a). Discrepancies occur only for small times: At the first time step the error is about 8%; by the second it has fallen off to about 4% (2 min.); and by ten minutes the error is less than 1%. Even though q_L is considered constant over Δt in the temporal discretisation (Eqn. 12) when it clearly is not, especially at short times, the resulting error is acceptably small for almost all applications.

Lumped versus pseudo-2D model predictions of fluid loss

Figures 3.2 compare predictions of total fluid loss made by the lumped and the pseudo-2D models for propagating fractures. For all three cases considered (constant fracture pressure, constant wellbore pressure, constant volume growth rate) the deviation is small, less than 6%; the results are almost

identical when a self-similar pressure distribution is used (Figures 3.2b and c). Predictions are most disparate when a constant pressure difference is specified along the fracture (Figure 3.2a). The area averaging technique of the lumped model can really only be evaluated when the fracture pressure is kept constant, since any other pressure distribution confounds the result: The lower fracture tip pressure of the self-similar distribution (Figure 2.3e) tends to reduce the rapid variation in the loss distribution and make more accurate the averaged loss approximation used in the lumped model.

Total loss in oil and gas reservoirs

Given identical fracture pressure and propagation histories, the total loss into oil and gas reservoirs need not be as similar as it is in Figure 3.3. This result can mostly be explained by a fortuitous choice of parameters; however, mitigating reservoir conditions in part explain the tendency toward similar results. For instance, the permeabilities of gas reservoirs, generally much lower than those of oil, can produce a greater resistance to leakoff in the leakoff penetration zone and thus can compensate for the lack of resistance to leakoff otherwise found in the gas reservoir.

Fracture Efficiency

The standard definition of the fracture efficiency η_T is fracture volume divided by total pumped volume. Fracture efficiency can also be defined as the fracture volume opposite the reservoir divided by the total pumped fluid η_R . The latter definition has the advantage of being a more realistic description in that it treats any volume of fracture which has grown out of zone for what it really is: lost volume. Figures 3.4 illustrate these definitions of fracture efficiency. The total efficiencies (30% average) run almost twice as high as the reservoir efficiencies (15% average) after 100 minutes. For the specified fracture growth rate cases, fracture efficiencies decrease through time. This is caused by an overall decrease in fracture pressure during the fracturing history which

results in thin fractures with small volumes. If constant pressure is specified the total efficiency increases through time. In this case the higher pressure causes a wider fracture width resulting in a greater volume. The oil reservoir efficiencies are about 5% higher than those for the gas. This is consistent with Figure 3.3, which shows lower losses to the oil than to the gas reservoir.

Single and two fluid models

In some but not all reservoirs it is necessary to take into account the effect of the leakoff penetration layer in order to obtain accurate estimates of loss. Figure 3.5a shows the total loss in an oil reservoir for single and two fluid models. The single fluid model assumes that the leakoff layer has the same properties as the reservoir proper, whereas the two fluid model takes into account the differences in viscosity and permeability between the two zones. The single and two fluid models predict almost identical loss rates: in both models the stiffness of the oil reservoir provides almost all of the resistance to loss.

As shown in Figure 3.5b, the situation is much different for a gas reservoir. The single fluid model predicts almost 6 times more loss than the two fluid model (for the typical gas reservoir $C_L = 14$). The gas in the reservoir is very compliant (compressible) and tends to make the reservoir much less resistant to leakoff than an oil reservoir. Consequently, resistance to loss in the leakoff zone is the dominant effect. Figure 3.5b indicates that leakoff cannot be modeled accurately without taking into account the leakoff zone.

Figure 3.6 essentially conveys the same information as Figure 3.5b except loss is expressed in terms of 1D loss rate (q_L) instead of total loss (Q_L) for a propagating fracture. The magnitude of the total loss depends on fracture propagation history as well as pressure difference, whereas the 1D loss rate is independent of the fracture propagation and depends only on the pressure difference (both, of course, depend on reservoir and leakoff zone properties).

Therefore, the loss information provided in Figure 3.6 is independent of any particular fracture propagation history.

2D fluid loss

Comparisons of 2D and pseudo 2D loss for a 50 foot stationary fracture in an oil reservoir are made in Figure 3.7a. A constant pressure along the fracture is assumed. Loss rates for the two models nearly coincide, except over the last 5 ft or so of the fracture. In this region, only the 2D solution can pick up the high loss due to the curving (reservoir) flow pattern near the fracture tip. Note also that the effect of the tip has propagated only half the distance from the fracture tip to the wellbore in 100 minutes. Even for a short fracture such as this one the loss along most of the fracture is unaffected by the flow conditions at the fracture tip, at least for the time periods required for hydraulic fracturing.

It is difficult for most numerical techniques to determine a solution which behaves so differently in two regions. In the case of 2D loss, the solution along the fracture differs radically from the solution at the tip. It resembles a boundary layer problem for which the standard technique is to break the problem into an inner region where the solution varies rapidly, and an outer region where the solution varies slowly. Even though such a technique often reduces computational demands, it requires the two solutions to be patched together which can lead to some inaccuracy. Our technique finds the solution everywhere at once, on a Chebychev grid, which provides a high concentration of grid nodes at the fracture tip. Because the singularity occurs over such a small region near the tip, a large number of Chebychev points must be used. For the 50 ft stationary fracture shown in Figure 3.7a 50 grid nodes were required. If an insufficient number of grid nodes is taken, a most unsatisfactory pathology develops. In attempting to capture the singularity, the solution underestimates the loss along the region of fracture length just before the

fracture tip and bulges out near the wellbore. If the time step is small enough, the pathology will develop for any number of grid nodes: As the time duration becomes small the singularity becomes more localised, thus requiring a greater grid node density for resolution. In the case of propagating fractures, this pathology develops even when a sufficient number of grid nodes is used initially: As the fracture grows the singular loss region covers a smaller and smaller percentage of the total fracture length. Since fracture length is determined by elapsed time, taking a larger time step just exacerbates the problem by creating a longer fracture. Unfortunately, this pathology develops for the time and growth scales of hydraulic fracturing. There are two solutions for the problem: Either the number of grid nodes must be increased initially, in order that there be enough to resolve the singularity at later times, when the fracture is longer; or remeshing must be done from time to time in order to increase the number of grid nodes as the fracture grows. Neither of these solutions were attempted in the present study. The former was computationally too intensive and the latter was beyond the scope of the study. Instead, we studied a slower growing fracture, one that grows from 50 ft to 200 ft over 100 minutes. All the important characteristics of 2D loss and backstress can be understood from studying this case, even given the slower growth rate.

Figure 3.7b compares 2D and pseudo-2D loss for propagating fractures. The 2D loss has essentially the same character here as it does for the stationary fracture, except there is higher loss near the fracture tip. This occurs because the propagating fracture is continually breaking into new reservoir where there has been no previous loss: in this region, the loss rate is higher. The pseudo-2D loss captures the same effect, which appears as a stepwise increase in loss near the fracture tip. Each step corresponds to the length over which the fracture has grown at previous times, and can be thought of as an artifact of the fracture growth discretisation. The pseudo-2D model slightly

underestimates but otherwise tracks the loss predicted by the 2D model fairly well.

2D loss corresponding to constant and self-similar fracture pressure distributions are compared in Figure 3.8. Firstly, since the variation in pressure along the fracture occurs only in the excess pressure (order 50 psi) which is a small portion of the total pressure difference that causes fluid leakoff (order 700 psi), one would expect any difference in loss distributions to be relatively small. Secondly, since the self-similar pressure distribution differs from the constant distribution mostly near the fracture tip (see Figure 2.3e), and the diffusion time scale is small compared to the fracture growth scale, the solutions should differ only near the fracture tip. This behavior can be observed in Figure 3.8. At the wellbore, where the pressures are equal, the loss rates are similar. The effect of the differing pressure out along the fracture has not had the time to diffuse into the region near the wellbore. The solutions are also similar at the fracture tip because the finite pressure in both cases causes the singularity in the loss there. It is only in between that the solutions differ, and the difference is minor because the change in pressure that drives the loss is small when the variation in excess pressure along the fracture is taken into account, compared with the total pressure difference that drives fluid loss.

3.3 Backstress

Wellbore backstress

Wellbore backstresses calculated for an oil reservoir are compared in Figure 3.9a. When based on fluid loss occurring over the vertical height of the oil reservoir, the wellbore backstress prediction is much higher (65 psi in after 100 minutes) than when based on fluid loss over the length of the propagating fracture (4 psi after 100 minutes). This result can be explained easily in terms of the misfit wedge concept. The equivalent misfit wedge for the reservoir

height model has a length equal to the reservoir half-height and a thickness that increases by the square root time. The wedge width in the vicinity of the wellbore is the same for the fracture length model; however, its' wedge length equals the fracture length which is typically much larger than the reservoir half-height. Since the backstress depends inversely on the length scale, the fracture length model should predict a smaller wellbore backstress than the reservoir height model. The magnitude of the difference depends on how fast the fracture propagates: In this case the fracture propagation rate is so rapid that the wellbore backstress is almost completely determined by the reservoir height contribution.

The numerical and the approximate square root calculations of wellbore backstress compare very well for the reservoir height model over the 100 minute period. Of course, the two will eventually diverge since the square root approximation is unbounded in time, whereas the long time upper limit of the backstress is ηp . The comparison is not quite as good for the fracture length model, although the square root approximation captures the trend and reasonably estimates the magnitude.

The square root and influence function approximations are compared to the numerical calculation for longer times in Figure 3.9b. All three predict similar wellbore backstresses for the first 100 minutes. After that, the square root approximation increases faster than the numerical result, for the reason discussed above. The influence function approximation follows the numerical solution longer, and for long time converges to a finite value $.7/.56$ times as great. This occurs because the curve fitting coefficient b was chosen to be $.7$ for the best fit over short to medium times. When b is $.56$, the influence function approximation will converge to the correct long time solution, but the short time approximation will be less accurate.

In oil reservoir, the contribution of the leakoff zone to the backstress is

less than 1%. The equivalent misfit wedge width is on the order of the pressure penetration depth, which is much greater than the leakoff penetration depth. In the gas reservoir, the wellbore backstress based on reservoir height is about a third as large as in the oil reservoir (Figure 3.10). After 100 minutes the backstress is 22 psi in the gas reservoir compared with 65 psi in the oil reservoir. The equivalent misfit wedge for the reservoir component in the gas reservoir is much smaller than in the oil reservoir; consequently, the leakoff component becomes important. In fact, the backstress due to leakoff (12 psi after 100 minutes) is larger than the backstress due to the reservoir component (8 psi after 100 minutes).

2D backstress

The 2D and pseudo-2D backstress results, shown in Figures 3.11, can best be understood in terms of the misfit wedge analogy. Consider the 2D and pseudo-2D backstress distributions for a stationary fracture presented in Figure 3.11a. For 2D loss at short times (5 min), the elliptical shape of the pressure penetration region can be approximated by a rectangle; the resulting backstress resembles that generated by a misfit wedge of constant width. The backstress is lowest at the wellbore and increases inversely with the distance to the fracture tip (r). For longer times (40, 100 minutes), the elliptical shape of the penetration region must be considered. The corresponding misfit wedge narrows out towards the fracture tip, producing a smaller backstress in the tip region than the rectangular wedge.

In the case of pseudo-2D loss, the constant loss rate produces a different wedge shape out along the fracture. Where for short times a singular loss (2D) produces an equivalent misfit wedge of approximately rectangular shape, constant loss (pseudo-2D) along the fracture corresponds to an equivalent wedge of negligible width at the fracture tip. As shown in Figure 3.11a, a misfit wedge of this shape produces a backstress distribution that decreases near the

fracture tip. At the wellbore, where the effect of the fracture tip is minimal, the 2D and pseudo 2D losses produce similar wedge widths so that the backstresses there are practically identical. Out toward the fracture tip, the 2D backstress increases because the equivalent misfit wedge is approximately rectangular, or at least elliptical. The pseudo-2D backstress follows the 2D for some distance out along the fracture where wedge widths are similar, whereas further out, the pseudo-2D width rapidly falls to zero, causing the stress also to fall off.

The backstress distribution for a propagating fracture (Figure 3.11b) differs from the stationary fracture in three important ways. Firstly, since it not only depends on misfit wedge width at the wellbore, but also on the current length of the fracture, the wellbore value does not increase with square root time. Secondly, there is a dip in the backstress before the tip of the fracture. Out towards the tip of the propagating fracture, the misfit wedge width narrows much more. There, penetration is always small in extent because loss duration is so short. Thirdly, the increase of backstress near the fracture tip is sharp and localised. Due to the low penetration, the backstress tends to decrease as the fracture tip is approached; however, some local region near the tip can always be found where the material misfit produces a sharp increase in the stress. The narrower the wedge width, the more localised the high stress will be. If an initial length of zero rather than 50 feet is used, the backstress does not bulge, instead it decreases monotonically out along the fracture, except at the fracture tip where the localised effect of the material misfit dominates.

2D and pseudo-2D backstresses are compared in Figure 3.11c for a propagating fracture. Note that up to 100 feet there is little disparity between the 2D and pseudo-2D results. After this point the pseudo-2D begins to oscillate widely about the 2D predictions. To understand the oscillations consider what happens as the fracture grows through one time step. After the

first time step the backstress distribution is similar to that of a stationary fracture (Figure 3.11a). On the next time step the fracture has grown, and if no previous loss has been taken into account, the backstress will again assume the same shape except the distribution will be stretched over the new fracture length. If the backstress of the previous time level is now superposed on the backstresses due to current loss, taking into account diffusion effects occurring over the time step, a dip will appear in the resulting backstress distribution at the previous position of the fracture tip. As the fracture grows further, the same interpretation can be repeatedly applied to explain the fluctuations down the fracture. Because of diffusion, the ones from early time steps become less noticeable. In fact, as shown in Figure 3.11c, the pseudo-2d solution matches the 2D solution very well out over two-thirds of the fracture, where diffusion has been given time to smooth the contributions of the early time steps. Along the fracture near the tip however, the tip effects from previous time levels remain pronounced. Thus only in an averaged sense can the pseudo-2D method be thought of as useful in predicting backstress near the fracture tip. At the tip, of course, only the 2D method accurately predicts backstress.

2D backstresses for constant and self-similar pressure distributions are similar in the wellbore region and at the fracture tip; some deviation occurs in the region near the fracture tip where there is the greatest disparity between the constant and the self-similar pressure distributions (Figure 3.12). Since the similarity of the two predictions depends on fluid loss, the reader is referred to the discussion of Figure 3.8, where fluid losses for these two distributions are shown.

3.4 Heat transfer

Comparison of 1D reservoir heat transfer solutions

Exact (for constant velocity), variational and influence functions solutions are compared in Figure 3.13 for the extreme case where convection accounts for 88% of the heat exchange between fracture and reservoir. The average error in temperature is 15% for the variational solution ($c=0.25$), and 6 and 13%, respectively, for influence functions solutions with 7 and 3 reservoir nodes. The influence function solutions predict more accurate results, but at the cost of having to integrate out into the reservoir. For typical reservoirs, where convection accounts for less than 15% of the heat exchange, the error associated with either method is small, less than 6 or 7%.

Sensitivity of variational solution to c

Although c should be determined by variational analysis (Section 2.3.1b), the error in reservoir temperature is relatively insensitive to variation in c , as is shown in Figure 3.14. Therefore, reasonably good estimates of temperature can be obtained by choosing any value of c between 0.25 and 0.75. When greater accuracy is required, c can be estimated from κ and β_v for any specified reservoir and pressure difference.

Lumped and pseudo-2D predictions of average fracture temperature

For a propagating fracture, average fracture temperatures predicted from lumped and 2D models differ at most by 3% (Figure 3.15). If small enough time steps were taken, and if the fracture was grown from zero initial volume, the fracture and wellbore temperatures would be equal initially. Within a short time, the fracture temperature would rise to the temperature range shown in Figures 3.15, as heat from the reservoir passed into the fracture. For these examples, the time step size and the initial non-zero fracture volume prevent the resolution of this transient.

In Figure 3.16, the lumped model predicts small variation in average fracture temperature (at most 4%) for 4 different fracture growth histories in which wellbore pumping rates vary from 15 to 22 bbl/minute. In two important determinants of fracture temperature, wellbore pumping rate and fracture surface to volume ratio the fractures considered do not differ greatly; hence, this result should not be thought of as general.

Variation of temperature along the fracture

Fracture temperature profiles for several fractures grown to final lengths between 1000 and 1500 feet in oil and gas reservoirs are presented in Figures 3.17. , For the fracturing periods considered (up to 100 minutes), the temperature of the fracture fluid is indistinguishable from the reservoir temperature by 700 ft down the fracture. Although it cannot be said that the temperatures along the fractures have reached steady state, our work has shown that after some time the temperature distributions along most fractures stabilise; the temperature distributions presented at 100 minutes are not far from stabilised profiles. Pumping rate and the fracture area to volume ratio determine the temperature distributions along the fracture for the various fracture cases studied. Note for the gas reservoir in Figure 3.17b, reservoir temperature is achieved by 400 feet down the fracture; whereas in Figure 3.17d, it is not until 700 feet that the reservoir value is reached.

3.5 Production

The flowrate distribution into the fracture for specified well production rate shown in Figures 3.18 and 3.19 were obtained from an earlier model (Cleary et al., 1983). The reader is referred to this work for a discussion of these results. The stabilised flowrate distribution shown in Figure 3.19 agrees with results obtained by Cinco et al. (1978). Results obtained with the current model agree in every way with these results, except that they can only be

generated with fracture conductivities an order of magnitude smaller than those used in the previous two studies. Although the weight of prior research is against it, there is some reason to believe that the new results are correct. For a fracture that is 1000 ft long and 0.2 inches wide in a 1 md permeability oil reservoir the fracture permeability would have to be 38000 md in order to produce the curve in Figure 3.19 that corresponds to stabilised drainage for a fracture conductivity of 0.2 (Of all those presented this case is most like radial drainage). Given that fracture permeabilities usually run between 4 and 1000 md, these older results would seem to indicate that long hydraulic fractures would only marginally improve well production. Since this is probably not the case, the predictions for lower fracture conductivities may be correct.

4 Summary and Conclusions

Schemes have been presented for calculating fluid loss, backstress, fracture temperature, and well production. The character of the models varies from simple to complex, depending on the model. The wellbore lumped model is easy to use and provides clear physical insight, but produces only first order estimates; the pseudo-2D takes into account the spatial variation of quantities over the fracture length and is computationally inexpensive; and, the 2D model calculates very precise solutions, especially in the vicinity of the fracture tip, but is more expensive to run. The well production model can determine either the wellbore flowrate or pressure buildup based on 2D drainage in the reservoir.

A number of results have been obtained for both stationary and propagating fractures, in gas and oil reservoirs. Propagating fracture results were based on four fracture growth histories generated by a lumped fracture model, without taking into account the effects fluid loss, backstress, and temperature on fracture propagation.

Fluid loss was determined by all three fracture models. Total loss predictions by the lumped and pseudo-2D models compared well, and the pseudo-2D accurately described spatial variation of loss, except at the fracture tip, where only the 2D model could capture the singularity in loss rate. The effect of the leakoff layer on loss was found to be very important in the gas reservoir and negligible in the oil, and the loss calculated for the constant and self-similar pressure distributions differed only slightly.

The analysis of backstress divided into a study of backstress at the wellbore, and a study of the variation of backstress over the fracture. Some important observations on wellbore backstress follow: 1) The wellbore backstress was found to be much greater when it was calculated using the reservoir height than when the fracture length was used; 2) several simple

approximations predicted the wellbore backstress accurately; 3) the effect of the leakoff layer was only important in the gas reservoir. As regards the variation in backstress, the high backstress at the fracture tip could only be modeled accurately by the 2D scheme; and, backstress calculations for the constant and self-similar pressure distributions were similar.

A simple criterion for the importance of convective heat exchange between fracture and reservoir was established; for the gas and oil reservoirs studied, it was found that only 10% of the total heat exchanged occurred by convection. Based on comparisons with the pseudo-2D predictions, the lumped model predicted accurately the average fracture temperature for propagating fractures. Fracture temperature profiles were determined for several propagating fractures with the pseudo-2D model. In all cases reservoir temperature was achieved well before the fracture tip.

Results for the production model agreed with previous work, except in terms of fracture conductivity. Current model predictions need either to be justified physically, or reconciled with previous work.

A continuation of this study should begin with a coupling of the models developed with appropriate fracture propagation models in order to determine the effect of fluid loss, backstress, and heat transfer on fracture growth. After that, the models could be turned on end in order to study a fracture cross section. If several cross sections were put together in a row, a 3D fracture could be analysed, P3DH style. Later, 3D influence functions for loss and backstress could be developed and implemented, first for a circular fracture, and then for the general 3D fracture, perhaps taking into account the impermeability of the adjacent strata.

References

1. Advani, S. H., Finite element model simulations associated with hydraulic fracturing, Paper No. SPE/DOE 8941, 1980.
2. Barr, D. T., and M. P. Cleary, Thermoelastic fracture solutions using distributions of singular influence functions - I: Determining crack stress fields from dislocation distributions, *Int. J. Solids Structures*, **19**, 73-82, 1983a
3. Barr, D. T., and M. P. Cleary, Thermoelastic fracture solutions using distributions of singular influence functions - II: Numerical modelling of thermally self-driven cracks, *Int. J. Solids Structures*, **19**, 83-91, 1983b
4. Boley, B. A., and J. H. Weiner, Theory of Thermal Stresses, John Wiley and Sons, Inc., 1960
5. Carslaw, H. S., and J. C. Jaeger, Conduction of Heat in Solids, 2nd edn., Oxford University Press, 1959
6. Chang, Y. P., C. S. Kang and D. J. Chen, The use of fundamental Green's functions for the solution of problems of heat conduction in anisotropic media, *Int. J. Heat Mass Transfer*, **16**, 1905-1918, 1973
7. Cheng, P., Heat transfer in geothermal systems, in: T. F. Irvine and J. P. Harnett (Eds.), Advances in Heat Transfer, Volume 14, Academic Press, New York, 1978, p. 1-105
8. Cinco, H., F. Samaniego and N. Dominguez, Transient pressure behavior for a well with a finite-conductivity vertical fracture, *SPEJ*, **18**, 253-264, 1978
9. Cleary, M. P., Moving singularities in elasto-diffusive solids with applications to fracture propagation, *Int. J. Solid Structures*, **14**, 81-97, 1978
10. Cleary, M. P., A. R. Crockett, J. I. Martinez, V. M. Narendran, and S. Slutsky, Surface integral schemes for fluid flow and induced stresses around fractures in underground reservoirs, SPE/DOE 11632, 1983 SPE/DOE Joint Symposium on Low Permeability Gas Reservoirs, Denver, Colorado, March 13-16, 1983

11. Cleary, M. P., R. G. Keck, and M. E. Mear, Microcomputer models for the design of hydraulic fractures, SPE/DOE 11628, 1983 SPE/DOE Joint Symposium on Low Permeability Gas Reservoirs, Denver, Colorado, March 13-16, 1983
12. Cleary, M. P., S. K. Wong, V. M. Narendran and A. S. Settari, General solutions for unsymmetric unidirectional hydraulic fracture propagation in reservoir structures, to be submitted for publication
13. Closmann, P. J., and D. M. Phocas, Thermal stresses near a heated fracture in transversely isotropic oil shale, *SPEJ, Feb*, 59-74, 1978
14. Gringarten, A., and H. Ramey, The use of sources and Greens's functions in solving unsteady-flow problems in reservoirs, *Trans. SPE AIME*, 255, 285-296, 1973
15. Hirth, J. P., and J. Lothe, Theory of Dislocations, McGraw-Hill, Inc., New York, 1968
16. Keung, C. S., and G. A. Domoto, The use of sources and sinks in solving two-dimensional heat conduction problems with change of phase in arbitrary domains, ASME Publication No. 80-HT-7, Joint ASME/AIChE National Heat Transfer Conference, Orlando, Florida, July 27-30, 1980
17. Narendran, V. M., and M. P. Cleary, Analysis of growth and interaction of multiple hydraulic fractures, SPE 12272, Seventh SPE Symposium on Reservoir Simulation, San Francisco, November 16-18, 1983
18. Rice, J. R., and M. P. Cleary, Some basic stress diffusion solutions for fluid-saturated elastic porous media with compressible constituents, *Rev. Geophys. Space Physics*, 14, 227-241, 1976
19. Settari, A. and H. Price, Simulation of Hydraulic Fracturing in Low Permeability Reservoirs, Paper SPE/DOE 8939, SPE/DOE Symposium on Low Permeability Gas Reservoirs, Pittsburgh, 1980
20. Settari, A. and M. P. Cleary, Development and testing of pseudo-three-dimensional model of hydraulic fracture geometry (P3DH), Paper No. SPE 10505, Proceedings of the Sixth SPE Symposium on Reservoir Simulation, New Orleans, February 1-3, 1982a

21. Settari, A. and M. P. Cleary, , Three-dimensional simulation of hydraulic fracturing, Paper No. SPE 10504, Proceedings of the Sixth SPE Symposium on Reservoir Simulation, New Orleans, February 1-3, 1982b
22. Shippy, D. J., Application of the boundary-integral equation method to transient phenomena in solids, *Boundary-Integral Equation Method: Computational Applications in Applied Mechanics*, ASME, 15-30, 1975
23. Sinclair, A. R., Heat fracture effects in deep well fracturing, *Journal of Petroleum Technology*, Dec, 1484-1492, 1971
24. Smith, M. B., Stimulation design for short precise hydraulic fractures, Paper No. SPE 10313, 1981
25. Tsai, Y. M., Thermal stress in a transversely isotropic medium containing a penny shape crack, *Journal of Applied Mechanics*, 1983 AMD/ASME Discussion Paper Number 83-APM-8, 1983
26. Wong, S. K., and M. P. Cleary, Numerical Analysis of Axisymmetric and other crack problems related to Hydraulic Fracturing, Report No. REL-81-4, MIT Resource Extraction Laboratory, June, 1981
27. Wong, S. K., V. M. Narendran and M. P. Cleary, Formulations and numerical methods for solving 2-D displacement discontinuity problems, submitted for publication to *Int. Jour. Num. Meth. Geomech.*, 1981

Table 1a
Non-Dimensionalisation of Parameters

<u>Dimensional Form</u>	<u>Non-Dimensional Form</u>
(t, τ)	$\frac{l^2}{c_R} (\hat{t}, \hat{\tau})$
$(x, y, \delta_h, \delta_l, l(t))$	$l(\hat{x}, \hat{y}, \hat{\delta}_h, \hat{\delta}_l, \hat{\delta}_f, \hat{l}(\tau))$
$(\theta - \theta_R)$	$(\theta_w^o - \theta_R) \Delta \hat{\theta}$
$(P - P_R)$	$\Delta p \Delta \hat{p}$, usually $\Delta p = p_F - p_T$
σ_B	$\Delta p \hat{\sigma}_B$
(\underline{v}, q_L)	$\frac{k_R(\Delta p)}{\mu_R \cdot l} (\hat{v}, \hat{q}_L)$
\dot{Q}_{rel}	$\frac{k_R \Delta p l}{\mu_R} \dot{Q}_{rel}$
h_L	$K_h (\theta_w^o - \theta_R) \hat{h}_L / l$
$\mu_L(\theta)$	$\mu_L(\theta_R) \hat{\mu}_L(\theta)$
$\mu_R(\theta)$	$\mu_R(\theta_R) \hat{\mu}_R(\theta)$
Vol	$l^3 \hat{V}ol$
A	$l^2 \hat{A}$

Table 1b
Non-Dimensional Parameters

$$\hat{\kappa} = \frac{\kappa}{c_R}$$

$$\hat{\beta}_V = \frac{k_R (p_w^o - p_R)}{\mu_R \mu_L}$$

$$\hat{\kappa}_L = \frac{\kappa_L}{c_R}$$

$$\hat{\kappa}_F = \frac{\kappa_F}{c_R}$$

$$\hat{C}_L = \frac{k_R \mu_L}{k_L \mu_R}$$

$$\hat{C}_F = \frac{k_R \mu_F}{k_F \mu_R}$$

Table 2a

Typical Reservoir Parameters for a Low to
Fair Permeability Oil Reservoir

ϕ	= 0.10	K_{hL}	= 0.393 BTU/hr.ft. ^{°F}
$\mu_L(\theta_R=250^\circ\text{F})$	= 0.21 cp	K_{hs}	= 1.058 BTU/hr.ft. ^{°F}
$\mu_L(\theta_w^0=125^\circ\text{F})$	= 0.5 cp	K_h	= 0.99 BTU/hr.ft. ^{°F}
$\mu_R(\theta_R=250^\circ\text{F})$	= 0.6 cp	ρ_L	= 1.869 Slug/ft ³
$\mu_R(\theta_w^0=125^\circ\text{F})$	= 4 cp	C_{pL}	= 32.3 BTU/slug ^{°F}
Δp	= 200 psi	ρ_s	= 4.269 Slug/ft ³
p_F	= 965 psi	C_s	= 5.453 BTU/slug ^{°F}
p_T	= 465 psi	k_L	= .83 md
θ_w^0	= 125 ^{°F}	k_R	= 1 md
θ_R	= 250 ^{°F}	v	= .3
K_f	= 6.25×10^4 psi		
l	= 60 ft.		

Diffusivities

κ	= 0.1×10^{-4} ft ² /sec
κ_L	= 0.46×10^{-5} ft ² /sec
κ_F	= 0.46×10^{-5} ft ² /sec
C_R	= 0.02675 ft ² /sec

Non-dimensional Parameters

$\hat{\beta}_v$	= 5.343
$\hat{\kappa}$	= 0.38×10^{-3}
$\hat{\kappa}_L$	= 0.17×10^{-3}
$\hat{\kappa}_F$	= 0.17×10^{-3}
\hat{c}_L	= 0.42

Table 2b

Typical Reservoir Parameters for a Low
Permeability Gas Reservoir

ϕ	= 0.05	K_{hL}	= 0.393 BTU/hr.ft. ^{°F}
$\mu_L(\theta_R=250^\circ\text{F})$	= 0.21 cp	K_{hs}	= 1.058 BTU/hr.ft. ^{°F}
$\mu_L(\theta_w^\circ=125^\circ\text{F})$	= 0.5 cp	K_h	= 0.99 BTU/hr.ft. ^{°F}
$\mu_R(\theta_R=250^\circ\text{F})$	= 0.03 cp	ρ_L	= 1.869 Slug/ft. ³
$\mu_R(\theta_w^\circ=125^\circ\text{F})$	= 0.03 cp	C_{pL}	= 32.3 BTU/slug. ^{°F}
Δp	= 200 psi	ρ_s	= 4.269 Slug/ft. ³
P_F	= 6500 psi	C_s	= 5.453 BTU/slug. ^{°F}
P_T	= 4000 psi	k_L	= .005 md
θ_w°	= 125 ^{°F}	k_R	= .01 md
θ_R	= 250 ^{°F}	K_f	= 4000 psi
		l	= 60 ft.
		v	= .3

Diffusivities

κ	= 0.11×10^{-4} ft ² /sec
κ_L	= 0.47×10^{-5} ft ² /sec
κ_F	= 0.47×10^{-5} ft ² /sec
κ_R	= 0.68×10^{-3} ft ² /sec

Non-dimensional Parameters

$\hat{\beta}_V$	= 1.034
$\hat{\kappa}$	= 0.16×10^{-1}
$\hat{\kappa}_L$	= 0.69×10^{-2}
$\hat{\kappa}_F$	= 0.69×10^{-2}
\hat{C}_L	= 14.0

Table 3

Fluid, heat penetration and heat exchange characteristic of the typical oil and gas reservoirs.

%heat exchange due to connection	OIL 9%	GAS 10%
Penetration depths after one hour:		
δ_L	.3 ft.	.66 ft.
δ_f	35.3 ft.	5.5 ft.
δ_{hc}	.68 ft.	.72 ft.
δ_h	.7 ft.	.75 ft.

TABLE 4

Fracture propagation cases generated by a lumped fracture propagation model (ellipsoidal shapes)

$$1) \quad \Delta p_w = 100 \text{ psi}, \quad \bar{E}_A/\bar{E}_R = 2, \quad \Delta\sigma_C = 50 \text{ psi}$$

$$l(t) = 50 + 1580(t/120 \text{ min})^{.92} \text{ ft}$$

$$h(t) = 50 + 190(t/120 \text{ min})^{.53} \text{ ft}$$

$$2\delta(t) = .045 + .17(t/120 \text{ min})^{.53} \text{ in}$$

$$2) \quad \dot{Q}_F = 5 \text{ bbl/min}, \quad \bar{E}_A/\bar{E}_R = 2, \quad \Delta\sigma_C = 50 \text{ psi}$$

$$l(t) = 50 + 1190(t/120 \text{ min})^{.68} \text{ ft}$$

$$h(t) = 50 + 150(t/120 \text{ min})^{.35} \text{ ft}$$

$$2\delta(t) = .063 + .092(t/120 \text{ min})^{.33} \text{ in}$$

$$3) \quad \dot{Q}_F = 5 \text{ bbl/min}, \quad \bar{E}_A/\bar{E}_R = 4, \quad \Delta\sigma_C = 100 \text{ psi}$$

$$l(t) = 50 + 1420(t/120 \text{ min})^{.72} \text{ ft}$$

$$h(t) = 50 + 110(t/120 \text{ min})^{.30} \text{ ft}$$

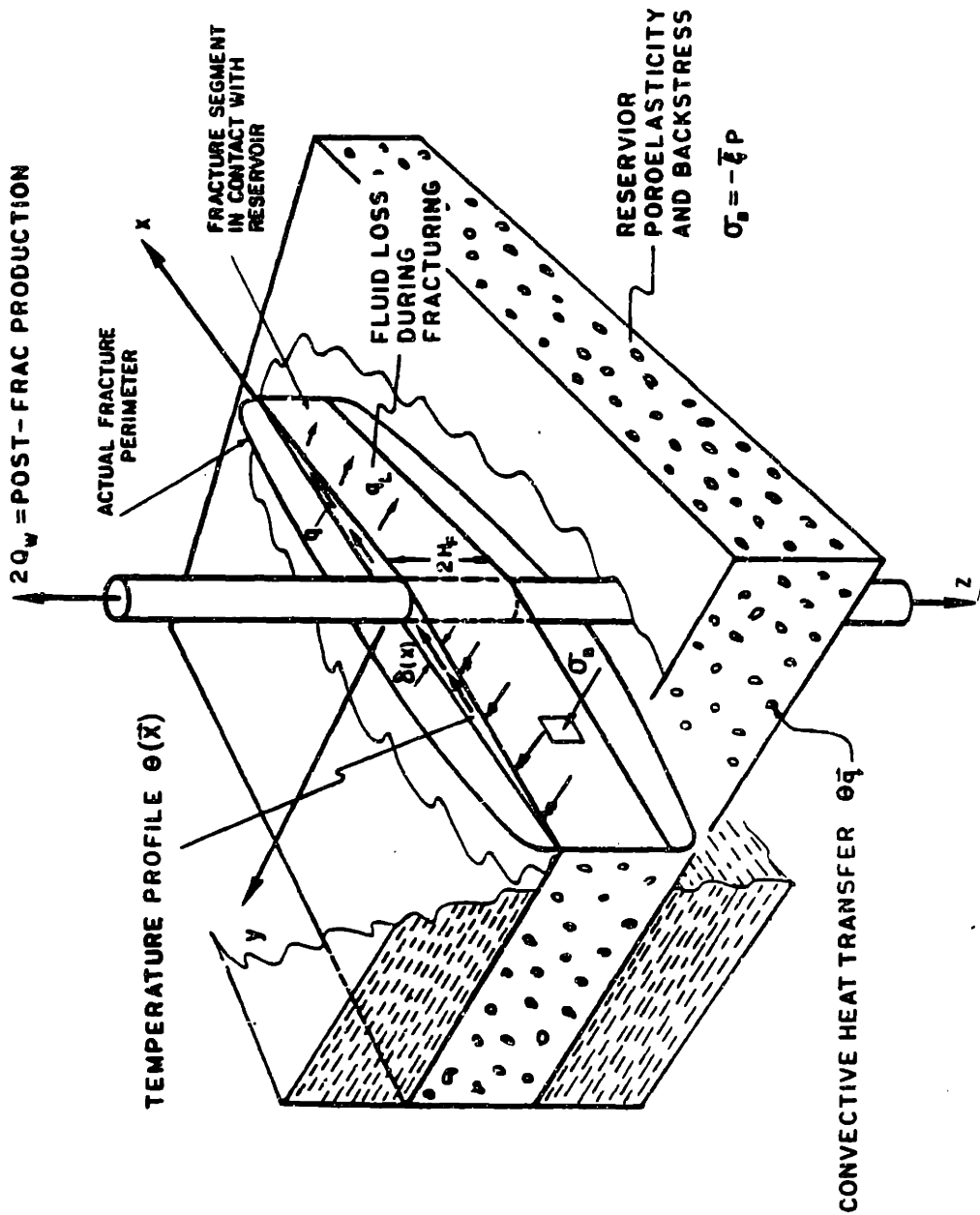
$$2\delta(t) = .063 + .10(t/120 \text{ min})^{.34} \text{ in}$$

$$4) \quad \dot{Q}_F = 5 \text{ bbl/min}, \quad \bar{E}_A/\bar{E}_R = 4, \quad \Delta\sigma_C = 150 \text{ psi}$$

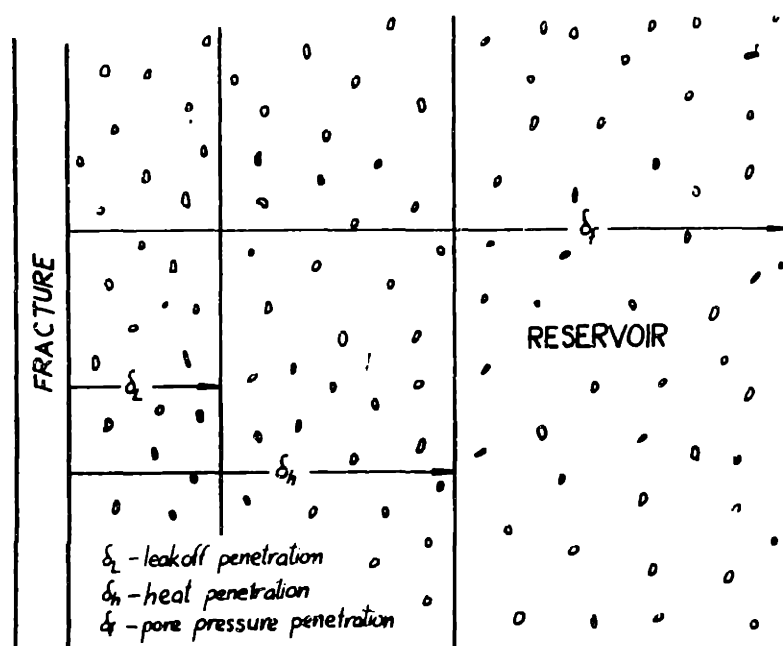
$$l(t) = 50 + 1690(t/120 \text{ min})^{.74} \text{ ft}$$

$$h(t) = 50 + 80(t/120 \text{ min})^{.28} \text{ ft}$$

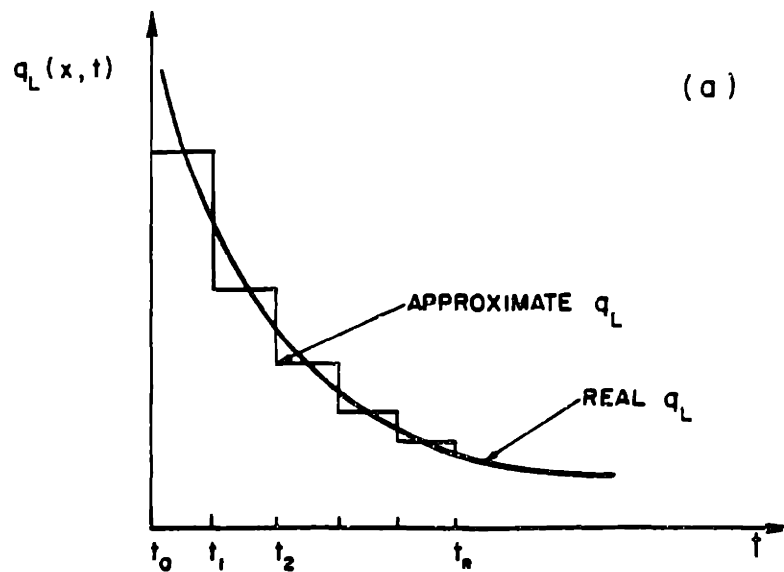
$$2\delta(t) = .063 + .11(t/120 \text{ min})^{.34} \text{ in}$$



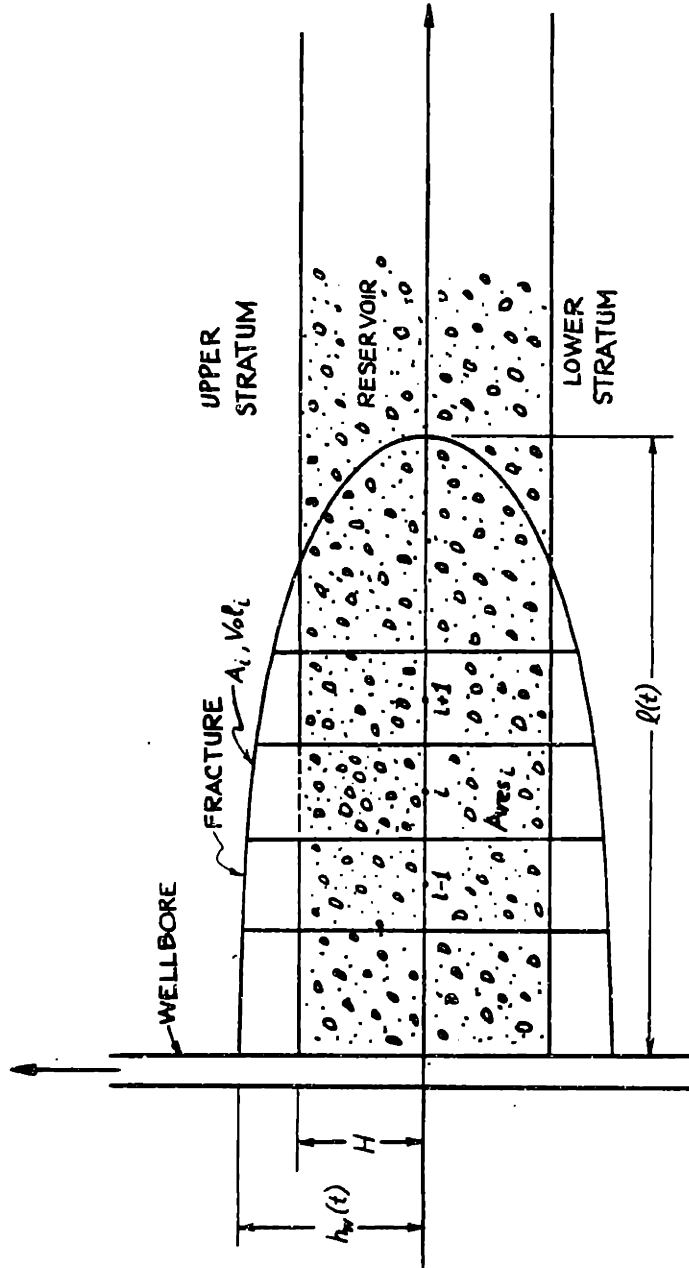
2.1 Fracture surroundings with relevant events noted



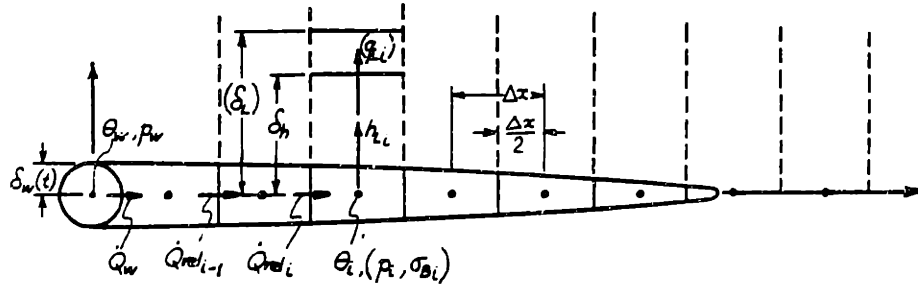
2.2 Heat and fluid penetration into the reservoir normal to the fracture



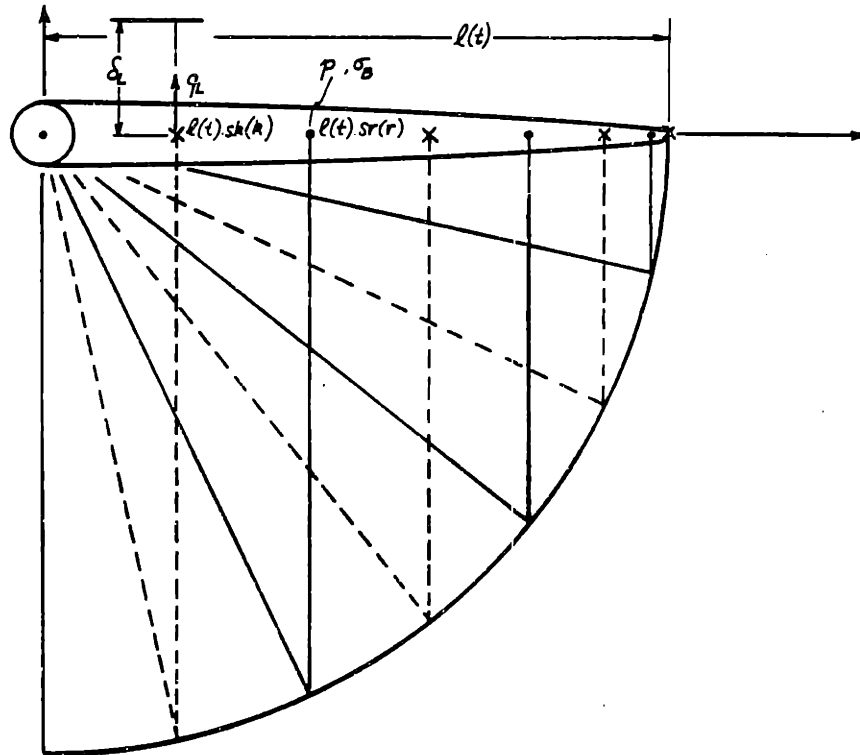
2.3a Discretisation of fluid exchange with time



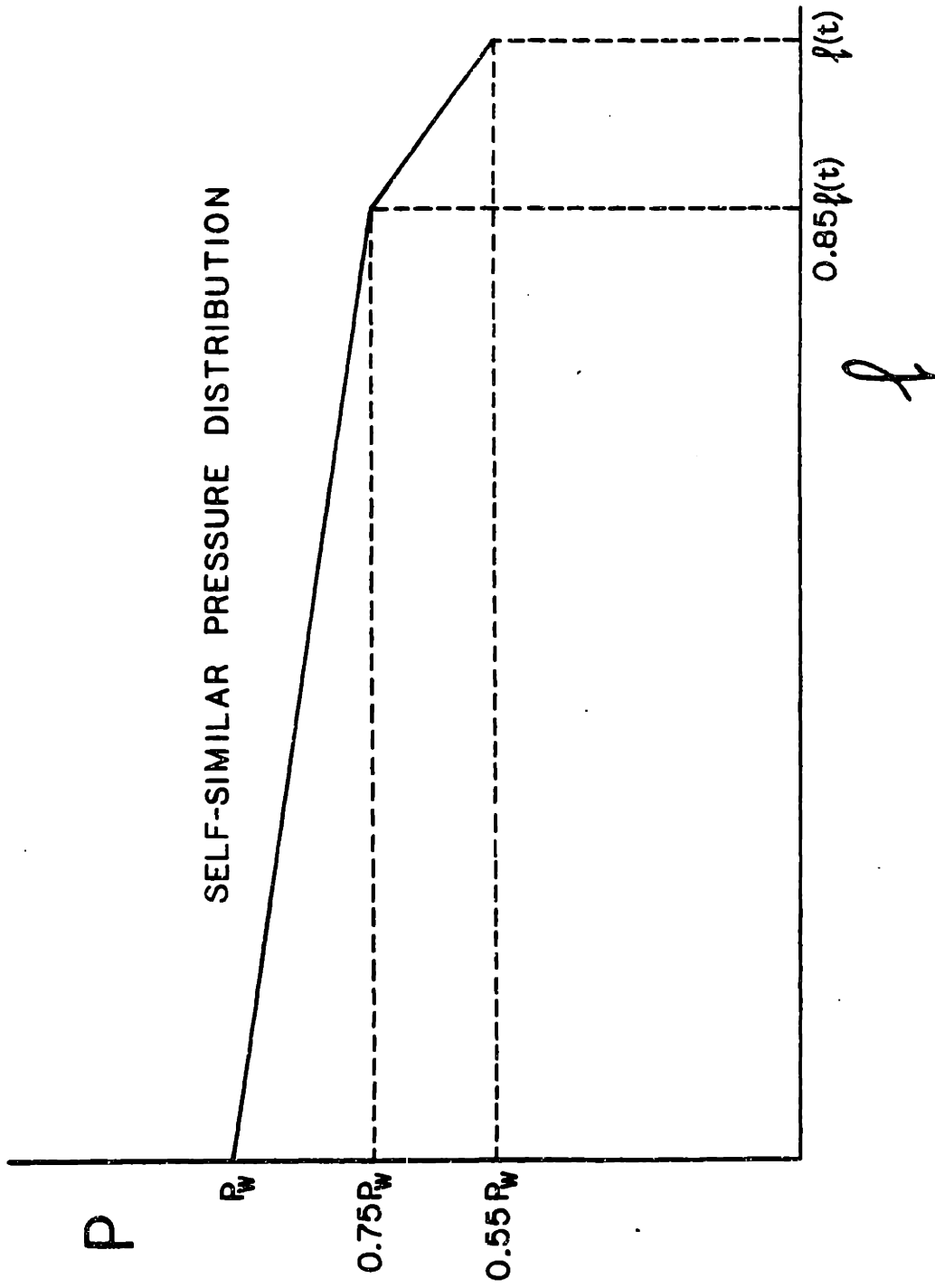
2.3b Fracture geometry; discretisation of fracture volume and surface area



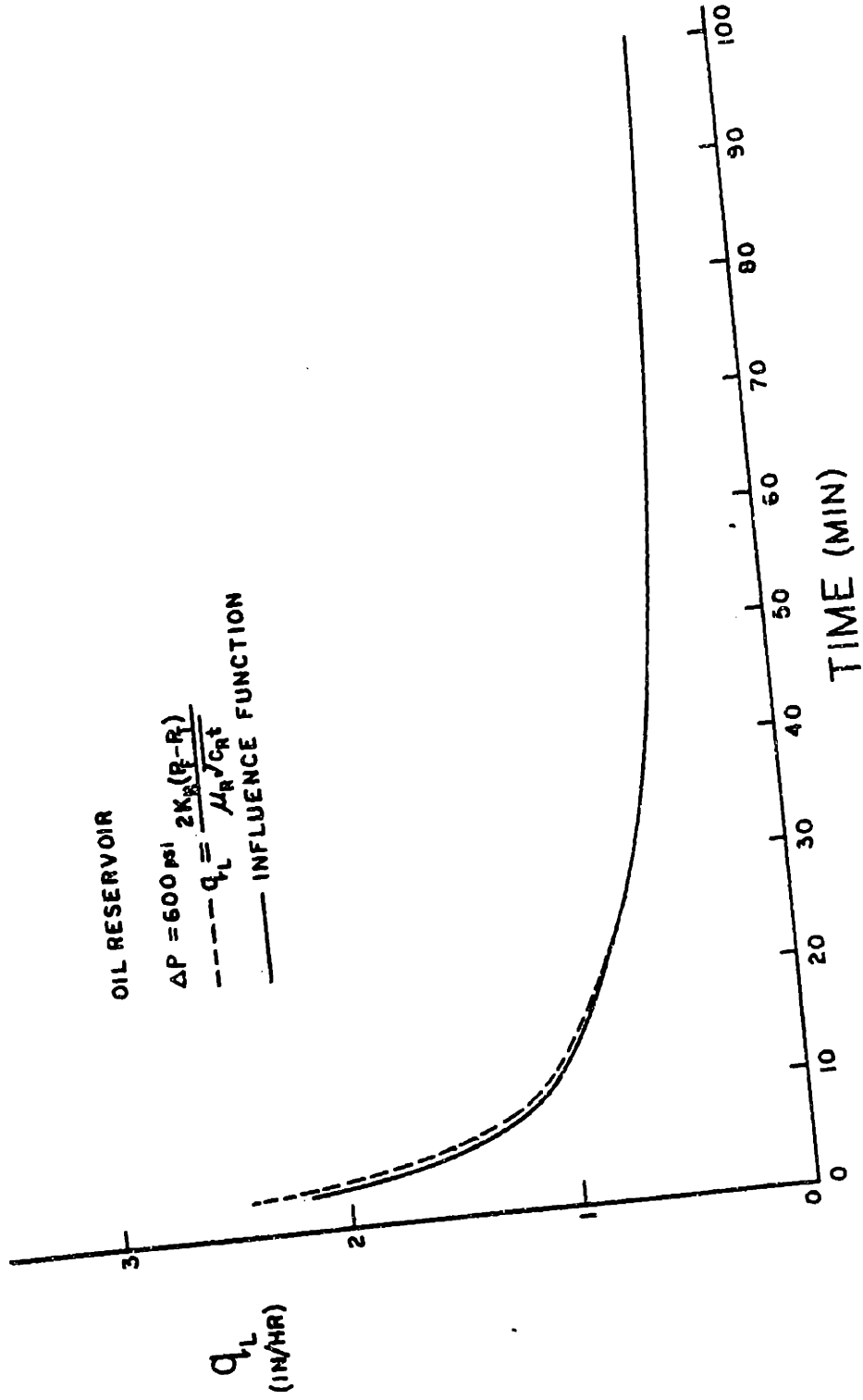
2.3c Stationary grid that fracture grows over;
variables associated with stationary grid



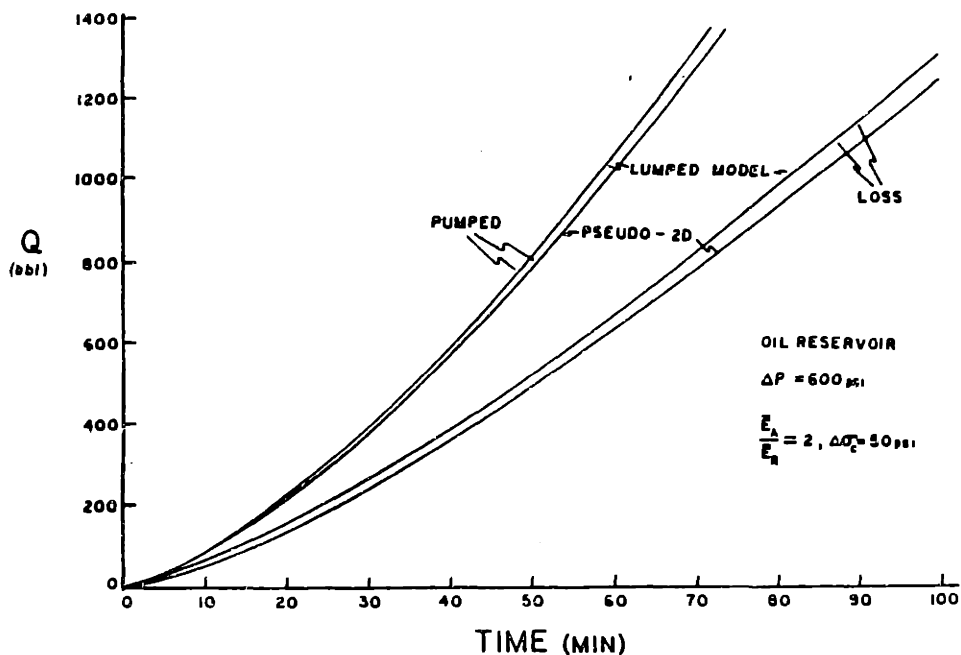
2.3d Chebychev grid that stretches over fracture as it grows;
variables associated with Chebychev grid



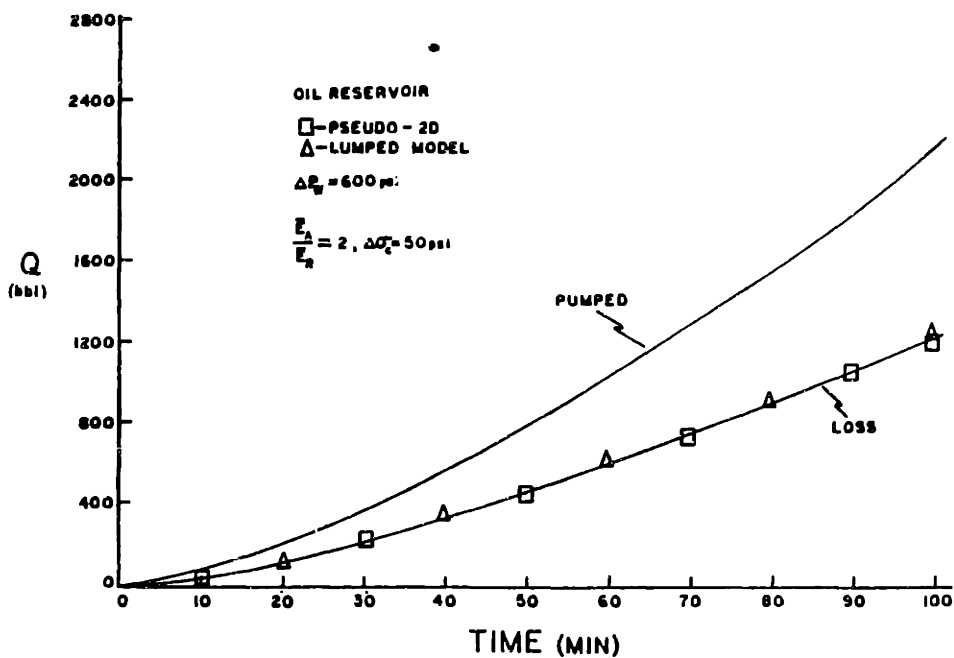
2.3e Pressure distribution for propagating fractures



3.1 1D exact versus influence function solutions of the fluid loss rate for constant fracture pressure

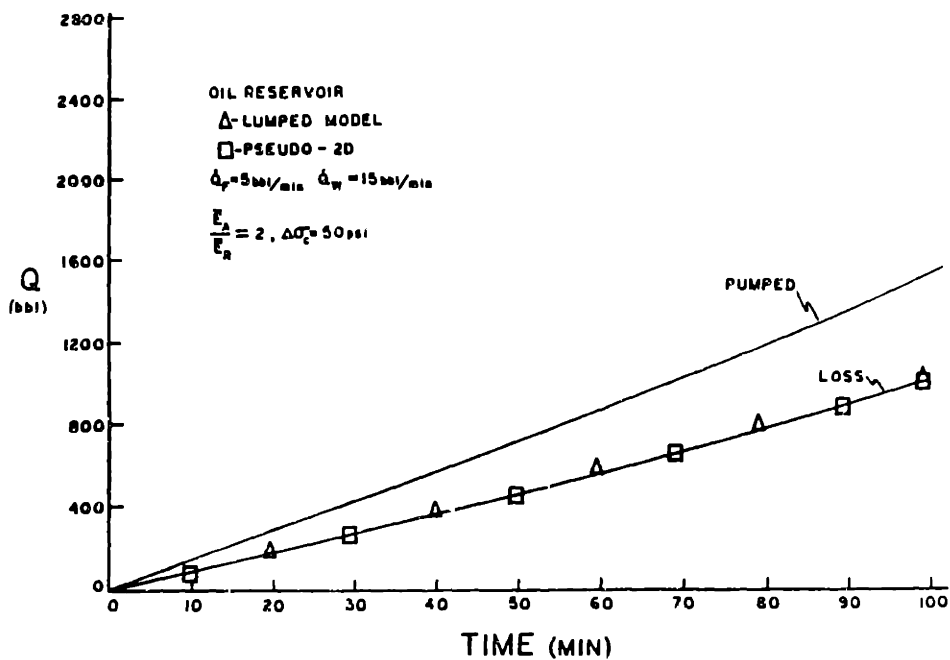


3.2a

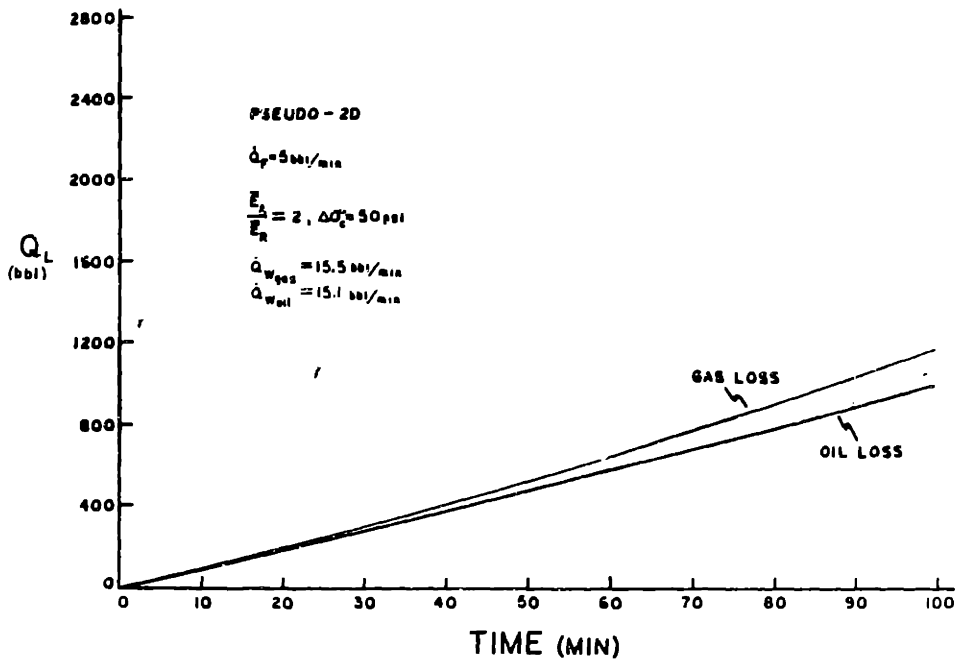


3.2b

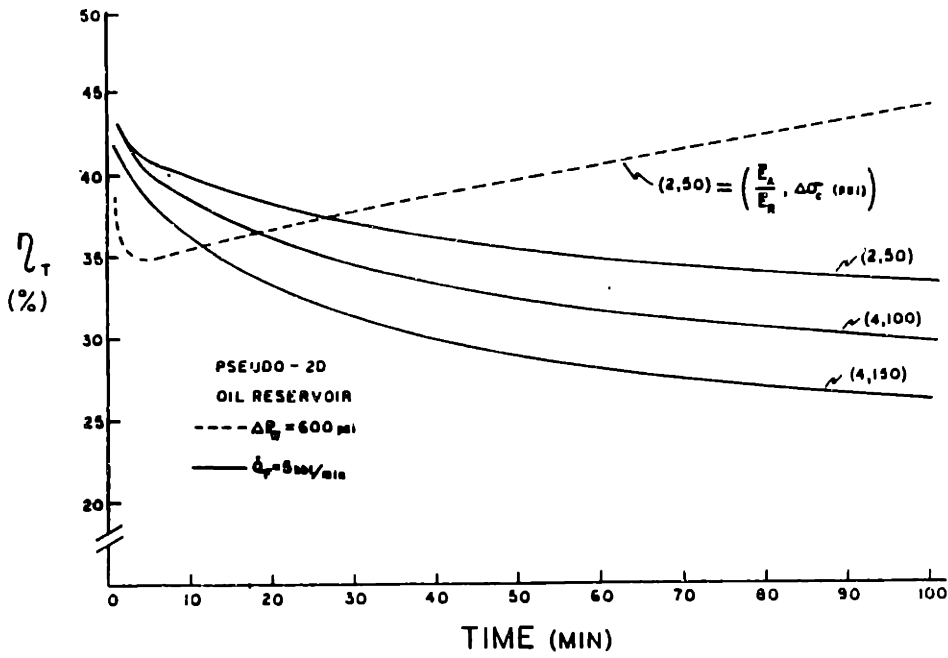
3.2 Lumped and pseudo-2D model predictions of the total fluid lost for propagating fractures; a) constant fracture pressure; b) constant wellbore pressure; c) constant fracture volume growth rate



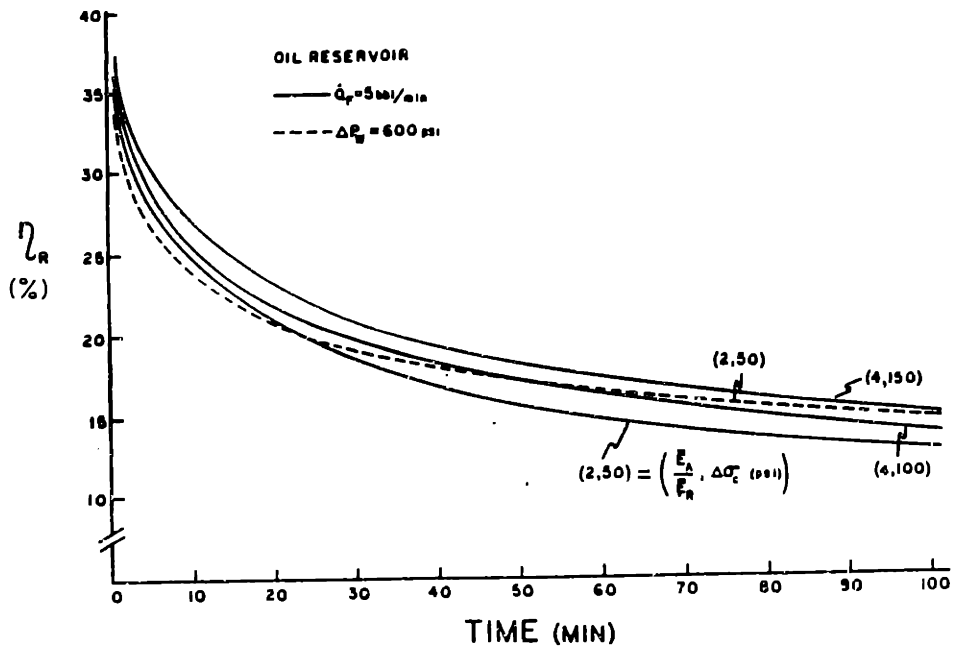
3.2c



3.3 Predictions of total fluid lost for propagating fractures in gas and oil reservoirs

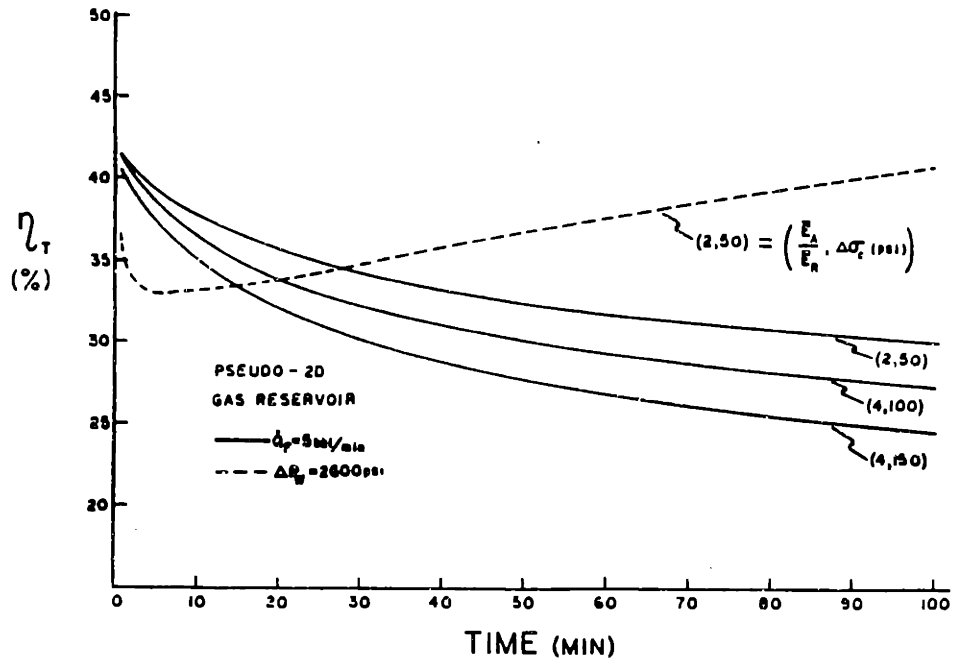


3.4a

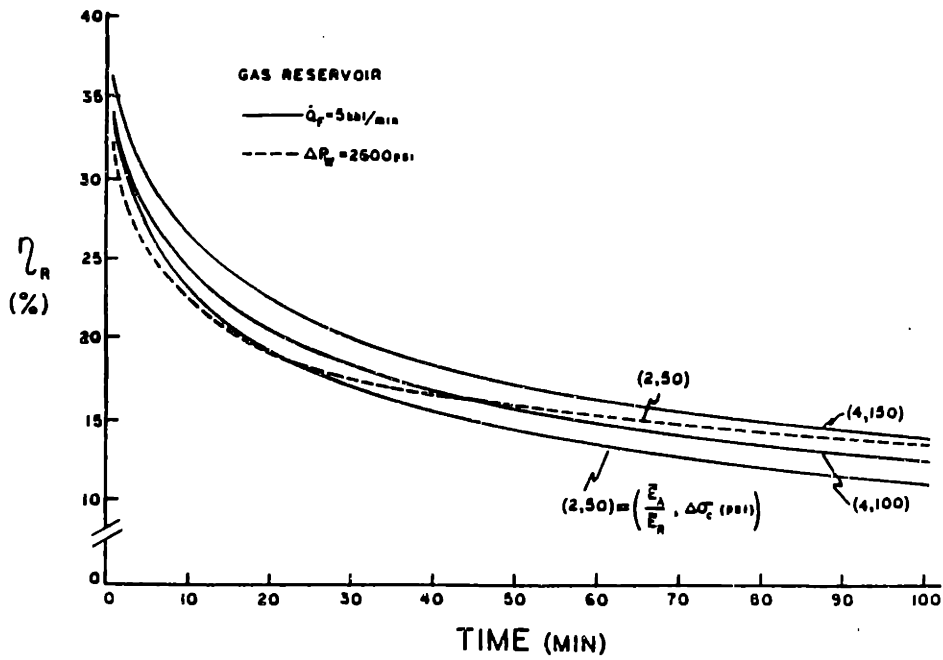


3.4b

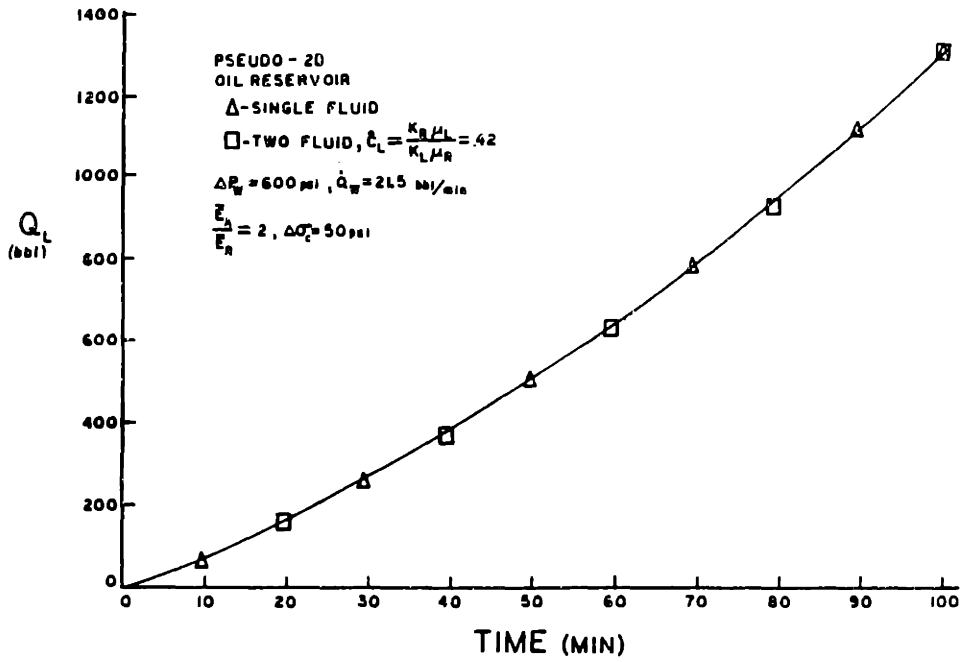
3.4 Two definitions of fracture efficiency shown for various fracture propagation conditions: a) and c) total fracture efficiency; b) and d) fracture volume opposite reservoir efficiency



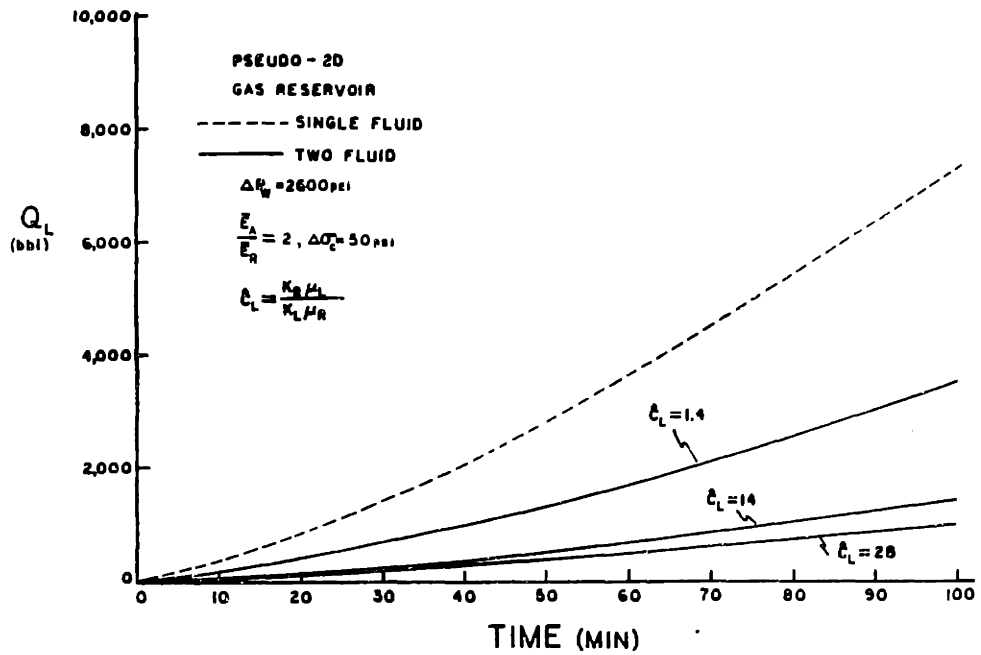
3.4c



3.4d

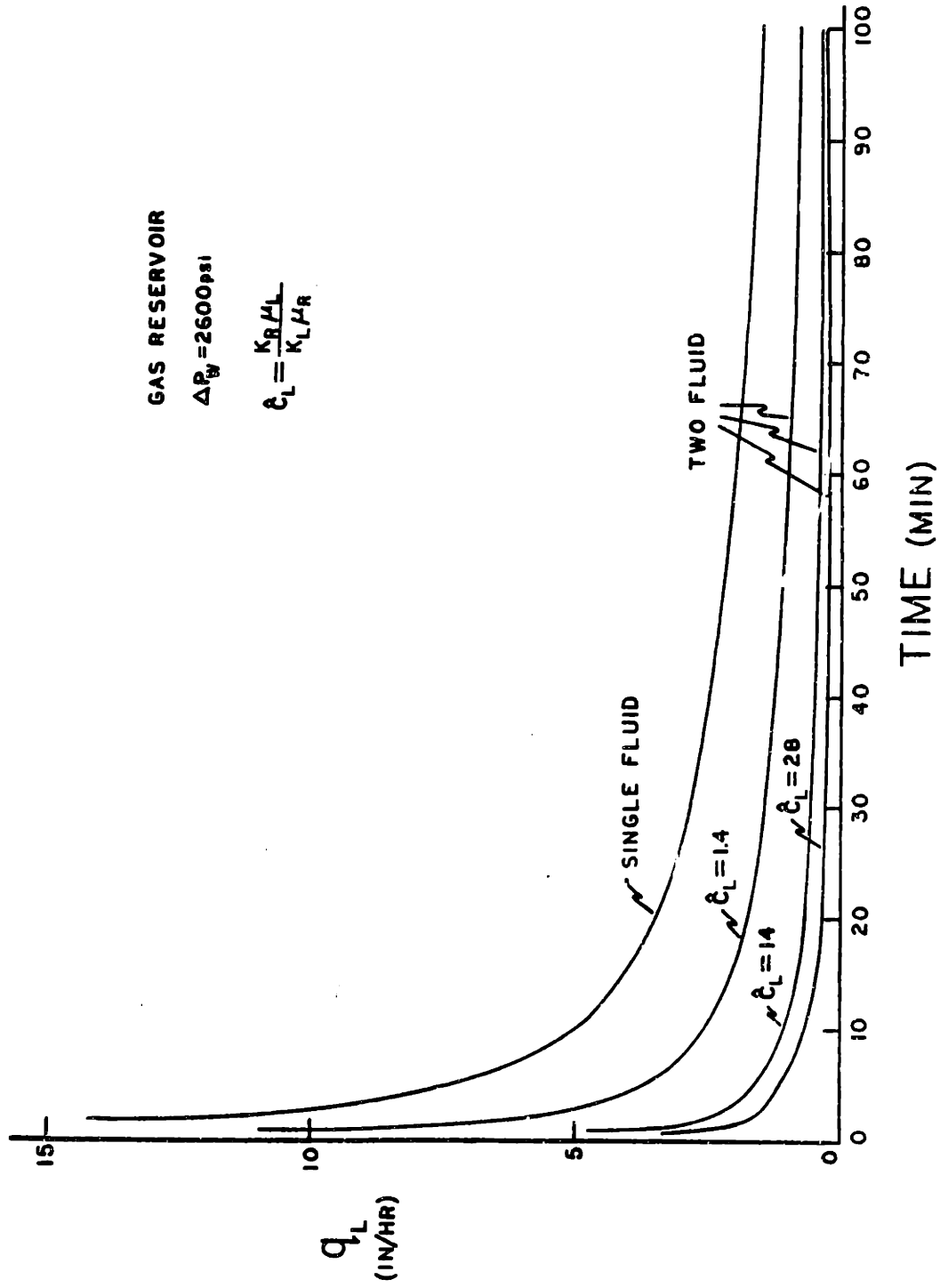


3.5a

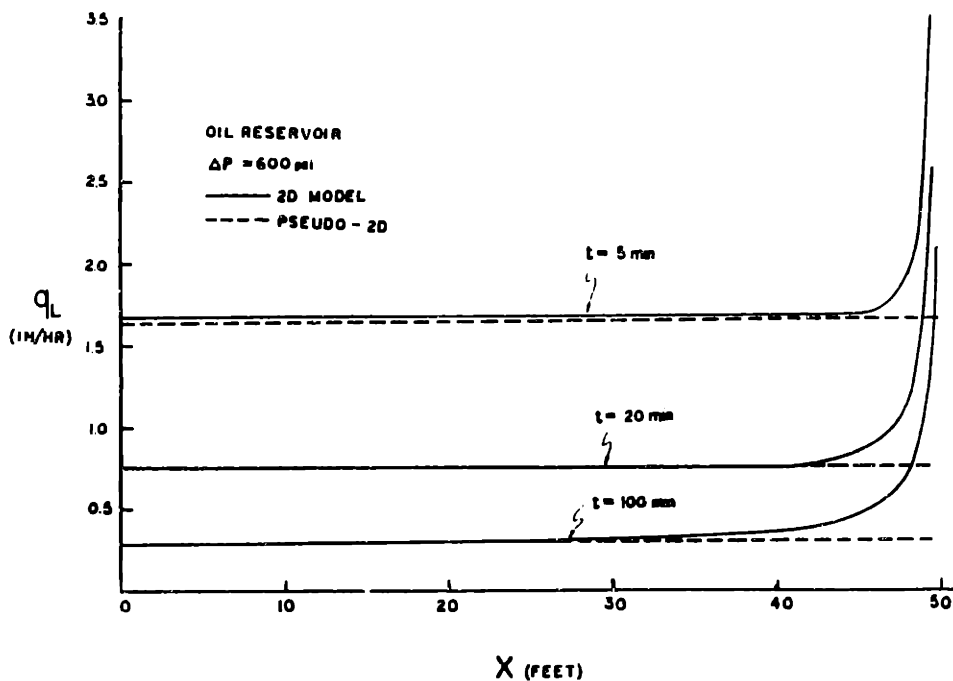


3.5b

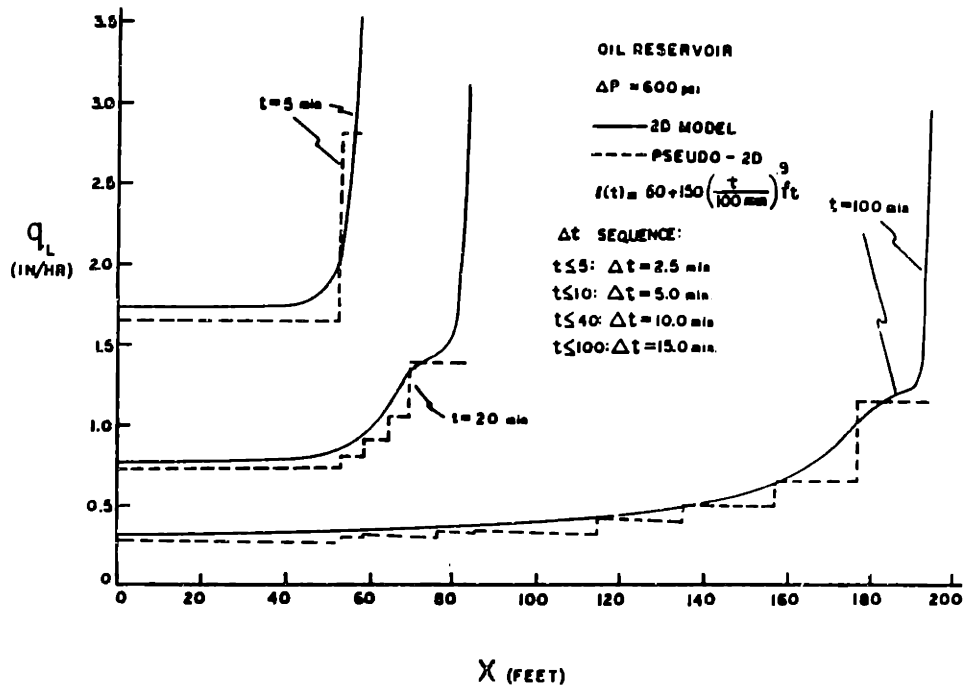
3.5 One and two fluid model predictions of total leakoff for a propagating fracture: a) oil reservoir; b) gas reservoir



3.6 One and two fluid model predictions of fluid loss rate

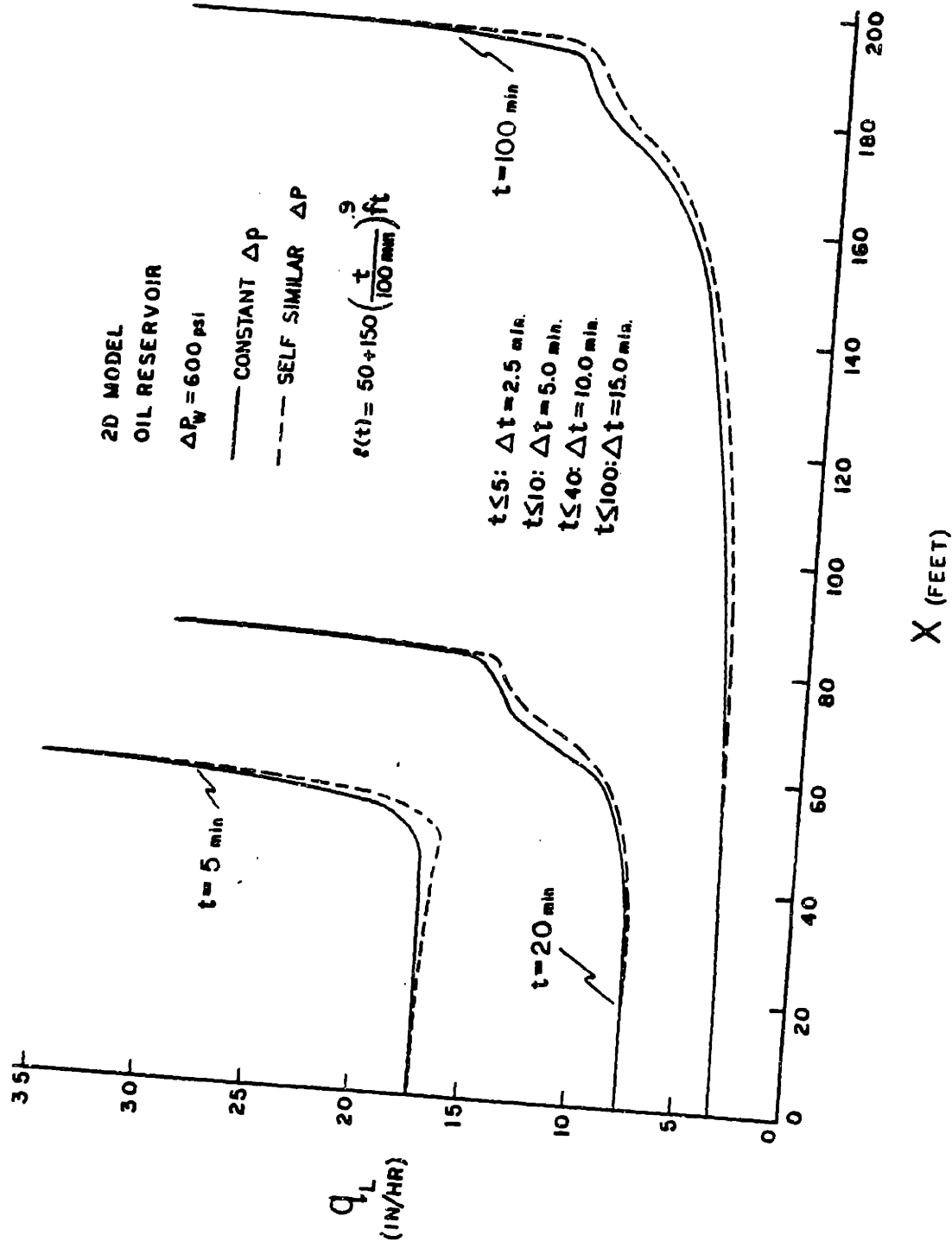


3.7a

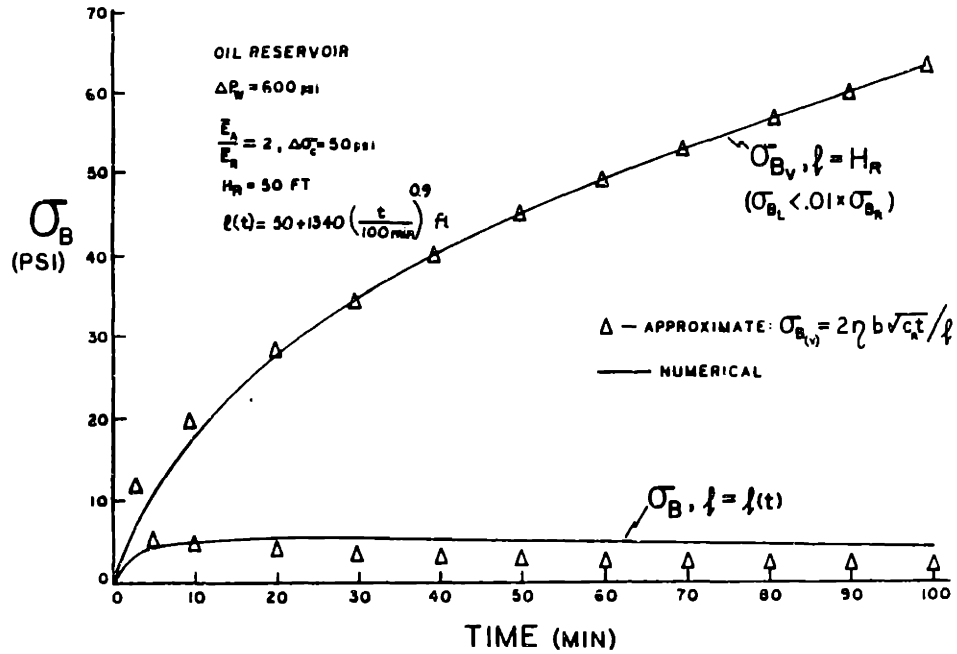


3.7b

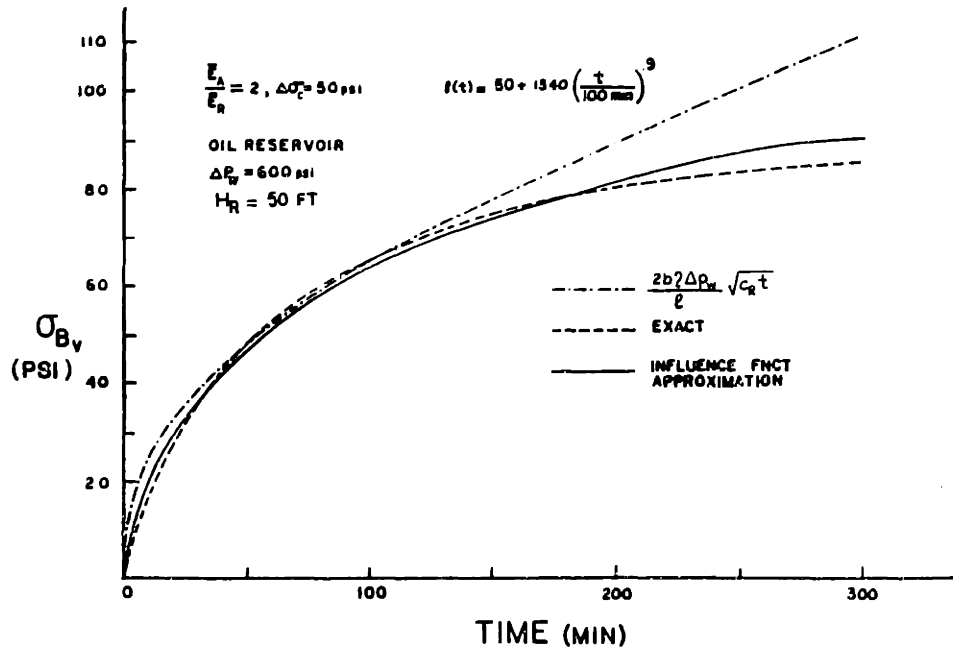
3.7 Comparison of 2D and pseudo-2D fluid loss rates:
 a) stationary fracture; b) propagating fracture



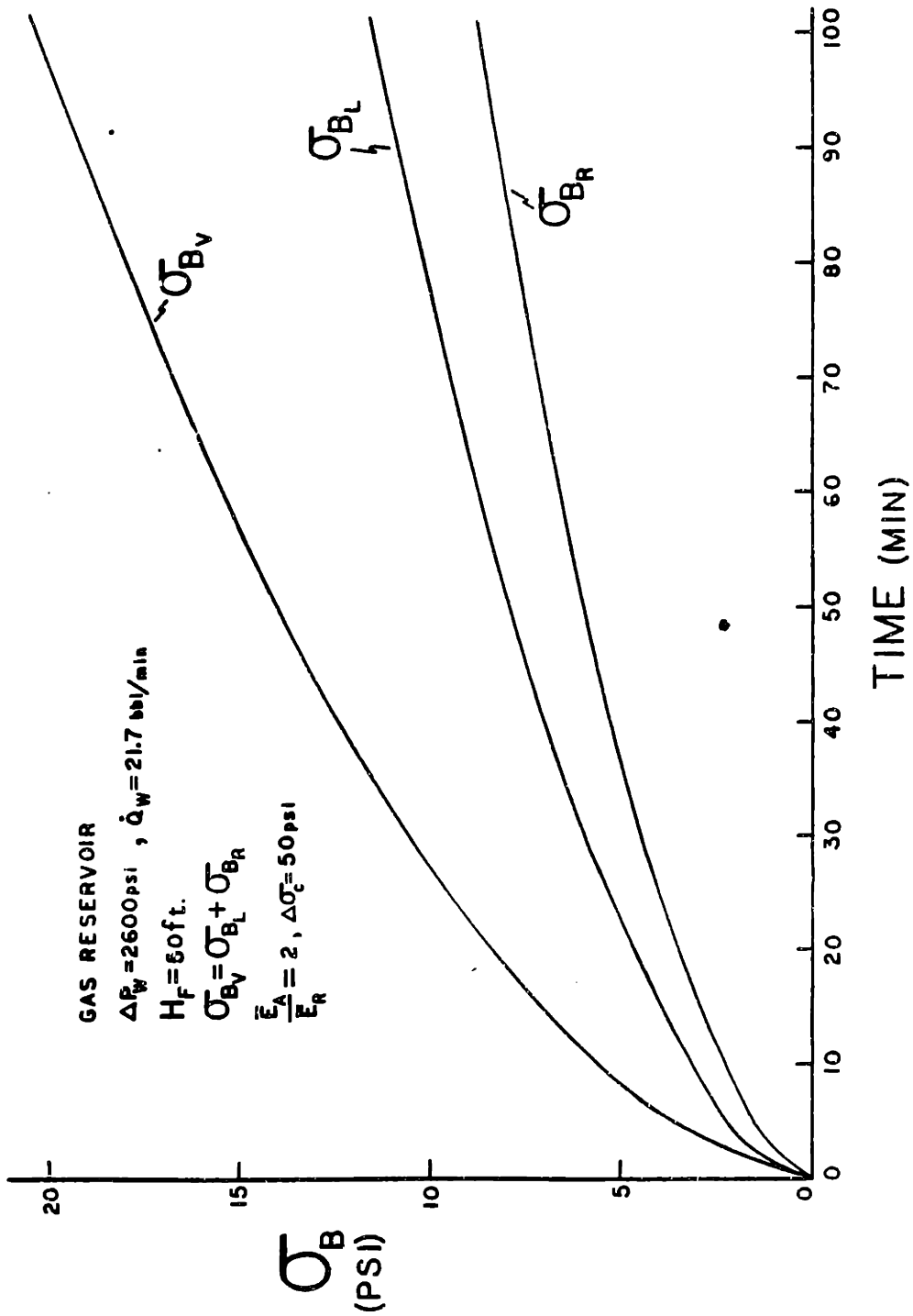
3.8 2D fluid loss rates for constant and self-similar pressure distributions along the fracture



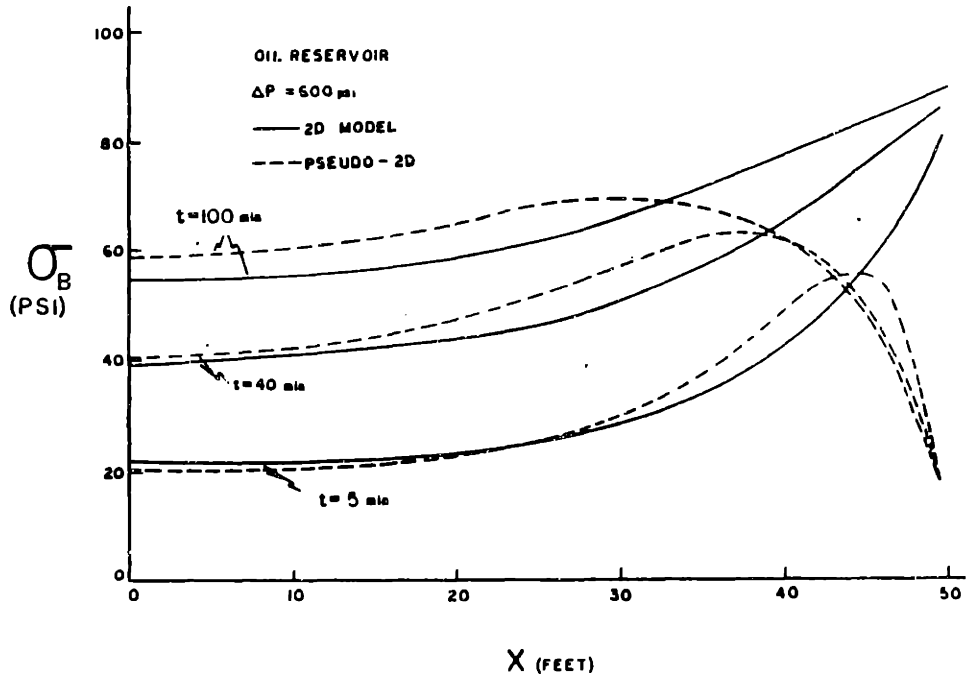
3.9a "Approximate", reservoir height, and fracture length model predictions of wellbore backstress for a propagating fracture in an oil reservoir



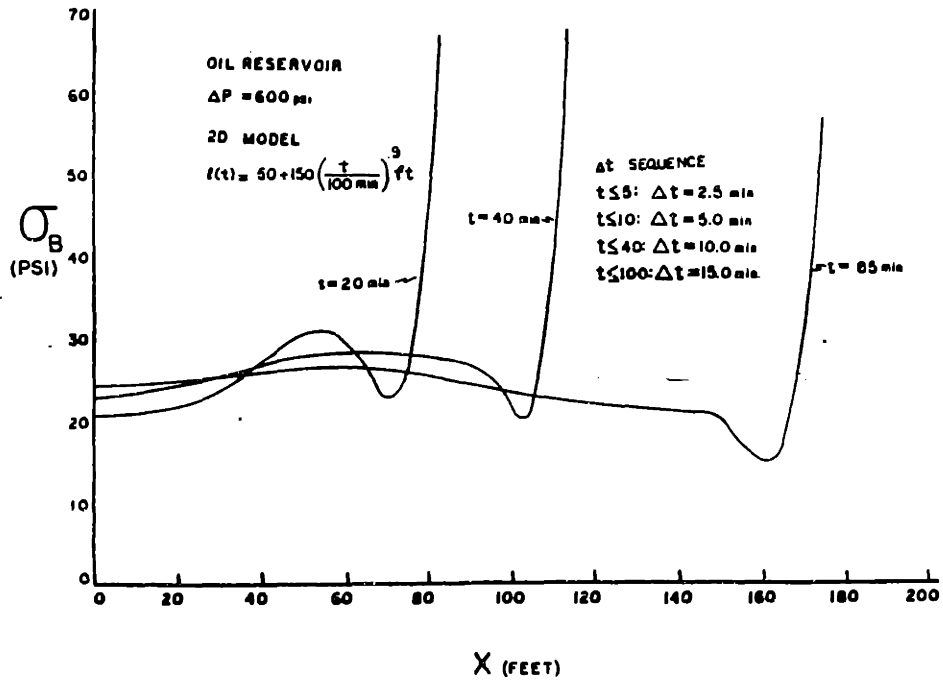
3.9b Comparison of approximate wellbore backstress predictions



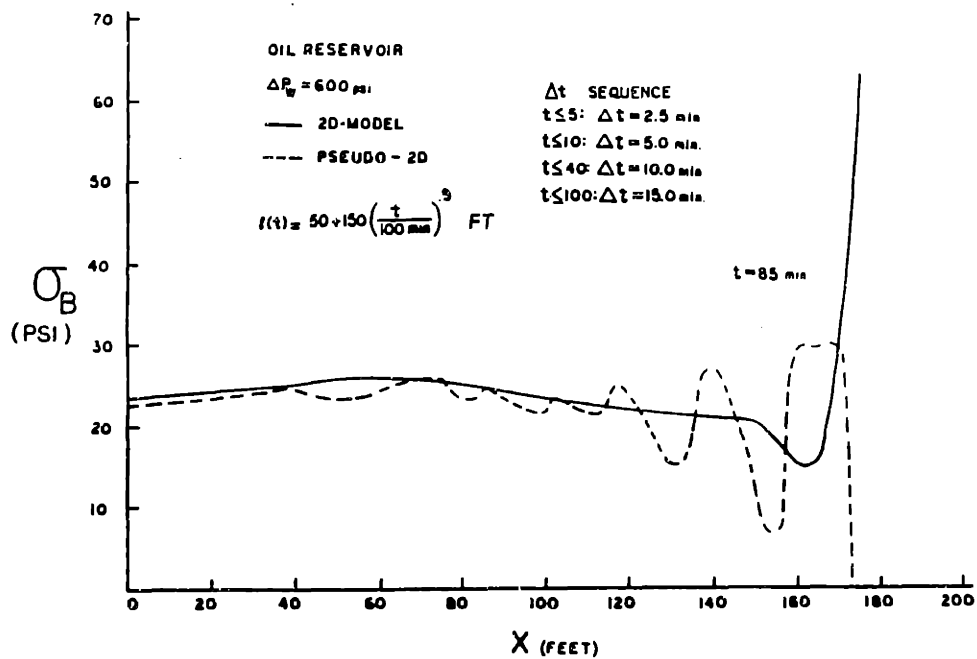
3.10 Decomposition of wellbore backstress for a propagating fracture in a gas reservoir into leakoff layer and reservoir components



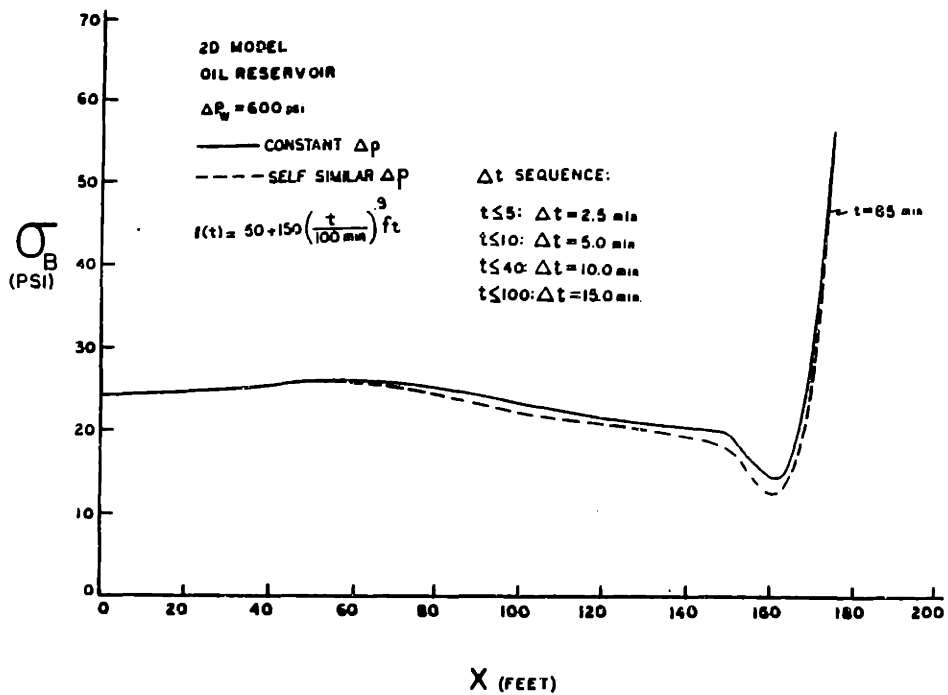
3.11a Comparison of 2D and pseudo-2D predictions of backstress for a stationary fracture



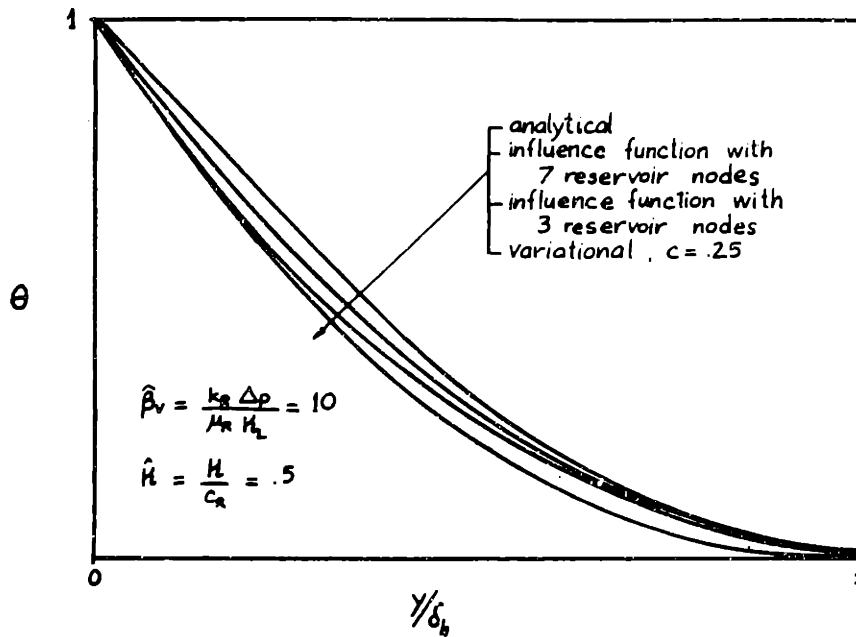
3.11b 2D predictions of backstress for a propagating fracture



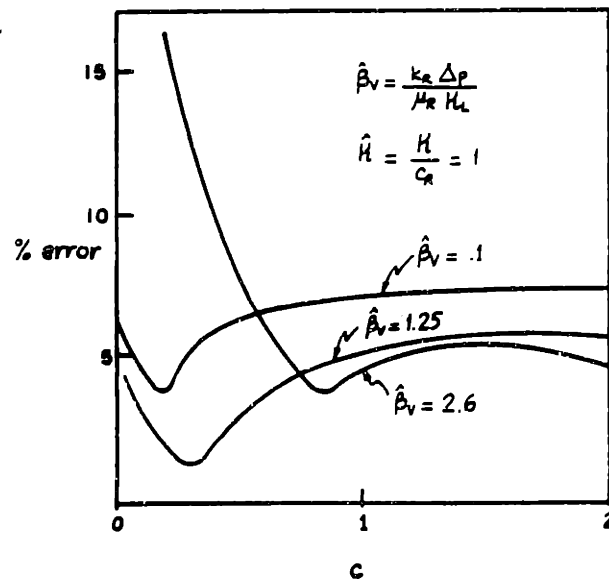
3.11c Comparison of 2D and pseudo-2D predictions of backstress for a propagating fracture



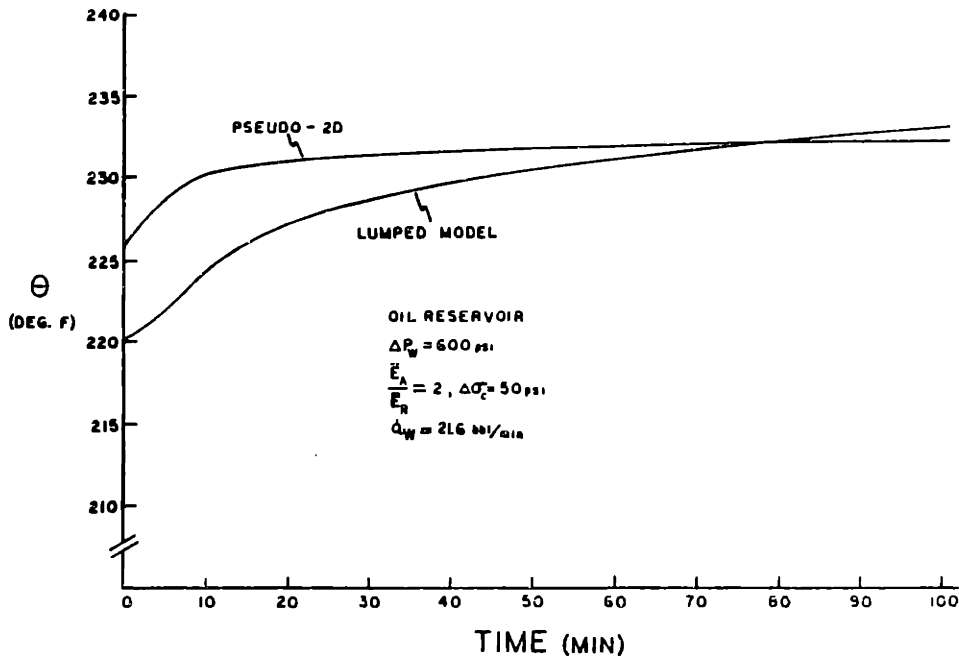
3.12 Comparison of 2D backstresses for constant and self-similar pressure distributions along the fracture



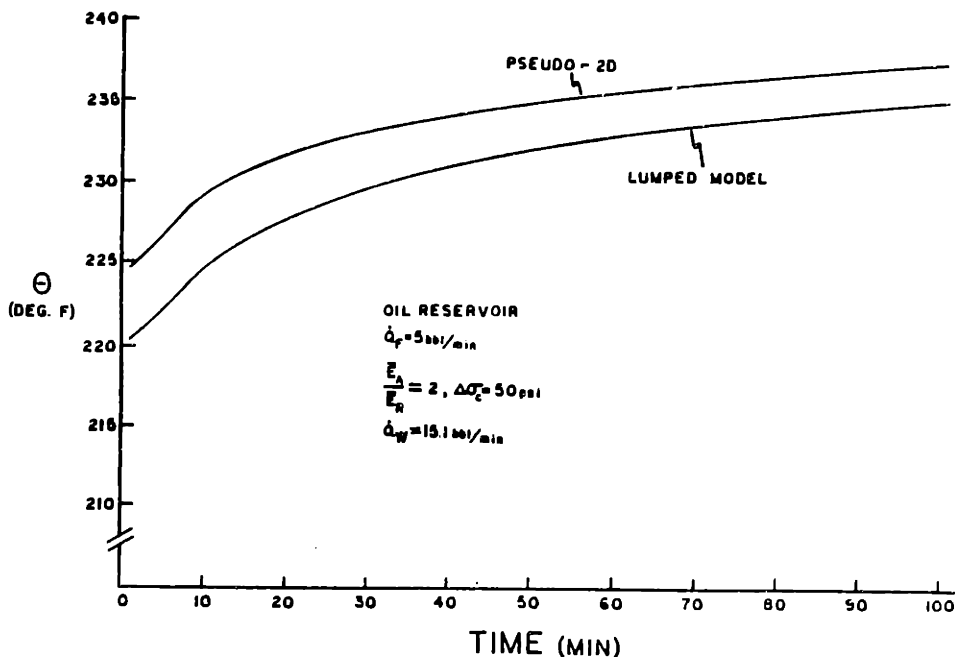
3.13 Comparison of 1D solutions for reservoir heat transfer



3.14 Sensitivity of the variational heat transfer solution to cubic curve fitting parameter (c)

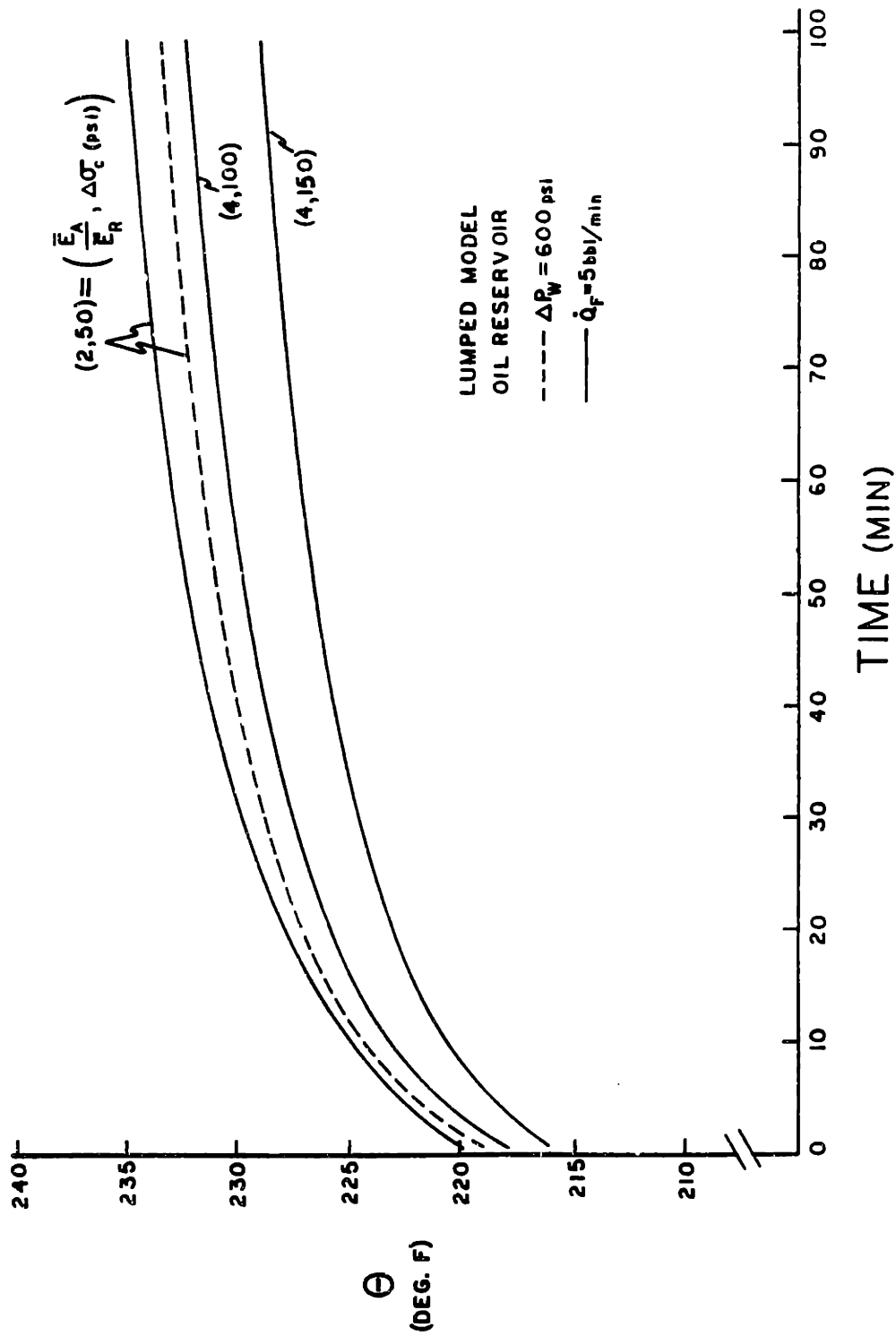


3.15a

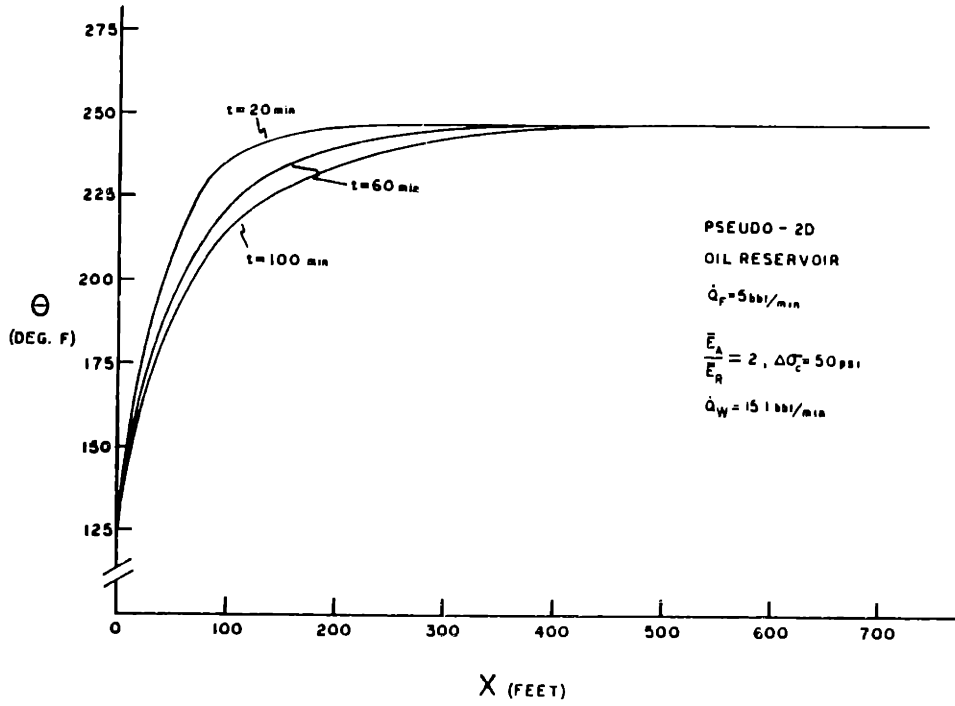


3.15b

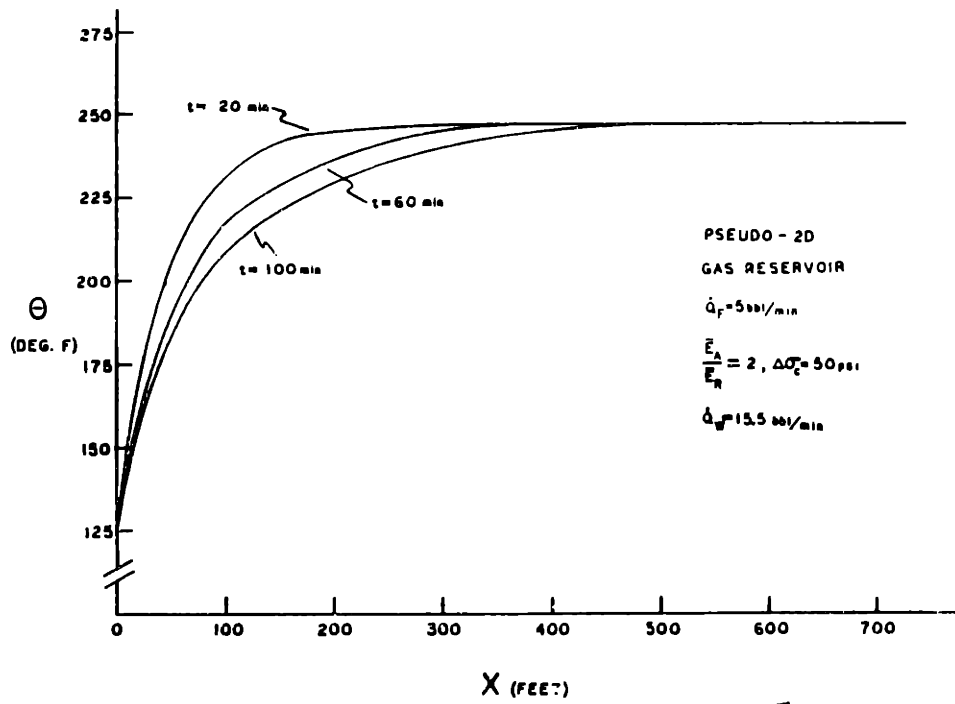
3.15 Lumped versus pseudo-2D predictions of average fracture temperature for propagating fractures: a) constant wellbore pressure; b) constant fracture volume growth rate



3.16 Lumped model predictions of average fracture temperature for propagating fractures

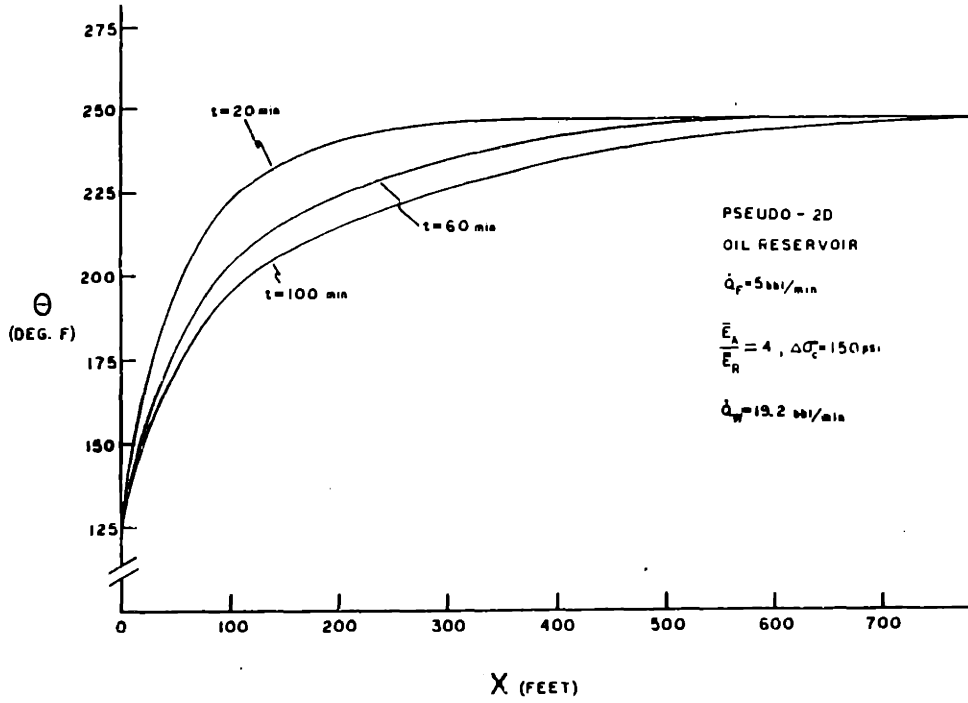


3.17a

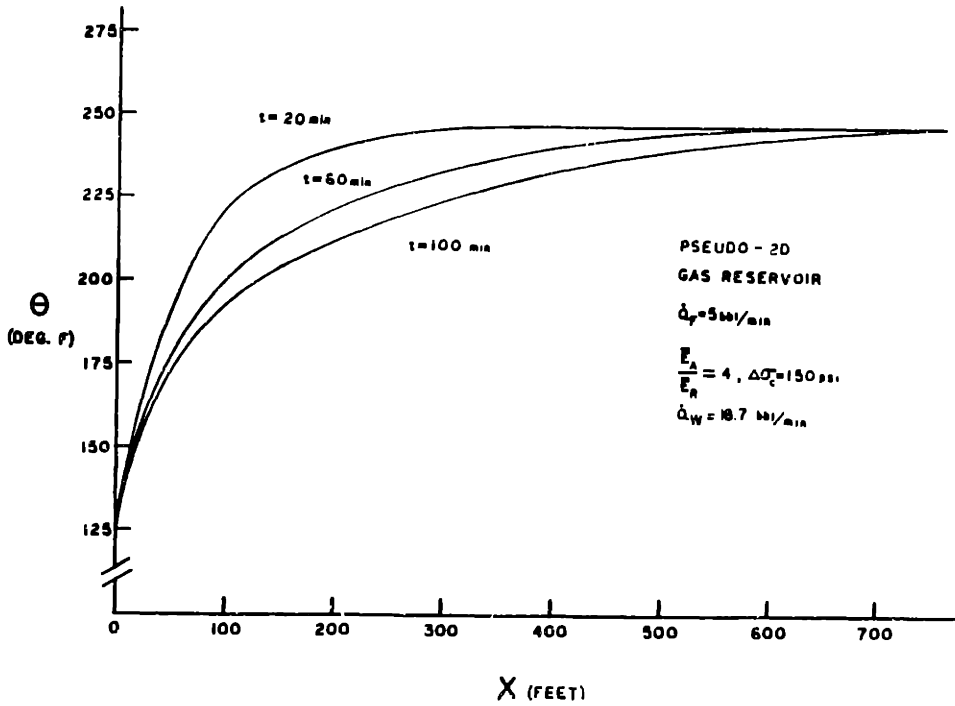


3.17b

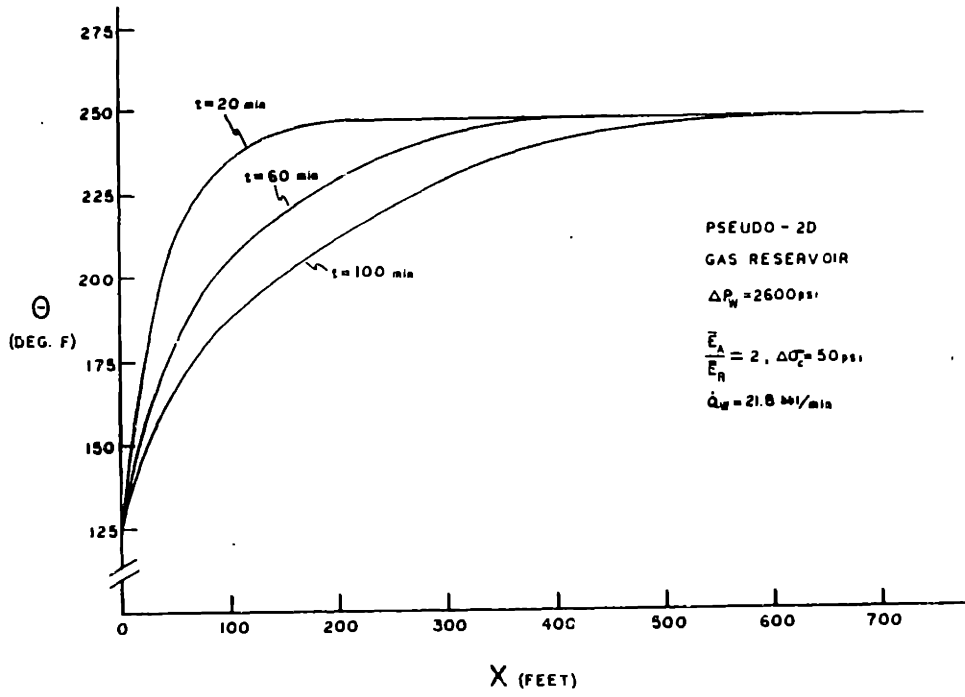
3.17 Pseudo-2D model predictions of fracture temperature for propagating fractures (Figures 3.17a - f)



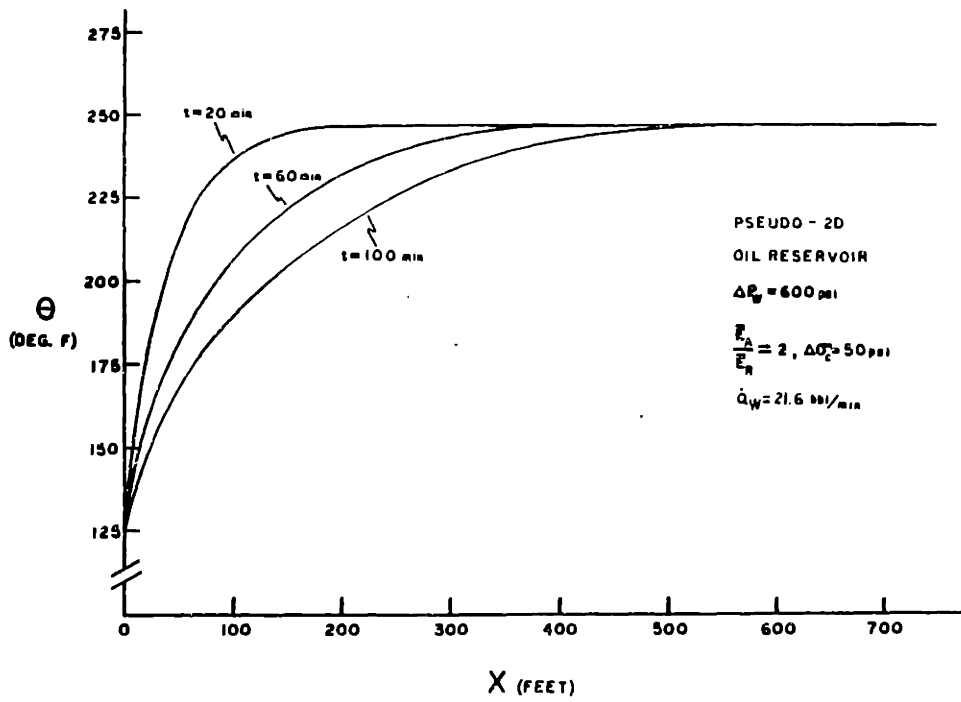
3.17c



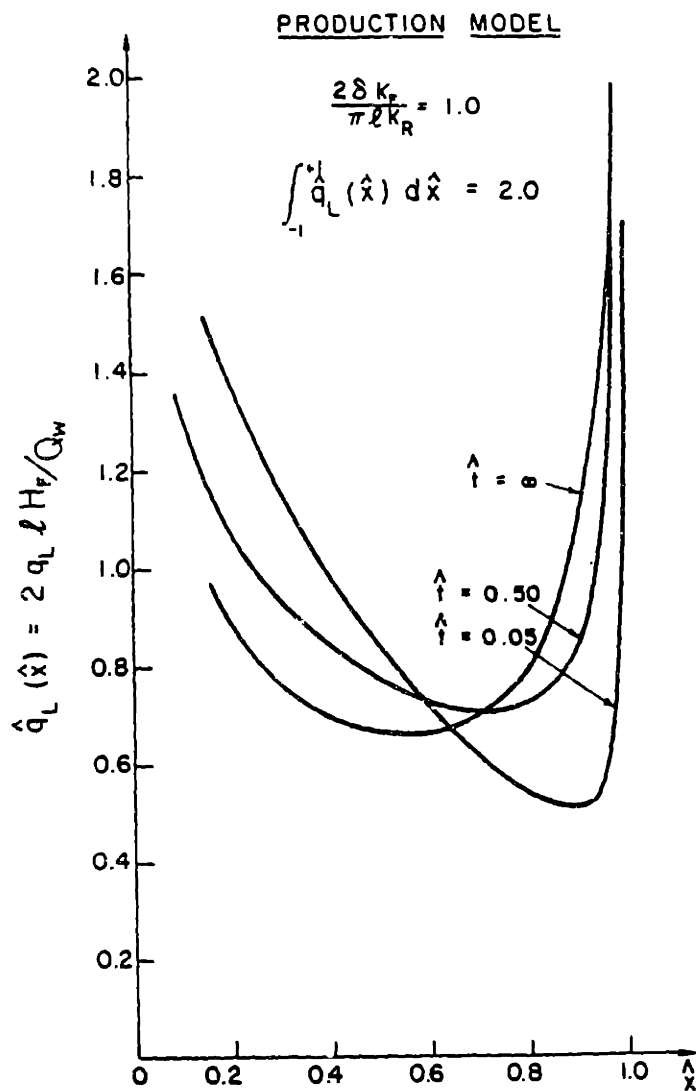
3.17d



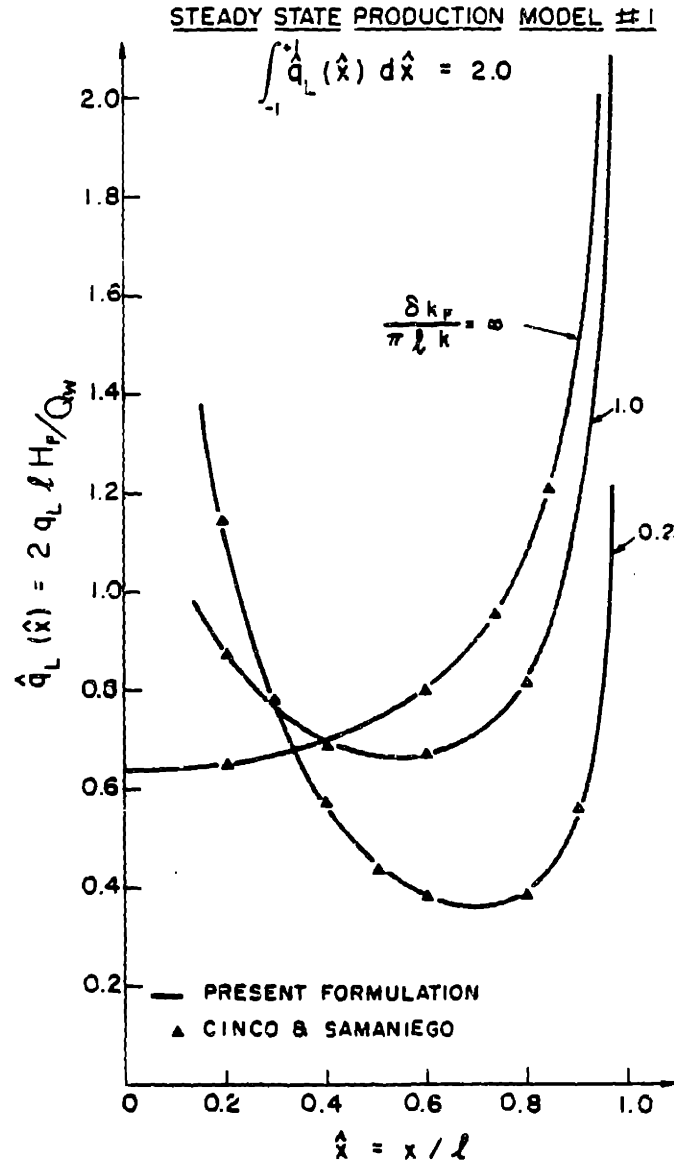
3.17e



3.17f



3.18 2D well production model predictions of flow rates into the fracture



3.19 2D well production model predictions of stabilised flowrates into the fracture